



THE UNIVERSITY *of* EDINBURGH

This thesis has been submitted in fulfilment of the requirements for a postgraduate degree (e.g. PhD, MPhil, DClinPsychol) at the University of Edinburgh. Please note the following terms and conditions of use:

- This work is protected by copyright and other intellectual property rights, which are retained by the thesis author, unless otherwise stated.
- A copy can be downloaded for personal non-commercial research or study, without prior permission or charge.
- This thesis cannot be reproduced or quoted extensively from without first obtaining permission in writing from the author.
- The content must not be changed in any way or sold commercially in any format or medium without the formal permission of the author.
- When referring to this work, full bibliographic details including the author, title, awarding institution and date of the thesis must be given.

Non-covalent interactions in solution

Lixu Yang



Doctor of Philosophy
The University of Edinburgh
2013

Declaration

I declare that the thesis has been composed by the myself, and the work described in this thesis is carried out by my own, except as specified. The work has not been submitted for any other degree or professional qualification.

Signature:

Date:

Acknowledgements

The most important person I should thank is my supervisor Dr Scott L. Cockroft. Scott gave me this precious opportunity to pursue a scientist's dream and lots of brilliant ideas on the projects. Scott not only offered me valuable advice on science, but also restored my optimism when I was experiencing a down period during my PhD.

My sincere thanks also go to Dr. John Brazier, who worked on the aromatic stacking project with me. This work could not have been done without his effort and contributions. I also like to thank Hayat P. H. Saifuddin who previously worked on alkyl-alkyl dispersion project and Catherine Adam who finished the project. Besides, I am very grateful to the rest of the group, for providing a very friendly environment and kind help. I would like to express my very great appreciation to the support teams of School of Chemistry.

I truly thank the financial support of overseas research scholarship (ORS) and MTEM scholarship.

Finally, I specially thank my family and friends for their support and encouragement throughout my study.

Abstract

Non-covalent interactions taking place in solution are essential in chemical and biological systems. The solvent environment plays an important role in determining the geometry and stability of interactions. This thesis examines aromatic stacking interactions, alkyl-alkyl interactions, edge-to-face aromatic interactions, halogen bonds and hydrogen \cdots hydrogen interactions in solution.

Chapter 1 briefly introduces the different classes of non-covalent interactions, in addition to the state-of-the-art models and methods for investigating these weak interactions. The chapter finishes with a focus on dispersion interaction in alkanes and arenes.

Chapter 2 investigates dispersion interactions between stacked aromatics in solution using a new class of complexes and thermodynamic double mutant cycles (DMCs). In extended aromatics, dispersion was detected as providing a small but significant contribution to the overall stacking free energies.

Chapter 3 concerns the experimental measurement of alkyl-alkyl dispersion interactions in a wide range of solvents using Wilcox torsion balances. The contribution of dispersion interactions to alkyl-alkyl association was shown to be very small, with DMC, QSPR method and Hunter's solvation model.

Chapter 4 studies edge-to-face aromatic interactions in series of solvents. In the open system, edge-to-face aromatic interactions were found to be sensitive to the solvent environment. The solvent effects were complicated and cannot be rationalised by a single parameter. Further analysis is needed.

Chapter 5 describes a preliminary approach to investigate organic halogen $\cdots\pi$ interactions in solution using supramolecular complexes and torsion balances.

Chapter 6 is a preliminary investigation of the ability of hydrogen atoms to act as H bond acceptors in silane compounds. Computations and ^1H NMR demonstrated a weak interaction between silane and perfluoro-*tert*-butanol.

List of papers

1. Lixu Yang, John Brazier, Scott L. Cockroft* "Measurement of interactions in extended aromatic contacts" in preparation.
2. Lixu Yang, Scott L. Cockroft* "Can Non-polar Hydrogen Atoms Accept Hydrogen bonds?" in preparation.
3. Lixu Yang, Catherine Adam, Gary S. Nichol and Scott L. Cockroft* "How much do van der Waals dispersion forces contribute to molecular recognition in solution?" submitted.

Abbreviations

1D	one dimensional
ADD	acceptor-donor-donor
AFM	atomic force microscopy
Ar	aryl
B3LYP	Becke, three-parameter, Lee-Yang-Parr
BSSE	basis set superposition error
Bu ₃ PO	tri-n-butylphosphine oxide
CCDC	Cambridge crystallographic data centre
CCSD(T)	Coupled-Cluster with Single and Double and Perturbative Triple excitations
COSY	correlation spectroscopy
d	doublet
<i>d</i>	deuterated
DCC	<i>N,N'</i> -Dicyclohexylcarbodiimide
DCM	dichloromethane
DEPT	Distortionless Enhancement by Polarization Transfer
DFT	density functional theory
DMAP	4-Dimethylaminopyridine
DMC	double mutant cycle
DME	Dimethoxyethane
DMSO	Dimethyl sulfoxide
DPPA	Diphenylphosphoryl azide
<i>E</i>	entgegen
EI	electron ionization
ESI	electrospray ionization
ESP	electrostatic surface potential
H bond	hydrogen bond

HF	Hartree-Fock
HMBC	Heteronuclear Multiple Bond Correlation
HSQC	Heteronuclear Single-Quantum Correlation
IR	Infrared
ITC	Isothermal Titration Calorimetry
IUPAC	International Union of Pure and Applied Chemistry
m	multiplet
m.p.	melting point
M06	Minnesota 2006
M ⁻¹	mol/L
MP2	Møller-Plesset perturbation theory
MS	mass spectroscopy
<i>n</i>	normal
NMR	Nuclear magnetic resonance
NOE	nuclear Overhauser effect
PEG	Polyethylene glycol
PFTB	Perfluoro-tert-butanol
QSPR	quantitative structure–property relationships
s	singlet
sat.	saturated
t	triplet
Tf	Trifluoromethanesulfonic
THF	tetrahydrofuran
UV-Vis	Ultraviolet–visible
vdW	van der Waals
Z	zusammen

Contents

Declaration	i
Acknowledgements	ii
Abstract	iii
List of papers	iv
Abbreviations	v
Chapter 1 Non-covalent interactions	1
1.1 General classes of non-covalent interactions.....	1
1.2 Methods for measuring non-covalent interactions	5
1.2.1 Supramolecular complexes	6
1.2.2 Folding molecules	7
1.2.3 Other methods for probing non-covalent interactions	10
1.2.4 Comparison of methods for measuring non-covalent interactions	10
1.3 Solvent effects on non-covalent interactions	11
1.4 Dispersion interaction theory.....	13
1.5 Dispersion in alkanes.....	15
1.5.1 Experimental and computational studies of dispersion interactions in alkanes.....	15
1.5.3 Solvent competition in dispersion interactions in alkanes	20
1.6 Dispersion in aromatic interactions	23
1.6.1 Computational studies of aromatic stacking interactions.....	24
1.6.2 Experimental study of aromatic stacking interactions in the gas-phase	29
1.6.3 Experimental study of aromatic stacking interactions in solution	31
1.6.4 Aromatic CH \cdots π interactions	38
1.7 Summary.....	41
References	42
Chapter 2 Measurement of interactions in extended aromatic contacts	47
2.1 Introduction	47
2.2 Methodology and initial project design	48
2.3 Synthesis and evolution of the complex design.....	52
2.4 Results and Discussion	64
2.4.1 Dilution experiments.....	64
2.4.2 Complex conformation analysis.....	68
2.4.3 Physicochemical parameters for analysing aromatic interactions	69
2.4.4 Binding studies.....	71
2.5 Conclusion.....	81
2.6 Experimental Section.....	81

References	101
Chapter 3 Solvent effects on alkyl dispersion interactions.....	103
3.1 Introduction	103
3.2 Project design and methodology.....	104
3.3 Synthesis	107
3.4 Results and Discussion	108
3.4.1 Structure determination	108
3.4.2 Solvent studies	110
3.4.3 Enthalpy and entropy determination	120
3.4.4 Computation studies.....	123
3.5 Conclusion	124
3.6 Experimental Section.....	125
References	138
Chapter 4 Solvent effects on edge-to-face aromatic interactions.....	140
4.1 Introduction	140
4.2 Project Design and Synthesis	141
4.3 Results and Discussion	143
4.4 Conclusion and Future Work	150
4.5 Experimental Section.....	150
References	152
Chapter 5 Halogen bonding in solution	153
5.1 Introduction	153
5.2 Iodide-aromatic complexes.....	154
5.3 Molecular torsion balances	156
5.4 Conclusion and Future work.....	159
5.5 Experimental Section.....	159
References	163
Chapter 6 Hydrogen as a Hydrogen Bond Acceptor	164
6.1 Introduction	164
6.2 Design and Aims.....	166
6.3 Results and Discussion	168
6.4 Conclusion and Future work.....	170
6.5 Experimental Section.....	170
References	172

Chapter 1 Non-covalent interactions

Abstract

This chapter gives general overview of non-covalent interactions. It introduces different classes of non-covalent interactions and goes on to present popular models and methods for quantifying these weak interactions. The chapter concludes with a focus on dispersion interactions in gas phase and in solution.

1.1 General classes of non-covalent interactions

The covalent bond, as has long been known by chemists, involves two atoms sharing a pair of electrons.¹ Since covalent bonds commonly have energies of hundreds of kJmol^{-1} , breaking a bond always requires large energy input either from an external energy source or from energy differences in other bonds that might be broken or formed in a chemical reaction. In contrast to strong covalent bonds, non-covalent interactions are relatively weak, and do not involve fully overlapping valence orbitals. Although weak, non-covalent interactions are fundamental parts in biological systems. Taking advantage of the non-bonded nature of interactions, which are normally reversible and easy to control, chemists are keen to exploit non-covalent interactions in building blocks for materials², molecular recognition³ and in molecular machines⁴. The classification of non-covalent interaction is sometimes indistinct and classification boundaries are often blurred, or overlapping. Here we introduce several typical types of non-covalent interactions, including ionic interactions, hydrogen bonds (H bonds), halogen bonds, the hydrophobic effect, Van der Waals forces and aromatic interactions (Fig 1.1).

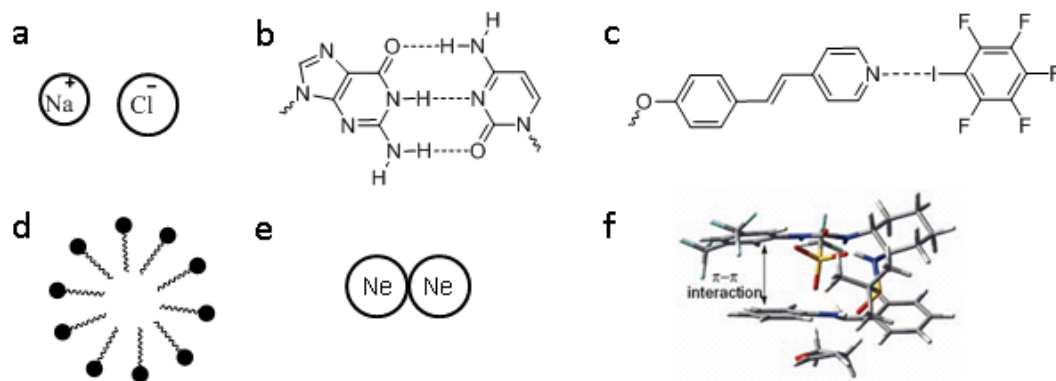


Figure 1.1. a) Ionic interaction in NaCl.⁵ b) H bond in a base pair in DNA.⁶ c) Halogen bond in liquid crystals.⁷ d) Hydrophobic assembly of a micelle.⁸ e) Van der Waals interaction between Ne atoms.⁹ f) Aromatic interaction in a catalyst.¹⁰

Ionic interactions occur between two charged elements, such as that occurring in salts like NaCl (Fig 1.1a). These types of interactions are considerably strong and sometimes comparable to the strength of a covalent bond. These types of interaction play an important role in drug and gene therapy, ion transport through membranes, artificial sensors, as well as in commercial and industrial applications such as those encountered in batteries.⁵

H bonds (Fig 1.1b) are perhaps the most well-recognised non-covalent interaction that chemists make use of and are defined by IUPAC as "*attractive interaction between a hydrogen atom from a molecule or a molecular fragment X–H in which X is more electronegative than H, and an atom or a group of atoms in the same or a different molecule, in which there is evidence of bond formation*".¹¹ H bonds are of moderate strength, for example the cooperative effect of four simultaneous H-bonds can have an energy of 71 kJ mol^{-1} .¹² Conventional H bonds take place between donors, such as halogen-H, NH, OH and SH, and acceptors such as N, O, S, and

aromatics. Recent studies have also considered non-conventional H bond interactions such as the dihydrogen bond, where hydride-like hydrogen atoms may act as H-bond acceptors (this is discussed in more detail in Chapter 6).¹³

Unlike the heavily studied H bond, halogen bonding interactions have only attracted the interests of scientists within the last decade (Fig 1.1c). Halogen bonds are very similar to H-bonds. Halogens with electron deficient sites, which are known as σ holes,¹⁴ act as halogen-bond donors, while halogen-bond acceptors are the same as those found in H-bond interactions. Halogen-bond donor ability increases in the order of $\text{Cl} < \text{Br} < \text{I}$, while F does not possess a significant σ hole (Fig 1.2). Although halogen bonds have only been studied for a short period of time and many properties remain unclear, they are now frequently employed in drug designs and supramolecular chemistry.¹⁵⁻¹⁸

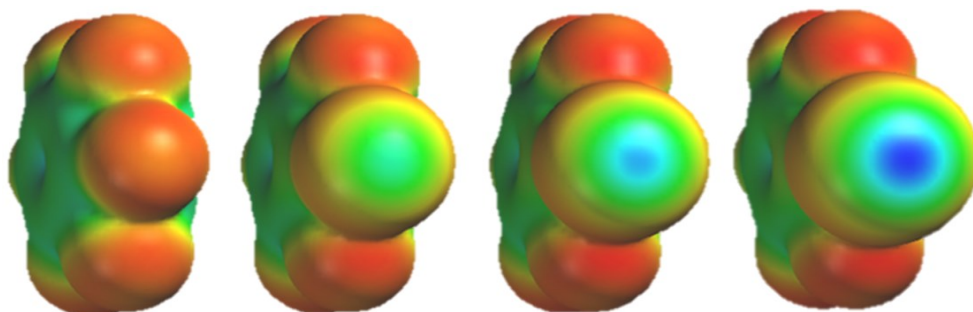


Figure 1.2. Electrostatic surface potentials (ESP) of hexafluorobenzene, chloropentafluorobenzene, bromopentafluorobenzene, iodopentafluorobenzene. ESPs are computed at the DFT/B3LYP/6-31G* level using *Spartan*. Colours are scaled from red to blue (-100 kJ mol^{-1} to $+100 \text{ kJ mol}^{-1}$).

The solvophobic effect describes the tendency of poorly solvated molecules to aggregate in solvents that form significant cohesive interactions (Fig 1.1d). The

hydrophobic effect is a special case of the solvophobic effect that arises due to the formation of extended networks of H-bonded water molecules. The view that hydrophobic effects are entropically driven is a deeply rooted point of view, but it is not true in all cases. Solvation free energy is attributed to entropy in small molecules, but controlled by enthalpy in larger surfaces.¹⁹ Enthalpic effects also appear to manifest themselves in binding to small cavities.²⁰⁻²² Solvophobic effects are hard to dissect from other effects, such as van der Waals dispersion forces because of their non-specificity, and because both classes of interaction are governed by differences in surface area contact. Though the definition is blurred and the origin is not always clear, solvophobic effects are often employed in constructing foldamers.²³

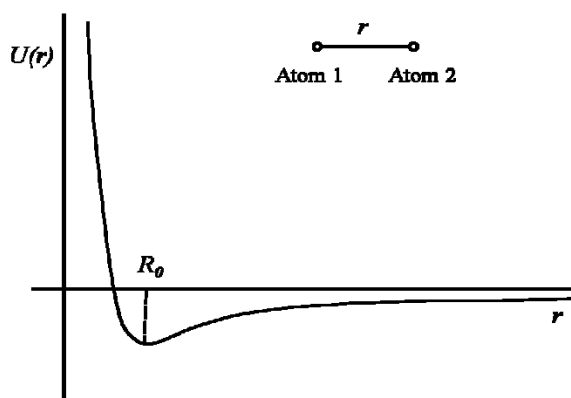


Figure 1.3. The Lennard-Jones potential as a function of distance.²⁴

Van der Waals forces consist of both repulsive and attractive forces between molecules (Fig 1.1e). As shown in Fig 1.3, at closer separations, repulsive interactions dominate, which falls off rapidly as the minimum potential energy reaches equilibrium separation, R_0 . Beyond this separation the attractive components become less favourable as distance increases. Dispersion interactions are the major contributor to the long-range part of the potential energy profile, and are discussed in

detail in the later section of this chapter. Dispersion forces are often loosely called van der Waals forces. It is generally regarded as being the weakest non-covalent interaction in solution, but experimental data is limited.

Aromatic interactions (Fig 1.1f) refer to non-covalent interaction between aromatics, which are often employed in chemical reactions, supramolecular chemistry and biological systems.²⁵⁻³¹ This kind of interaction will be discussed in more detail later in this Chapter, and in Chapters 2 and 4.

1.2 Methods for measuring non-covalent interactions

While covalent bond energies can be studied easily by chemical reactions, the weakness of non-covalent bonds makes their measurement much more challenging. Nonetheless, two main methods for the measurement of non-covalent interactions exist.

1.2.1 Supramolecular complexes

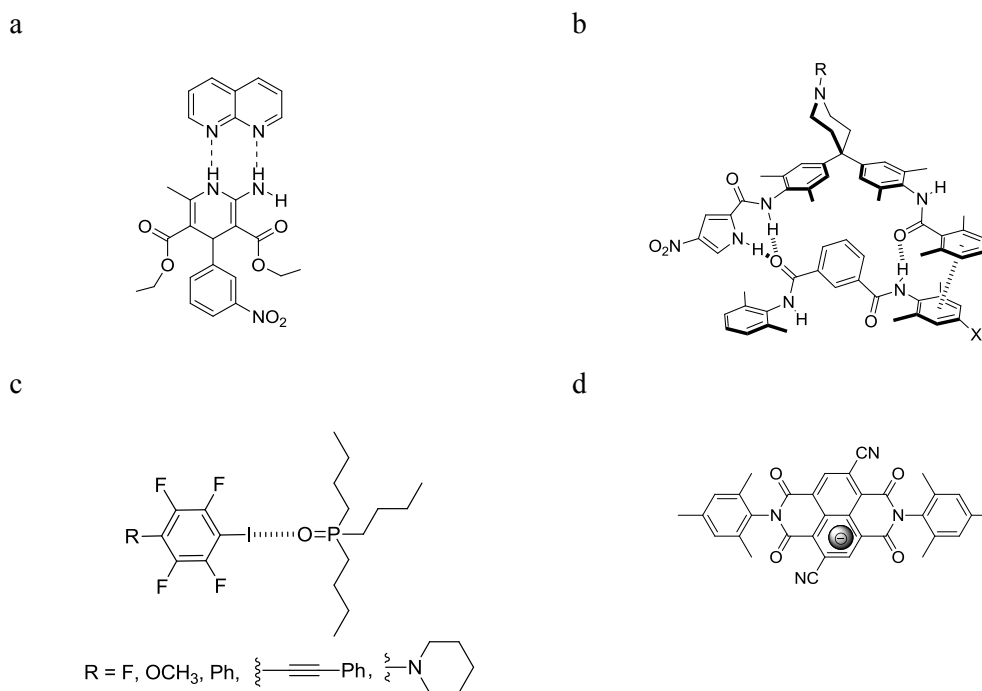


Figure 1.4. Supramolecular complexes used for the study of non-covalent interactions.

Supramolecular complexes are quite convenient in the systematic study of non-covalent interactions, since each half of a complex can be varied to generate multiple host-guest combinations (Fig 1.4). Binding constants of these complexes can be determined by titration experiments using modern techniques such as ^1H NMR, UV-vis spectroscopy, and ITC.³²

Fig 1.4a shows a double H-bond complex explored by Zimmerman.³³ This AA-DD architecture avoids repulsive secondary electrostatic interactions between adjacent H bonds, resulting in a stable complex with a binding constant $K = 260 \text{ M}^{-1}$. Inspired by this discovery, others^{12,34-35} adapted variations of these complexes to explore larger systems with multiple H-bonds, for example AAA-DDD and AAAA-DDDD systems, in which even higher binding energies were observed. Zipper

complexes³⁶⁻³⁷ designed by Hunter, also took advantage of multiple H bonds to offer a suitable geometry for studying aromatic interactions (Fig 1.4b). When replacing the aromatic group with a CX₃ group, these types of complexes were also used to study halogen- π interactions.³⁸ Most organic iodides are weak halogen-bond donors, however, binding to a strong acceptor such as tri-*n*-butylphosphine oxide (Bu₃PO) enabled investigation of halogen bond interactions in solution (Fig 1.4c).³⁹ Meanwhile, modified naphthalenediimides with highly electron-deficient cores accommodate anion binding, facilitating analysis of anion- π interactions (Fig 1.4d).⁴⁰ Other electron-poor aromatics and anion complexes have also been used to target anion- π interactions.⁴¹

1.2.2 Folding molecules

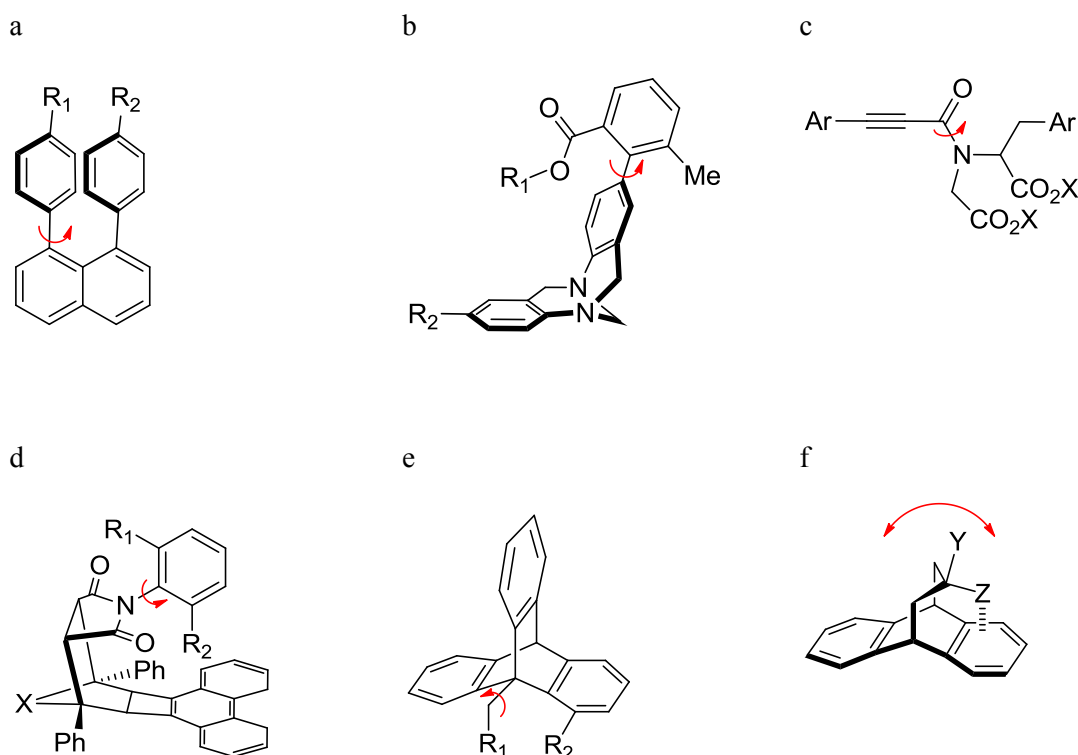


Figure 1.5. Folding molecules used to examine non-covalent interactions.

Two possible approaches exist for extracting thermodynamic information on non-covalent interactions from folding molecules or rotamers. The most popular approach involves studying conformer populations at equilibrium (as discussed with more examples below), while another involves measurement of the barrier to rotation about a hindered bond. For example, the early exploration of the barrier to rotation in 1,8-diarylbiphenylenes provided a tool for studying parallel-offset aromatic interactions (Fig 1.5a).⁴²⁻⁴³ Although the rotational barrier cannot be directly determined from a single ¹H NMR spectrum at room temperature, it can be determined by using variable temperature NMR. Similar approaches have been used by Cozzi and co-workers to examine other types of aromatic interactions using barriers to rotation.⁴⁴

As mentioned above, many so-called folding molecules feature a slowly rotating bond, which results in the generation of two conformations where the equilibrium population depends on the molecular contacts and the solvent environment in which the balance is placed. Thus, the preference for one conformer over another allows intramolecular interactions and solvent effects to be measured. Interaction free energies then can be obtained by ¹H NMR spectroscopy and calculated as follows:

$$\Delta G = -RT \ln (c_{\text{folded}}/c_{\text{unfolded}}) \quad \text{Equation 1.1}$$

In 1994, Wilcox introduced a particularly elegantly designed molecular balance, which has since become known as the Wilcox balance. This design involved introducing substituents on a biphenyl moiety to increase the rotational barrier, resulting in the observation of two conformations at room temperature (Fig 1.5b).⁴⁵ In

the following decades, use of these balances has assisted in the study of edge-to-face aromatic interactions,⁴⁶ CH- π ,⁴⁷⁻⁴⁸ and orthogonal dipolar interactions.⁴⁹⁻⁵¹

Sterically hindered amides have found application in molecular balances developed by Gellman (Fig 1.5c) and Shimizu (Fig 1.5d). Two ester groups improve solubility of Gellman's balances, which facilitated its use in probing aromatic stacking interactions in aqueous solution.⁵² In contrast, Shimizu's balances do not possess an aliphatic linker, and as a result provided a more rigid framework suitable for examining aromatic stacking⁵³ and deuterium isotope effects in CH/D- π interactions.⁵⁴⁻⁵⁵

Triptycenes (Fig 1.5e) synthesised by Òki and Gung operate based on their slowly interconverting *syn* and *anti*-conformers. Since the R1 and R2 groups are easily varied, these types of balance have been employed in various areas such as in the study of CH \cdots O, CH \cdots π , O \cdots π and aromatic stacking interactions.⁵⁶⁻⁵⁷

Other interesting folding molecules have been developed by Motherwell.⁵⁸ Unlike balances involving rotation of a single bond, this balance adopts a flipping movement, and equilibrium constants were derived from averaged coupling constants relative to control compounds (Fig 1.5f).

The above provides a simple overview of some of the most important classes of folding molecules employed by chemists to quantify non-covalent interactions, and other examples are discussed in a recent tutorial review.⁵⁷

1.2.3 Other methods for probing non-covalent interactions

Chemical reactions provide another option for the quantification of non-covalent interactions. Wheeler, Houk and others have applied Diels-Alder cycloaddition reactions for the study of aromatic interactions as is discussed in greater detail later in this chapter.⁵⁹ A similar approach has also been utilised based on examination of the differences in the standard molar enthalpies of formation between 1-phenylnaphthalenes and 1,8-diphenylnaphthalenes, to enable a gas-phase measurement of aromatic stacking interactions.⁶⁰

Alternatively, mechanical measurements provide a direct approach for measuring the strength of non-covalent interactions. To illustrate just one example, Venkataraman and co-workers⁶¹ have used atomic force microscopy (AFM) to quantify Van der Waals forces between Au particle and pyridine molecules at the single-molecule level. Finally, mass spectrometry has been employed as a useful tool for determining binding strength.⁶²⁻⁶³

1.2.4 Comparison of methods for measuring non-covalent interactions

In summary, each of the methods introduced above have their own advantages and disadvantages for the measurement of non-covalent interactions. Supramolecular complexes are quite flexible and facilitate combinatorial examination of interactions, but require tedious NMR titration work. Normally, these supramolecular complexes employ H bond motifs, which mean that competitive H bond solvents cannot be examined because they disrupt the structure of the complexes.⁶⁴ Meanwhile, folding molecules are harder to design and syntheses when special structural criteria need to

be satisfied for a particular investigation. However, folding molecules present the advantage of allowing data to be collected rapidly in a range of solvents once they have been synthesised.

1.3 Solvent effects on non-covalent interactions

When dealing with non-covalent interactions in solution, it is necessary to consider solvent competition. Hunter proposed a solvation model to rationalise complicated solvent effects. In the theory, all solvents can be treated simply by considering their H bond donor and acceptor abilities, while assuming that van der Waals dispersion interactions cancel out for a rearrangement of molecular surfaces in solution.⁶⁵ Non-covalent interactions in solution now can be considered as an equilibrium between solute-solute, solute-solvent and solvent-solvent interactions as shown in Fig 1.6. Hence a given interaction can be expressed by the equation:

$$\begin{aligned}\Delta\Delta G &= (\alpha\beta_s + \alpha_s\beta) - (\alpha\beta + \alpha_s\beta_s) + 6 \text{ kJ mol}^{-1} \\ &= -(\alpha - \alpha_s)(\beta - \beta_s) + 6 \text{ kJ mol}^{-1}\end{aligned}\quad \text{Equation 1.2}$$

Where α and β represent the solute's H-bond donor and acceptor constants respectively, and α_s and β_s represent the solvent's H-bond donor and acceptor constants respectively. α and β of most common solvents can be determined from experiment or by calculation, and these constants are listed in the literature.⁶⁶ The value of 6 kJ mol^{-1} is an estimate of the entropic cost associated with biomolecular association in solution.⁶⁵

In this point of view, solvophobic effects can be understood as arising from strong

solvent-solvent interactions outcompeting solute-solvent interactions, thereby leading the association of apolar solutes, even though the direct interactions between the solutes may be very weak.

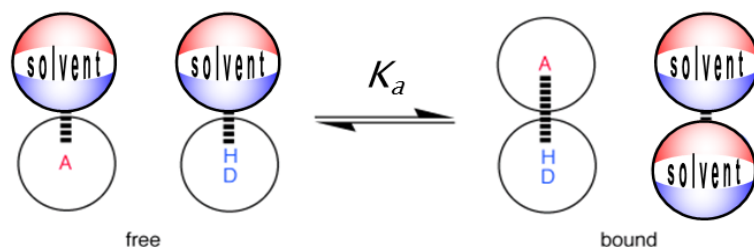


Figure 1.6. Hunter's solvent competition model.⁶⁶

Hunter's model (Fig 1.6) has been shown to be applicable to solvent effects on H-bonds, and is also useful for rationalising the behaviour of binary solvent system, where solutes may be preferentially solvated.⁶⁷⁻⁶⁸ When the model is applied in reverse, α_s and β_s values for non-polar solvents can be derived that are otherwise hard to obtain by conventional methods.⁶⁹ Furthermore, Cockroft and Hunter succeeded in applying this model to explain the discrepancy between the conclusions reached by Wilcox and Diederich's groups on aromatic edge-to-face interactions.⁷⁰⁻⁷¹

Although this solvent competition model is quite successful in predicting non-covalent interactions in solution, it is a very simple model based on just H-bond properties, which only consider electrostatic interactions. When other properties such as dispersion interactions become important relative to electrostatic interactions, experimental free interaction energies are expected to deviate from the predictions.

1.4 Dispersion interaction theory

The dispersion interaction, also known as London forces, is an attractive interaction between mutually induced, fluctuating dipoles/multipoles (in contrast to those occurring between permanent dipoles/multipoles).⁷² An example, a transient electric fluctuation generates an instantaneous dipole in one atom, which exerts influence on the neighbouring atom, which distorts in response to form a new dipole. When these two dipoles attract each other, this is referred to as dispersion (Fig 1.7).

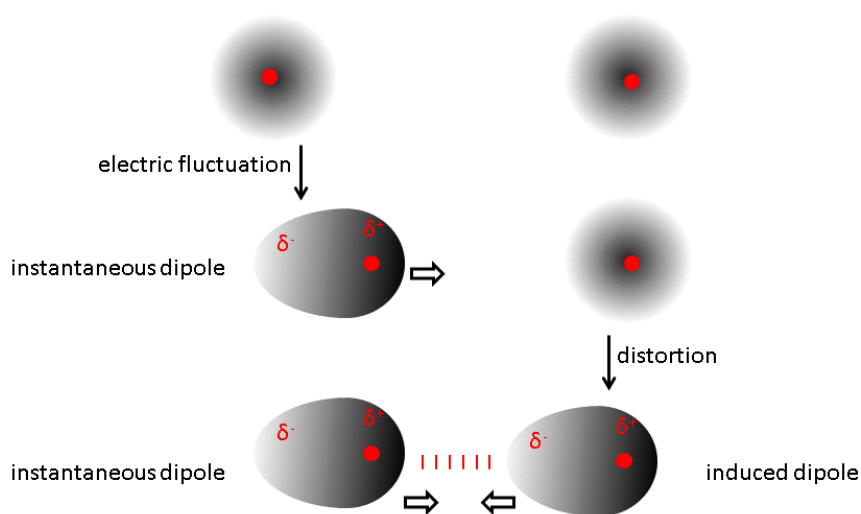


Figure 1.7. Representative of dispersion interaction

Dispersion interactions can be defined by quantum mechanical theory by the equation:

$$E_{ij} = \frac{B_{ij}}{r_{ij}^6} \quad \text{Equation 1.3}$$

$$B_{ij} = c \frac{\alpha_i \alpha_j}{\sqrt{\alpha_i / N_i} + \sqrt{\alpha_j / N_j}} \quad \text{Equation 1.4}$$

Where α is the polarisability, N is number of valence electrons, r is the distance

between two atoms. According to the definition formula, dispersion effects depend on the polarisability α , of the two interacting moieties. Generally speaking, the larger the molecular surfaces, the easier it is for the electron cloud to be distorted, and as a result, the polarisability is higher. For comparison, however, polarisability per unit surface area may be more appropriate (Table 1.1).⁶⁶

Table 1.1. Relative values of dispersion interaction per unit surface area of contact for some atoms from literature.⁶⁶

	C	N	O	F	P	S	Cl
C	1.0	1.0	1.1	1.1	1.5	1.4	1.1
N	1.0	0.9	1.0	1.1	1.5	1.3	1.1
O	1.1	1.0	1.0	1.1	1.6	1.4	1.2
F	1.1	1.1	1.1	1.1	1.6	1.5	1.3
P	1.5	1.5	1.6	1.6	2.1	1.8	1.5
S	1.4	1.3	1.4	1.5	1.8	1.6	1.4
Cl	1.1	1.1	1.2	1.3	1.5	1.4	1.2

With modern techniques, computational chemists are keen to analyse non-covalent interactions using quantum mechanical models. While accurate dispersion interactions are well estimated by large-basis-set post Hartree-Fock methods,⁷³ the original density functional theory (DFT) only considers electrostatics and poorly predicts dispersion dimers. Considering that the former method is computationally expensive, DFT methods capable of considering dispersion forces are emerging, such as dispersion-corrected DFT, parameterised functionals and dispersion-correcting potential.⁷⁴ Although lots of effort has been spent on correctly calculating dispersion, different methods give different results. One should examine the methods carefully with respect to experimental data before drawing conclusions.

1.5 Dispersion in alkanes

1.5.1 Experimental and computational studies of dispersion interactions in alkanes

Alkanes lack the ability to make polar cohesive interactions such as H bonds, and therefore any adhesion between molecules must be via dispersion forces. The cumulative addition of dispersion forces in alkanes is reflected in the boiling points of alkanes (Table 1.2). As the length of linear alkanes increase, boiling points increase dramatically, which means that intermolecular dispersion interactions must be responsible. Compared to linear alkanes, boiling points of corresponding cycloalkanes are higher by at least 9 °C. This is attributed to larger intermolecular surface contact for cycloalkanes, which arises from closer packing in the liquid state.

Table 1.2. Boiling points of linear and cyclo alkanes.⁷⁵

Linear alkane	Boiling point [°C]	Cycloalkane	Boiling point [°C]
Methane	-162	-	-
Ethane	- 89	-	-
<i>n</i> -Propane	- 42	cyclopropane	- 33
<i>n</i> -Butane	0	cyclobutane	13
<i>n</i> -Pentane	36	cyclopentane	49
<i>n</i> -Hexane	69	cyclohexane	81
<i>n</i> -Heptane	98	cycloheptane	118
<i>n</i> -Octane	126	cyclooctane	149
<i>n</i> -Nonane	151	cyclononane	178
<i>n</i> -Decane	174	cyclodecane	201

The patterns in the boiling points of alkanes illustrate how large the effects of dispersion interactions can be. Dispersion interactions are hard to measure on the molecular level. When Hunter *et al*⁶⁹ were investigating H-bonding properties in non-polar solvents using a H-bond donor and acceptor as a probe, they found that the experimental results for alkanes were larger than those calculated using the α/β model. This implied that dispersion in alkanes cannot be ignored, because the α/β model only considers electrostatic effects. Although, the precise contribution arising from dispersion forces was not determined in the original investigation, a more recent study of evaporation in alkanes revealed that van der Waals interactions between chains were a linear function of molecular surface area and, thus rearrangement of surfaces in contact in molecular recognition events occurring in solution should be associated by a small change in dispersion forces.⁷⁶

Alkanes, although simple, are not easy to fully simulate *in silico*. Tsuzuki's calculations revealed that interaction energies between longer *n*-alkanes are large; the intermolecular interaction energy for the *n*-hexane dimer was predicted to be $-19.2 \text{ kJ mol}^{-1}$ using the MP2 method, which is comparable to that of the H-bonded water dimer.⁷⁷ Later, Tsuzuki and co-workers compared the interaction energies from different methods and basis sets, and achieved similar results. With these values, they obtained a linear relationship between dimer interaction energies and the number of carbon atoms (Fig 1.8).⁷⁸

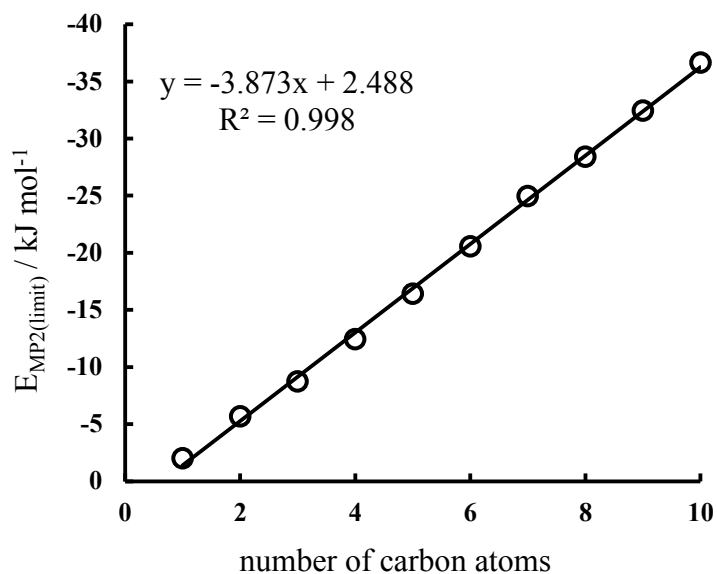


Figure 1.8. Estimated interaction energy of alkane dimers at MP2 level against number of C atoms.⁷⁸

Figure is remade using kJ mol^{-1} unit.

More recently, calculations have been performed on even longer *n*-alkanes. In order to reduce the computational cost of the MP2 method, Ferrighi and co-workers⁷⁹ evaluated the interaction energies of alkanes up to 10 carbons with the DFT/MGGA-M06-L method. The compromise between accuracy and cost make this method attractive for calculations on large molecules. $-45.23 \text{ kJ mol}^{-1}$ was reported for the decane dimer.

The claim that strong dispersion forces arise between long alkanes due to multiple contacts is also supported by the very recent work of Shaik and Alvarez.⁸⁰ They carried out a full computation on linear alkanes, branched alkanes and polyhedranes at the MP2 level, and compared the results with experimental melting points and crystal structures. The “dihydrogen contact”, as they describe it in their work, was calculated as being worth 1 kJ mol^{-1} per $\text{H}\cdots\text{H}$ interaction, and the dissociation

energy for dodecahedrane reached $-12.38 \text{ kJ mol}^{-1}$ (Fig 1.9).

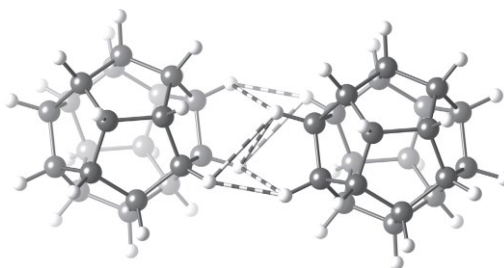


Figure 1.9. Structure of dodecahedrane dimers.⁸⁰

The increased stability of branched alkanes compared to their unbranched equivalents can also be attributed to dispersion forces (Fig 1.10). In 1956, Pitzer and Catalano⁸¹ found isobutane was 5.0 kJ mol^{-1} more stable than *n*-butane, and neopentane was 7.5 kJ mol^{-1} more stable than *n*-pentane, using Slater and Kirkwood's dispersion formula. With the assistance of modern computation techniques, Wodrich *et al.* demonstrated that the stabilisation energy is worth 9.54 to $11.84 \text{ kJ mol}^{-1}$ per alkyl-alkyl branch contact using a bond-separating reaction.⁸² Furthermore, the alkane isomerisation energy, which is another indicator for this branching effect, was reported as at least 2.5 kJ mol^{-1} per alkyl-alkyl branch contact.⁸³

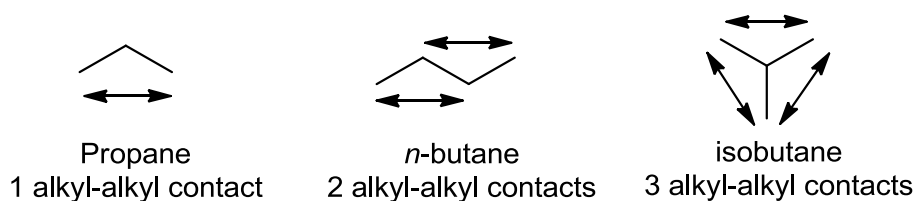


Figure 1.10. Intramolecular alkyl-alkyl contacts in some alkanes.

Similar types of intramolecular alkyl-alkyl dispersion forces have been proposed as significantly stabilising the longest known C-C bond.⁸⁴⁻⁸⁵ The C-C bond in ethane is 1.533 Å, which is typical for the unstrained C-C bond.⁷⁵ However, the cumulative effect of multiple H···H dispersion-mediated contacts allows the C-C length in compound **1** to be elongated to 1.704 Å despite the expected steric repulsion (Fig 1.11). Changing from triamantane to tetramantane (compound **2**) expands the dispersion contact area and pushes the C-C length boundary to 1.71 Å. The role of dispersion was confirmed by DFT calculations; only DFT calculations including dispersion corrections provided structures close to the X-ray crystal structures, while traditional DFT methods that do not take dispersion interactions were unsuccessful. It is worthy of note that these highly hindered diamondoid compounds prevent interpenetration of solvents and gases; hence dispersion forces between H···H contacts are undisturbed by competitive effects.

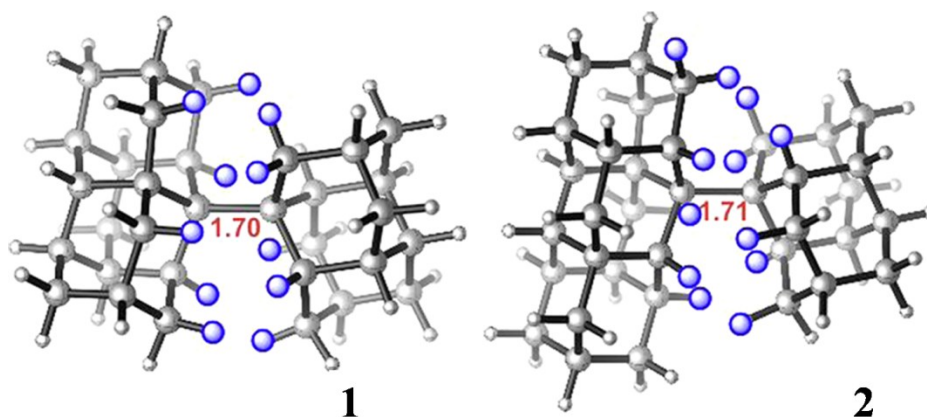


Figure 1.11. Structure of compound **1** and **2**.⁸⁵

The situation where dispersion interactions are able to overcome steric repulsion is verified in another case. Compound **3** is very unstable, with a dissociation energy as low as $-38.0 \text{ kJ mol}^{-1}$. In contrast, compound **4**, which shares the core structure of **3**,

has a melting point as high as 214 °C and a dissociation energy of + 57.3 kJ mol⁻¹, some 95.0 kJ mol⁻¹ higher than that of compound **3**.⁸⁶ The enhanced stabilisation is owed to twelve *t*-butyl groups contributing dozens of H···H contacts (Fig 1.12).

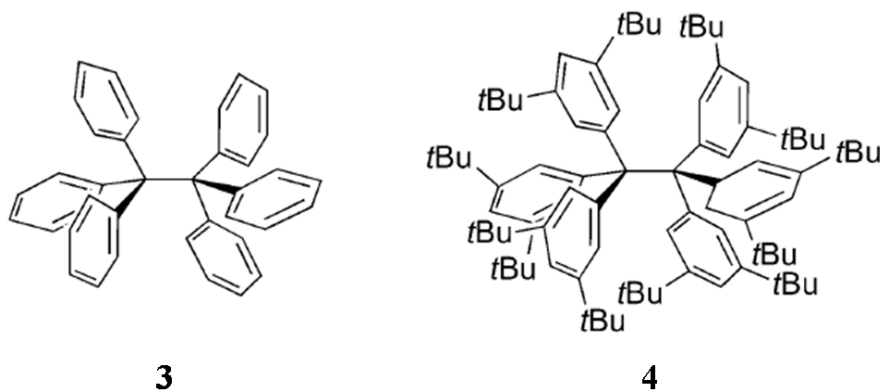


Figure 1.12. Structure of compounds **3** and **4**.⁸⁶

1.5.3 Solvent competition in dispersion interactions in alkanes

It has been shown that in the ideal condition where alkanes contain enforced intramolecular contacts, dispersion forces can be very strong. However, these intramolecular situations may be the exceptions rather than the rules, since many parts of chemical and biological systems are exposed to multiple competitive solvent molecules.

It is widely known that alkanes prefer to stick together in aqueous solution, while Rebek's group discovered that alkanes tend to maximise the dispersion interaction inside a molecular capsule.⁸⁷ More than 30 years ago, Abraham⁸⁸ showed that solvation of *n*-alkanes by hexane is preferred over solvation by water by 3.85 kJ mol⁻¹ per CH₂. More recently, Wu and Prausnitz⁸⁹ published their result on the interaction of alkanes in water. Interpretation of these results involves consideration

of the H-bond network of water, van der Waals interactions between the alkanes and water, and van der Waals interactions between the alkanes. The hydrophobic potential of alkanes was calculated from free energies of solvation, which was derived from Henry's constant. As shown in Fig 1.13, comparison between hydrophobic potential and the vdW energy indicated that when two methane molecules were in contact in water, the maximum vdW energy between methane was only half of the hydrophobic energy. In other words, the vdW energy has been masked by overwhelming hydrophobic effects, at least for short alkanes.

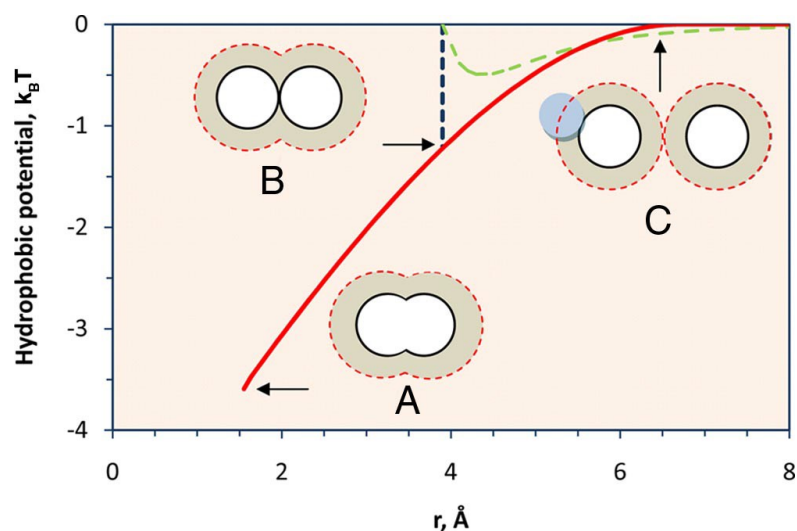


Figure 1.13. The red solid line corresponds to the hydrophobic potential between two methane molecules in water, against their distance. Two methane molecules are separated at C–C bond length ($r = 1.533 \text{ \AA}$) (A), at contact (B) and have non-overlapping solvation shells (C). The red dotted lines are the outer boundary of the solvation shell. The green dashed line is the Lennard–Jones potential between two isolated methane molecules. The black dotted line shows position (B) when the methane molecules are at contact.⁸⁹

Meanwhile Ray and Akhremitchev *et al*⁹⁰ successfully measured interactions between linear alkanes (decane, dodecane, tetradecane, hexadecane and octadecane) in water at the single-molecule level. Alkanes were bonded to either the substrate or

the AFM probe via PEG linkers, which also helped the alkanes to dissolve in water (Fig 1.14). The interaction energy was measured by the rupture force method, and the surface energy density was measured to be around $21 \text{ kJ mol}^{-1}\text{nm}^{-2}$, which was close to the value used in computer simulations of hydrophobic interactions ($17 \text{ kJ mol}^{-1}\text{nm}^{-2}$). Although it isn't discussed in this study, the small difference ($4 \text{ kJ mol}^{-1}\text{nm}^{-2}$) might be attributed to dispersion interactions, which are apparently weakened by water competition.

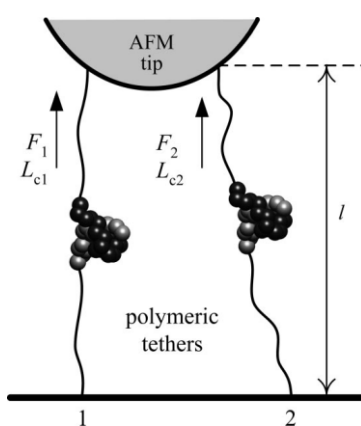


Figure 1.14. The set-up of AFM experiments. The soft black line is PEG, the ball models represent alkane chains.⁹⁰

While the delicate H-bond network and resulting hydrophobic effects on alkane association has been relatively well studied, alkane interactions in non-aqueous solvents are less studied. Solvation energies of alkanes in 16 organic solvents showed that alkanes are more easily solvated by non-polar solvents than polar solvents.⁸⁸ This work indicated a stronger contribution of solvent-solute interactions than alkane-alkane interactions in non-polar solvents. Research conducted to date has shown that dispersion interactions between alkanes in solution are frequently overshadowed by solvophobic effects.

1.6 Dispersion in aromatic interactions

Aromatic interactions can be classified into four geometric classes (Fig 1.15). Various different contributing factors have been proposed as governing the strength of aromatic interactions, including electrostatics, dispersion and solvophobic effects. The understanding of these contributors is fundamental to utilise aromatic interactions in applications of molecular assembly and the operation of molecular machines. Since stacked (sandwich and parallel-displaced) contacts have the largest surface contact areas, these types of interactions are likely to have the largest dispersion components.

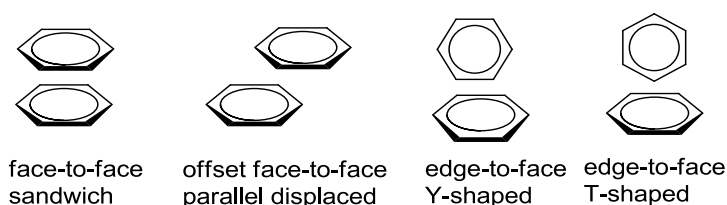


Figure 1.15. Diagrammatic pictures of arene-arene interaction geometries.

It has been argued whether ‘aromaticity’ really matters for dispersion interactions.⁹¹ Aromaticity is often known to stabilize a conjugated cyclic system through delocalisation of π electrons. Intuitively, the delocalisation displays a ‘soft’ π -electron cloud, which should be easily distortable. As softness is related to polarisability, one would think that dispersion forces in these types of systems would be significant. However, much controversy surrounds the study of aromatic interactions as detailed below.

1.6.1 Computational studies of aromatic stacking interactions

Theoretical decomposition of aromatic interaction energies in the gas-phase is often classified into four contributors: electrostatic, dispersion, induction and exchange repulsion. As briefly introduced previously, computations using DFT methods are frequently employed in studies of non-covalent interactions. However B3LYP is unable to properly characterise the medium-range correlation energies involved in van der Waals interactions. One approach to overcoming this limitation is to use highly computationally intensive methods such as benchmark coupled-cluster CCSD(T) level,²⁹ or second-order Møller-Plesset perturbation theory (MP2) calculations with large basis sets.⁹² Truhlar⁹³ invented the M06-class functionals as an alternative approach for modelling van der Waals interactions within the framework of DFT. For example, M06-2X, M05-2X, M06-HF, M06 and M06-L functionals have been suggested as being suitable for modelling non-covalent interactions.

Substituted benzene dimers have been widely studied by computation and experiment as recently reviewed by Wheeler.⁹⁴ Calculations by Sinnokrot and Sherrill⁹⁵ suggested that all monosubstituted benzene – benzene dimers were more stable than the benzene dimer. They indicated that electrostatic, dispersion, induction and exchange repulsion were all important to binding. A subsequent study revealed that substituted effects were additive in sandwich dimers.⁹⁶ Later, Ringer and Sherrill performed calculation on polysubstituted benzene dimers using counterpoise-corrected MP2 method. A very scattered plot of interaction energies against the sum of the Hammett constants of the substituents ($\Sigma\sigma_m$) suggested that electrostatic effects were not dominant. An extreme demonstration of this effect was

provided by the very electron-rich hexaaminobenzene ($C(NH_2)_6$), and the very electron-deficient 1,3,5-tricyano and hexafluoro-substituted benzenes ($C_6H_3(CN)_3$, C_6F_6), which shared similar interaction energies with benzene despite dramatic variation in their electrostatic potentials (Fig 1.16). This computational result has been attributed to major dispersion components,⁹² and even implied that two electron-rich aromatics would display an attractive stacking interaction. More examples on the importance of dispersion are also discussed in Sherrill's recent review.⁹⁷ Later calculations by Kim and co-workers⁹⁸ also agree with Sherrill.

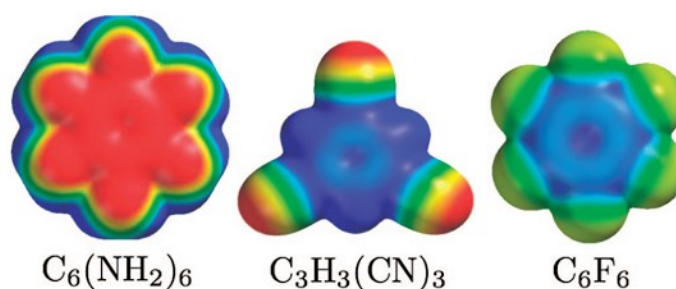


Figure 1.16. ESPs of hexaamino-, 1,3,5-tricyano-, and hexafluoro-substituted benzene calculated at Hartree-Fock/6-31G* level. Red represents negative electrostatic potentials and blue represents positive electrostatic potentials.⁹²

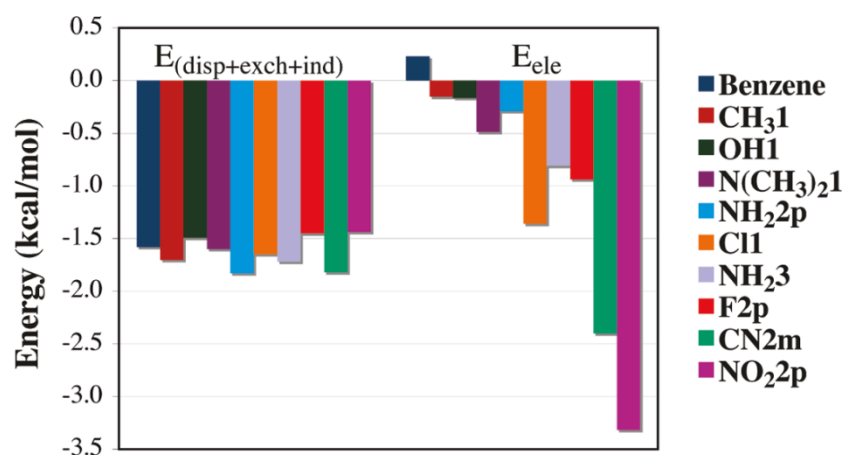


Figure 1.17. Decomposition energy of aromatic interaction for benzene derivatives.⁹⁹

Lewis and co-workers⁹⁹ provided greater insight to the findings of Sherrill. They also found that substituted-benzenes enhanced binding with benzene despite variations in the electrostatic potential surfaces of these molecules. Decomposition of stacking energy into dispersion, exchange, induction and electrostatic components revealed the sum of first three components were constant for all dimers (Fig 1.17). Thus, although dispersion was often the major energetic contributor, the trend in the interaction energies upon variation of substituents was clearly attributable to the electrostatic components. They concluded that both dispersion and electrostatic should be taken into consideration when predicting binding energies.

Azulene possesses a resonant zwitterionic form which possesses a large dipole moment (Fig 1.18a). Surprisingly, calculations found the antiparallel orientation in which the dipoles were opposed was not the most stable dimer. Eleven dimer structures were studied by three methods. The most accurate DFT-D method pointed to the most stable complex (Fig 1.18a) as having an interaction energy of 30.1 kJ mol⁻¹ with a minor dipole-dipole interaction and a dominant dispersion contribution.¹⁰⁰

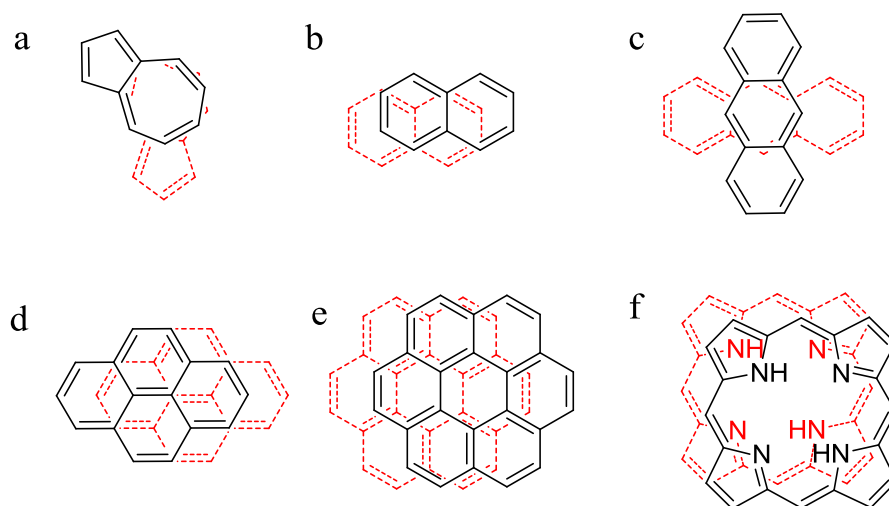


Figure 1.18. Favourable stacking geometries for azulene,¹⁰⁰ naphthalene,¹⁰¹ anthracene,¹⁰¹ pyrene,¹⁰¹ coronene¹⁰²⁻¹⁰³ and porphine.¹⁰⁴

Moving to larger systems, computational chemists have found that the interaction energy between benzene and polycyclic aromatic hydrocarbons exhibited a linear relationship with polarisability.¹⁰⁵ Dispersive effects have been identified as being important components in the parallel-stacked and offset-stacked aromatic geometries, with the dispersive component becoming stronger as the contact surface increased.¹⁰⁶ Nonetheless, calculated polyaromatic dimers^{101-102,104,107} have been shown to prefer parallel-displaced geometries (Fig 1.18b,d,e,f), except for anthracene (Fig 1.18c). The cross configuration adopted by the anthracene dimer was attributed to minimised valence repulsion, which did not overly compromise the dispersion component. Interaction energies between polycyclic aromatics also increased with the number of rings, with dispersion being the major contributor in all cases. A more persuasive example is charged porphyrin dimer, where “dispersion wins over coulomb repulsion”(Fig 1.19).¹⁰⁷⁻¹⁰⁸

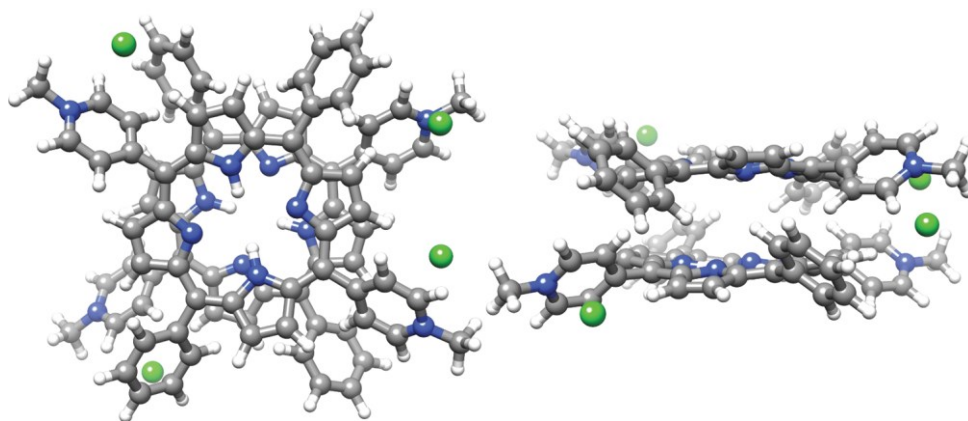


Figure 1.19. Structure of 5,15-diphenyl-10,20-bis[4-(*N*-methyl)pyridinium]porphyrin] dication dimer including counterions. top and side view. White balls represent H atom, grey balls represent C atoms, blue balls represent N atoms and green balls represent Cl⁻ ions.¹⁰⁷

Addressing the question of whether aromaticity is a requirement for enhanced dispersive forces in aromatic stacking interactions, Grimme compared the theoretical interaction energies of a series of saturated ring systems and aromatics. He found that the stacking interaction energy for small ring systems, either saturated or aromatic is virtually indistinguishable, with a special dispersion contribution from the aromatic character of rings only seeming significant when rings contained more than 10-15 carbon atoms.⁹¹ Indeed, Grimme recommends DFT-D3 for dispersion-corrected calculations of aromatic stacking since the method provides sp^2 carbon atoms with a larger dispersion coefficient than sp^3 carbon atoms.¹⁰⁷

Several computational results support Grimme's view that sp^2 and sp^3 carbon atoms behave differently with regards to dispersion interactions; Sherrill's follow-up study found pentacene dimers to be 54 kJ mol⁻¹ more stable than the corresponding saturated ring systems.¹⁰⁹ Janowski and Pulay¹⁰³ studied decalin, perhydrocoronene and their corresponding aromatic dimers at benchmark coupled-cluster CCSD(T) level, and found that σ -stacking energies were less stable than π -stacking energies.

Furthermore, Kim and co-workers¹¹⁰ performed comprehensive investigations on aromatic- π , aliphatic- π and non- π dimers, and he also declared that dispersion is most significant in aromatic- π stacking.

Contrasting with these results, Schreiner *et al.* studied large non-aromatic [*n*]graphane dimers containing between 10 and 97 carbon atoms mainly at the B97D level.¹¹¹ Association energies per carbon atom were found to be 5.0 kJ mol⁻¹, which was similar to that seen in graphene dimers. Meanwhile, Wheeler *et al.*¹¹² found that the delocalisation of π -electrons actually weakens stacking while non-aromatic polycenes exhibit better stacking.

In other words, it has been proposed that aromaticity is not absolutely necessary for stacking interactions, just complementary interatomic contacts. Thus, both Iverson¹¹³ and Wheeler¹¹² have suggested that the term ' π -stacking' should be used with caution. However, there appears to be no theoretical controversy involved in describing these types of interactions as 'aromatic interactions', and it always remains necessary to test, or verify the predictions of theory using experimental data.

1.6.2 Experimental study of aromatic stacking interactions in the gas-phase

From the aspect of experimental research, Santos and co-workers⁶⁰ analysed the formation enthalpies of 1,8-diphenylnaphthalenes and 1-phenylnaphthalenes in the gas-phase (Fig 1.20). The interaction energy increased as either OCH₃ or CHO substituents were added, and energies were additive as the number of substituents increase. The stacking energies correlated well with molecular polarisability tensors

α_{zz} . They concluded that these results gave support to the theoretical dominance of dispersion forces.

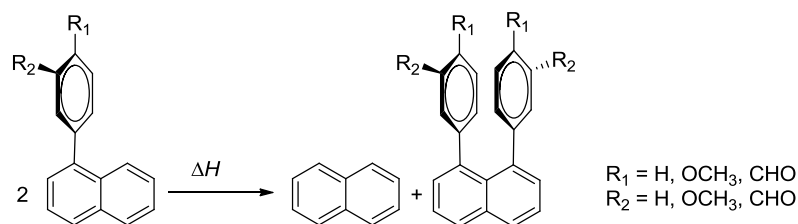


Figure 1.20. Reaction scheme for the formation of 1,8-diphenylnaphthalenes in the gas phase employed in Santos's study.

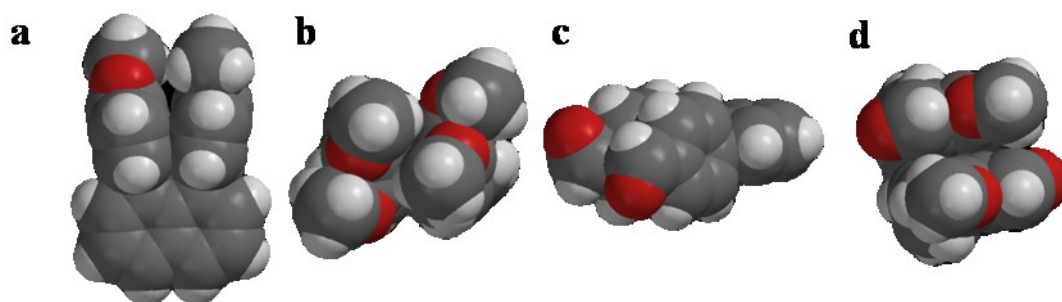


Figure 1. 21. a) $R_1/R_2 = \text{OCH}_3/\text{H}$ front view b) $R_1/R_2 = \text{OCH}_3/\text{OCH}_3$ top view c) $R_1/R_2 = \text{CHO}/\text{H}$ side view d) $R_1/R_2 = \text{OCH}_3/\text{CHO}$ top view.

However, many aspects of these experiments were not discussed that are crucial in constructing the correct conclusion. Firstly, a very limited range of substituents was examined. OCH_3 was the only substituent that was considered as an electron-donating group by the authors, yet calculations show that the OCH_3 group is electron-withdrawing with respect to the electrostatic potential of the face of the aromatic ring. Secondly, when looking closely at the space-filling model of the 1,8-diphenylnaphthalenes, interactions between the substituents themselves cannot be ignored. For example, where $R_1/R_2 = \text{OCH}_3/\text{H}$ a possible $\text{CH}\cdots\text{O}$ interaction may

be responsible for the total attractive energy (Fig 1.21a). Similarly, the additivity seen in $R_1/R_2 = \text{OCH}_3/\text{OCH}_3$ may be due to multiple $\text{CH}\cdots\text{O}$ contacts (Fig 1.21b). In the case of $R_1/R_2 = \text{CHO}/\text{H}$, the optimised structure shows that the antiparallel CHO dipoles may result in strong dipole-dipole interactions (Fig 1.21c). The last example $R_1/R_2 = \text{OCH}_3/\text{CHO}$ also features multiple $\text{CH}\cdots\text{OCH}_3$ and $\text{CH}\cdots\text{OHC}$ contacts (Fig 1.21d). The view of direct interaction between substituents is also advocated by Wheeler.⁹⁴ He proposed a direct, local interaction between substituents and the other aromatic without considering contribution from electrostatic, dispersion or other effects.

Some other studies of aromatic stacking interactions in the gas-phase have been performed, but stacking conformation could not be verified experimentally or the results were not quantitative.¹¹⁴⁻¹¹⁵

1.6.3 Experimental study of aromatic stacking interactions in solution

While gas-phase and computational results emphasise the importance of dispersion in stacking interactions, experimental studies in solution have mainly pointed to a subtle or indeterminable contribution from dispersion.

Cockroft and Hunter demonstrated that aromatic stacking interactions are mostly controlled by electrostatic components in CDCl_3 .³⁷ By varying substituents in the benzene dimers of a series of zipper complex, correlations between stacking interaction energies and Hammett constants was clearly shown (Fig 1.22). In another words, dispersion component can be neglected in solution for small aromatic systems.

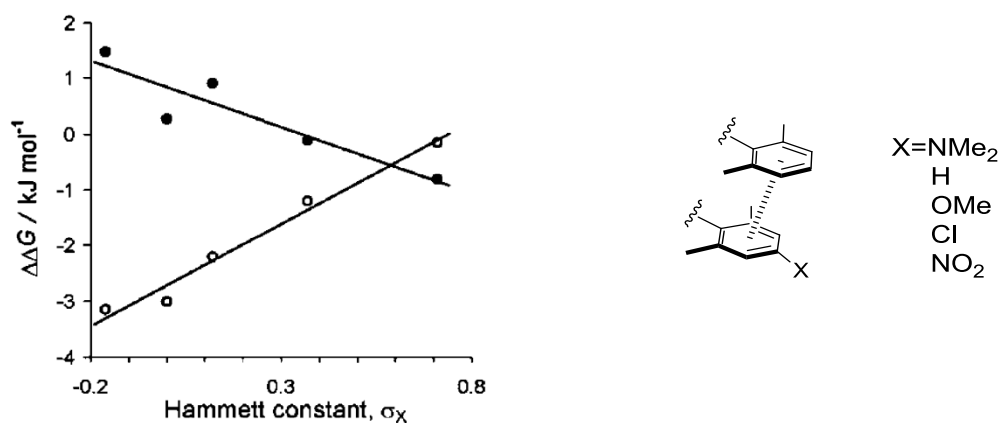


Figure 1.22. Aromatic interaction energy against Hammett constant in Hunter's work.³⁷

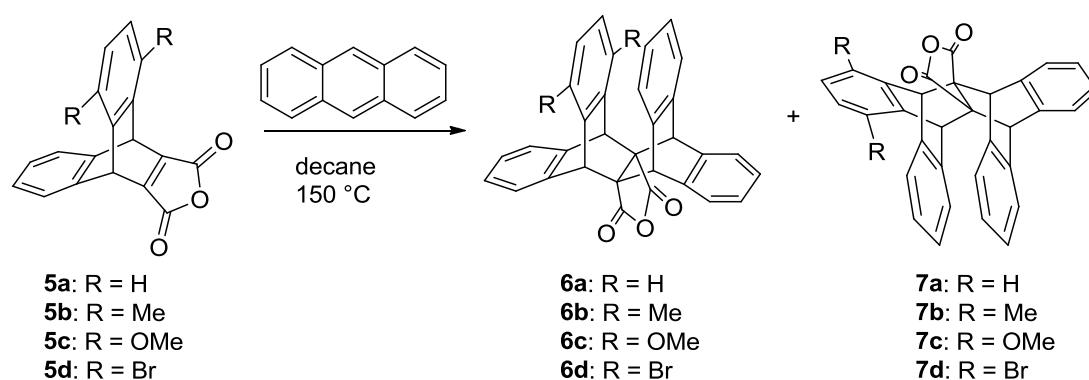


Figure 1.23. Diels-Alder reaction employed by Wheeler *et al.*⁵⁹

Wheeler⁵⁹ and co-workers restated that dispersion was not central to the stacking interaction based on the observations of Diels-Alder cycloadditions in decane. As shown in Fig 1.23, substrates with different substituents on the aromatic ring underwent Diels-Alder reactions with anthracene to give different product ratios, which was reasoned to be due to the differing intermolecular interactions between the species involved. As part of this work, Wheeler *et al.* performed a full examination of the transition state regarding the secondary effects of substituents and steric interactions by computation. This led to the conclusion that these effects were minor

and the barrier differences ($\Delta\Delta G^\ddagger$) can represent the stacking energy. Their stacking energies correlated with Hammett constants σ_m . Although Lewis and co-workers⁹⁹ argued the correlation with σ_m was due to the limited variation in substituents (all substituents in this work were electron-withdrawing groups), and that their results were in accordance with previous finding.^{37,116} Another point to consider is that transition states are far more complicated: the conformation of a transition state is not visible, and substituent stability and steric effects are hard to predict by computation.⁵⁷ Furthermore, Hunter found that aromatic interactions were stronger in transition states than in the products, with the difference depending on the substituent.¹¹⁷ Therefore it may not be appropriate to infer the properties of ground-state aromatic interactions based on transition-state $\Delta\Delta G^\ddagger$ measurements.

Molecular torsion balances have also been used to investigate aromatic stacking interactions in the ground state. Gung¹¹⁸⁻¹²⁰ prepared two triptycene series for the study of stacking interactions in the parallel displaced and near-sandwich configuration (Fig 1.24). The isomer ratios were determined by ¹H NMR in CDCl₃. This study revealed that aromatic stacking was not controlled by a single effect: electrostatic effects governed the interaction when an extremely electron-deficient arene was involved, while the dispersion component increased when parallel-displaced configuration allowed close contact.^{118,120} Finally, it was suggested that charge transfer might become significant when the NMe₂ substituted arene was present.¹¹⁸⁻¹¹⁹

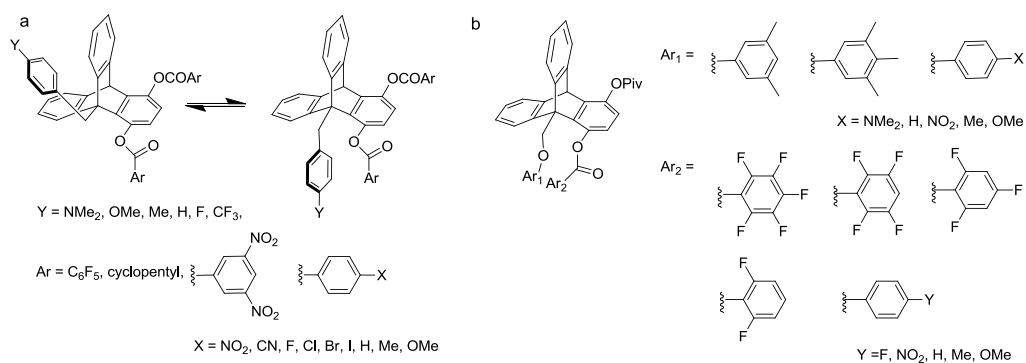
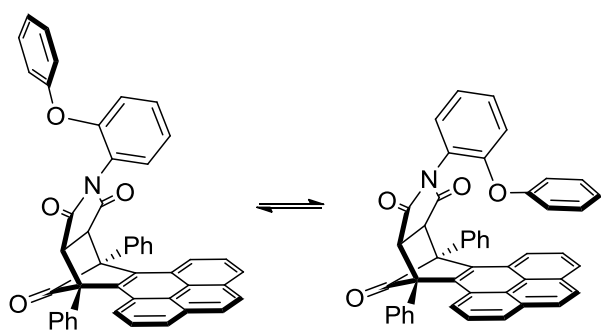
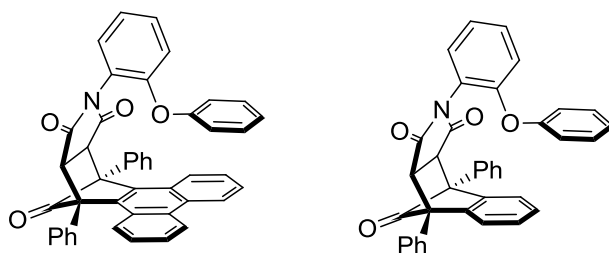


Figure 1.24. Triptycenes used by Gung *et al.*¹¹⁸⁻¹²⁰ aromatic interaction in a) parallel displaced and b) sandwich configuration.

Shimizu first designed a rigid molecular balance featuring a bicyclic *N*-arylsuccinimide framework, which provides a tool for investigating aromatic stacking interaction between benzene and polycyclic aromatics (Fig 1.25).⁵³ Higher folding ratios were observed for larger aromatics. A solvent study showed a linear relation between the folding energies and solvent polarity $E_T(30)$. Later he designed a naphthalenediimide-based molecular balance to study face-to-face aromatic interactions between electron-deficient and electron-rich polycyclic aromatics in d_2 -tetrachloroethane and d_6 -DMSO (Fig 1.26).⁶⁴ A non-linear trend of folding energies against arene surfaces (indicated by number of carbon) was observed. The interaction was much stronger for the larger pyrene system. It was uncertain whether this was due to solvophobic effects or larger dispersion.



pyrene



phenanthrene

benzene

Figure 1.25. Shimizu's molecular balances with bicyclic *N*-arylsuccinimide framework.⁵³

R = *tert*-Amyl

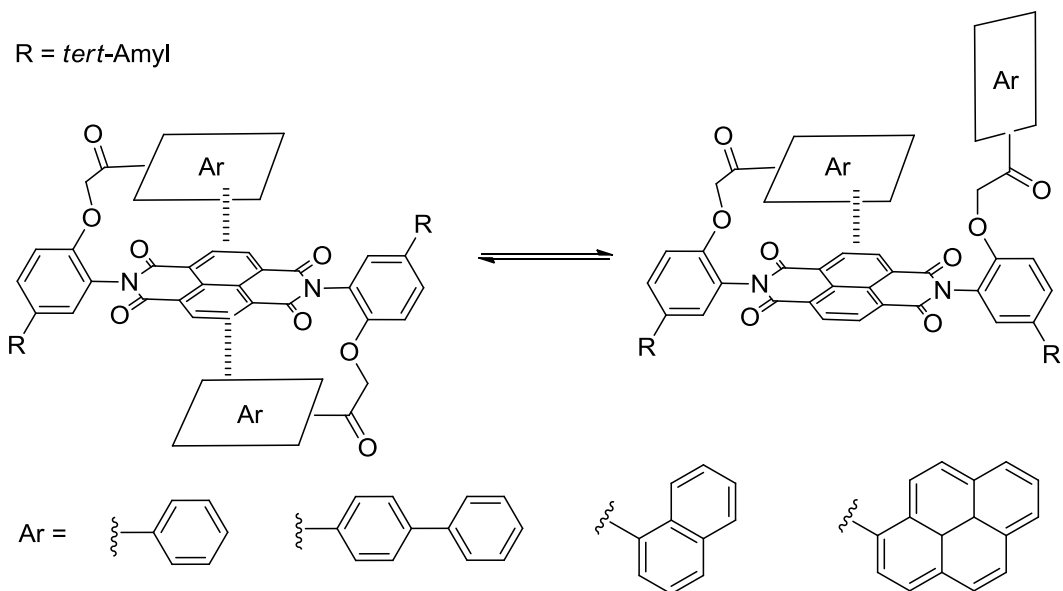


Figure 1.26. Shimizu's molecular balances with naphthalene diimide framework.⁶⁴

Aromatic stacking in water is typically assumed to be dominated by hydrophobic effects. Gellman¹²¹ compared the folding of carboxylate compounds in water (Fig 1.27). It was observed that compound **10** did not fold while compound **8** and **12** folded. This phenomenon excluded the classical hydrophobic effect and dispersion as driving forces. He later used another folding molecule model to reinvestigate stacking in water. However there is no certain conclusion whether dispersion plays a part or not.⁵² Rebek¹²² measured the association constant of adenine with aromatic receptors in water (Fig 1.28). Association constants increased as the aromatic surface became larger, and this was attributed to the hydrophobic effect without considering dispersion.

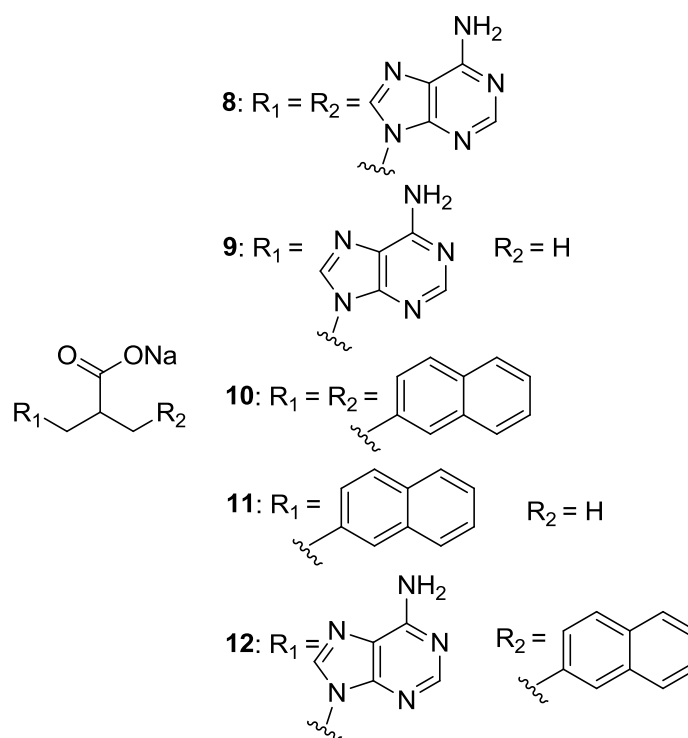


Figure 1.27. Folding molecules used in Gellman's work.¹²¹

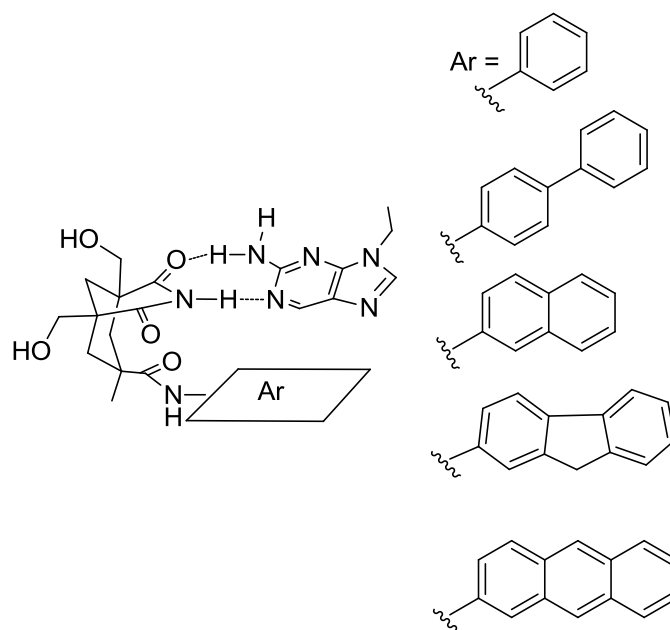


Figure 1.28. Model complex used in Rebek's work.¹²²

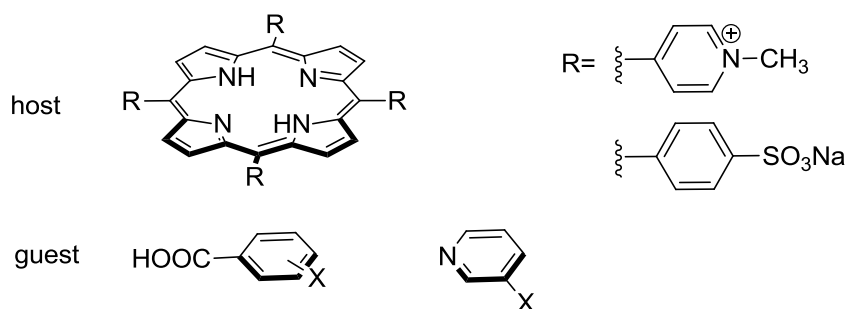


Figure 1.29. Porphyrin host and guest model used in Schneider's work.¹²³⁻¹²⁴

Schneider *et al*^{30,123-124} also investigated stacking interactions in water, but using a porphyrin and substituted benzene/pyridine or saturated guest (Fig 1.29). It was found that aliphatic guests showed little attractive interaction, while other guests with higher polarisability, for example, aromatics and halogens exhibited dispersive effects. However, no information concerning the geometry of this complex is known, and the results seem in stark contrast to other studies on dispersion forces.

While many chemists have focused on the study of aromatic interactions involving small aromatics like benzene, very little experimental data exists for interactions between polycyclic aromatic systems. However, the frequently encountered low solubility of large aromatic systems suggests the importance of dispersion in extended aromatic contacts.

1.6.4 Aromatic CH \cdots π interactions

There is no consensus of opinion on the role of dispersion in edge-to-face aromatic interactions (Fig 1.30). Given the smaller areas of molecular contacts involved, it can be expected that dispersion forces in aromatic CH \cdots π interactions are smaller than those encountered in aromatic stacking.

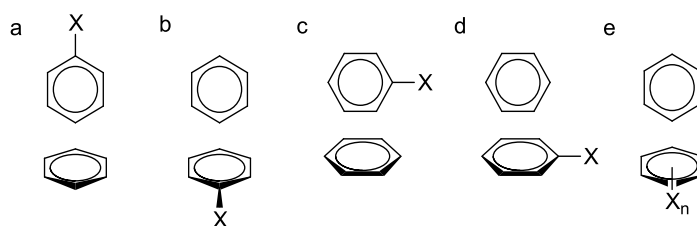
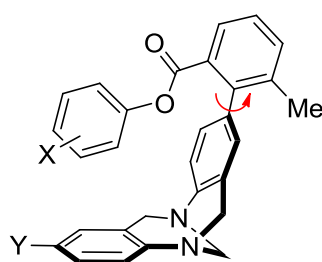


Figure 1.30. Several types of edge-to-face configurations studied.



X = *p*-H, *p*-CH₃, *p*-OCH₃, *p*-CF₃, *p*-CN, *p*-NO₂, *p*-I, 3-Me, 3-CN, 3,5-diMe
 Y = NH₂, CH₃, H, OH, NHAc, I, Br, Cl, CN, NO₂

Figure 1.31. Wilcox's balance for examining aromatic edge-to-face interactions as the X and Y substituents are varied.

In 1994,⁴⁵ Wilcox first used his torsion balances to study edge-to-face aromatic interactions (Fig 1.31). The conformations in these balances were tilted edge-to-face aromatics contacts with various substituents on the edge ring. Nakamura and Houk¹²⁵ examined these balances by computation, both in the gas phase, and with simple solvation fields. The calculated energies were overestimated, but the folding preferences were reproduced and folding was proposed to be a result of a compromise between dispersion and solvent effects. In the case of face-substituent effects (Fig 1.30 tilted conformation d), Wilcox *et al.*⁴⁷ found that the folding energies of balances with edge-to-face interactions were relatively insensitive to the effects of the substituents on the face ring, and proposed that this was due to the dominant effect of dispersion interactions. Orozco *et al.*¹²⁶ compared the simple edge-to-face aromatic model and Wilcox's folding model by computation. Decomposition of the total energy led to the conclusion that dispersion was dominant, with electrostatics contributing in part. However, using similar Wilcox balances with electron-withdrawing CF₃ substituents on the edge ring and varying the substituents on the face ring, Diederich *et al.* discovered a strong electrostatic relationship with interaction energy in C₆D₆.⁴⁹ This discrepancy was tackled by Cockroft and Hunter⁷⁰ using the α/β solvation model. They explained that Wilcox's study (in CDCl₃) and Diederich's study (in C₆D₆) were carried out in different solvents with different H-bond donor abilities, therefore the electrostatic effect for the more polar balances in a less polar solvent was detected (Diederich's study), while the same effect for the less polar balance in a more polar solvent was washed out by the effects of the solvent, which was responsible for the misunderstanding of the importance of dispersion.

So far, experimental work all points to the electrostatic nature of edge-to-face interactions. In response to the above explanation, Diederich *et al*⁴⁶ performed more comprehensive study. Folding energies of 14 balances with edge-to-face interaction were taken in CDCl₃ and C₆D₆ respectively. The correlation with Hammett constants (σ_m) remained. Compared with computational findings, they believed that the edge-to-face interaction was dominated by dispersion and balanced with electrostatic and exchange repulsion. A few months later Cockroft and Hunter⁷¹ analysed Diederich's new results. The original α/β solvation model still held for the new data-set when applied correctly. The same model was also shown to account for edge-to-face interaction energies obtained in supramolecular zipper complexes. Thus they insisted that the edge-to-face interaction in solution can be explained by an electrostatic solvation model.

The advantage of the Wilcox balance is that the backbone offers well-defined geometries, allowing studies in solution. The disadvantage, owing to the same backbone, is that it complicates the simple interaction due to geometric effects and secondary interactions.¹²⁶ In contrast, computational studies can focus on the net interaction in unconstrained equilibrium geometries. Sinnokrot and Sherill⁹⁵ found that the effects of varying both edge and face substituents cannot be explained by electrostatics alone (Fig 1.30a, b). In some examples, dispersion was larger than electrostatics. Kim considered dispersion¹²⁷ was the larger contributor in both edge or face substitution, but found that it is cancelled by exchange repulsion in the former and cooperates with exchange repulsion/electrostatics in the latter. Sherrill and others discovered that the T-shape interactions are controlled by electrostatic and dispersion.⁹⁶ Meanwhile, Wheeler and Houk *et al* stated that substituent effects arose

from the electrostatic interactions of the edge substituent with face ring, combined with the sum of the electrostatic and dispersion interactions of the face substituent with the edge ring (Fig 1.30c, d).¹²⁸

For edge-to-face interactions involving polysubstituted aromatics (Fig 1.30e), Sherril and others⁹⁶ implied that multi-substituent effects are irregular, and that it was necessary to consider close contact between the substituent and the hydrogen atoms on the other ring. Wheeler and Houk¹²⁸ suggested that substituent effects are additive in disubstituted dimers. In contrast, studies of aromatic CH \cdots π interactions in polyaromatic systems are rarely encountered; although it has been suggested that dispersion is the dominant factor in naphthalene and anthracene edge-to-face dimers.¹⁰¹

1.7 Summary

This chapter has introduced several classic non-covalent interactions, in combination with computational and synthetic models used to study these weak interactions. Hunter's α/β solvent competition theory is a very powerful tool for unravelling solvent effects and predicting interaction energies. Dispersion interactions both in aliphatic alkane and aromatic system are discussed in detail. No agreement has been reached on the importance of this non-specific dispersion forces, particularly in solution, and it seems most appropriate to discuss the role of dispersion in the context of interactions occurring in solution and the gas-phase separately. New experimental investigations are required to probe the understanding of dispersion in solution, since the most important molecular recognition events occur in solution rather than the gas-phase.

Supporting information: All compound numbers refer to compounds exclusively as presented in this chapter.

References

- (1) Langmuir, I. *J. Am. Chem. Soc.* **1919**, *41*, 868-934.
- (2) Tovar, J. D. *Acc. Chem. Res.* **2013**.
- (3) Ariga, K.; Ito, H.; Hill, J. P.; Tsukube, H. *Chem. Soc. Rev.* **2012**, *41*, 5800-5835.
- (4) Kay, E. R.; Leigh, D. A.; Zerbetto, F. *Angew. Chem., Int. Ed.* **2007**, *46*, 72-191.
- (5) Ciferri, A.; Perico, A. *Ionic Interactions in Natural and Synthetic Macromolecules*; John Wiley & Sons, 2012.
- (6) Betz, K.; Malyshev, D. A.; Lavergne, T.; Welte, W.; Diederichs, K.; Dwyer, T. J.; Ordoukhanian, P.; Romesberg, F. E.; Marx, A. *Nat. Chem. Biol.* **2012**, *8*, 612-614.
- (7) Metrangolo, P.; Meyer, F.; Pilati, T.; Resnati, G.; Terraneo, G. *Angew. Chem., Int. Ed.* **2008**, *47*, 6114-6127.
- (8) Haldar, J.; Aswal, V. K.; Goyal, P. S.; Bhattacharya, S. *Angew. Chem., Int. Ed.* **2001**, *40*, 1228-1232.
- (9) Israelachvili, J. N. *Intermolecular and Surface Forces*; Revised Third ed.; Academic Press: San Diego, 2011.
- (10) Xu, H.; Zuend, S. J.; Woll, M. G.; Tao, Y.; Jacobsen, E. N. *Science* **2010**, *327*, 986-990.
- (11) Arunan, E.; Desiraju, G. R.; Klein, R. A.; Sadlej, J.; Scheiner, S.; Alkorta, I.; Clary, D. C.; Crabtree, R. H.; Dannenberg, J. J.; Hobza, P.; Kjaergaard, H. G.; Legon, A. C.; Mennucci, B.; Nesbitt, D. J. *Pure Appl. Chem.* **2011**, *83*, 1637-1641.
- (12) Blight, B. A.; Hunter, C. A.; Leigh, D. A.; McNab, H.; Thomson, P. I. *Nat. Chem. Biol.* **2011**, *3*, 244-248.
- (13) Chen, X.; Bao, X.; Zhao, J.-C.; Shore, S. G. *J. Am. Chem. Soc.* **2011**, *133*, 14172-14175.
- (14) Clark, T.; Hennemann, M.; Murray, J.; Politzer, P. *J. Mol. Model.* **2007**, *13*, 291-296.
- (15) Auffinger, P.; Hays, F. A.; Westhof, E.; Ho, P. S. *Proc. Natl. Acad. Sci. U. S. A.* **2004**, *101*, 16789-16794.
- (16) Hardegger, L. A.; Kuhn, B.; Spinnler, B.; Anselm, L.; Ecabert, R.; Stihle, M.; Gsell, B.; Thoma, R.; Diez, J.; Benz, J.; Plancher, J.-M.; Hartmann, G.; Banner, D. W.; Haap, W.; Diederich, F. *Angew. Chem., Int. Ed.* **2011**, *50*, 314-318.
- (17) Erdelyi, M. *Chem. Soc. Rev.* **2012**, *41*, 3547-3557.
- (18) Beale, T. M.; Chudzinski, M. G.; Sarwar, M. G.; Taylor, M. S. *Chem. Soc. Rev.* **2013**.
- (19) Chandler, D. *Nature* **2005**, *437*, 640-647.
- (20) Biro, S. M.; Ullrich, E. C.; Hof, F.; Trembleau, L.; Rebek, J. *J. Am. Chem. Soc.* **2004**, *126*,

2870-2876.

- (21) Setny, P.; Baron, R.; McCammon, J. A. *J. Chem. Theory Comput.* **2010**, *6*, 2866-2871.
- (22) Rebek, J. *Acc. Chem. Res.* **2009**, *42*, 1660-1668.
- (23) Yan, Z.; Jeffrey, S. M. In *Foldamers (First Edition)*; Stefan Hecht, D. I. H., Ed. 2007, p 75-108.
- (24) Lennard-Jones, J. E. *Proc. Phys.Soc.* **1931**, *43*.
- (25) Krenske, E. H.; Houk, K. N. *Acc. Chem. Res.* **2012**, *46*, 979-989.
- (26) Klärner, F.-G.; Schrader, T. *Acc. Chem. Res.* **2012**, *46*, 967-978.
- (27) Nandwana, V.; Samuel, I.; Cooke, G.; Rotello, V. M. *Acc. Chem. Res.* **2012**, *46*, 1000-1009.
- (28) Pace, C. J.; Gao, J. *Acc. Chem. Res.* **2012**, *46*, 907-915.
- (29) Riley, K. E.; Hobza, P. *Acc. Chem. Res.* **2012**, *46*, 927-936.
- (30) Schneider, H.-J. *Acc. Chem. Res.* **2012**, *46*, 1010-1019.
- (31) Salonen, L. M.; Ellermann, M.; Diederich, F. *Angew. Chem., Int. Ed.* **2011**, *50*, 4808-4842.
- (32) Anslyn, E. V.; Dougherty, D. A. *Modern Physical Organic Chemistry*; University Science Books, 2005.
- (33) Zimmerman, S. C.; Murray, T. J. *Phil. Trans. R. Soc. Lond. A* **1993**, *345*, 49-56.
- (34) Djurdjevic, S.; Leigh, D. A.; McNab, H.; Parsons, S.; Teobaldi, G.; Zerbetto, F. *J. Am. Chem. Soc.* **2006**, *129*, 476-477.
- (35) Blight, B. A.; Camara-Campos, A.; Djurdjevic, S.; Kaller, M.; Leigh, D. A.; McMillan, F. M.; McNab, H.; Slawin, A. M. Z. *J. Am. Chem. Soc.* **2009**, *131*, 14116-14122.
- (36) Bisson, A. P.; Carver, F. J.; Eggleston, D. S.; Haltiwanger, R. C.; Hunter, C. A.; Livingstone, D. L.; McCabe, J. F.; Rotger, C.; Rowan, A. E. *J. Am. Chem. Soc.* **2000**, *122*, 8856-8868.
- (37) Scott L. Cockroft; Christopher A. Hunter; Kevin R. Lawson; Julie Perkins; Urch, C. J. *J. Am. Chem. Soc.* **2005**, *127*, 8594-8595.
- (38) Harry, A.; Scott, L. C.; Claudio, G.; Christopher, A. H.; Kevin, R. L.; Julie, P.; Sharon, E. S.; Christopher, J. U.; Rhonan, F. *Chembiochem* **2004**, *5*, 657-665.
- (39) Sarwar, M. G.; Dragisic, B.; Salsberg, L. J.; Gouliaras, C.; Taylor, M. S. *J. Am. Chem. Soc.* **2010**, *132*, 1646-1653.
- (40) Dawson, R. E.; Hennig, A.; Weimann, D. P.; Emery, D.; Ravikumar, V.; Montenegro, J.; Takeuchi, T.; Gabutti, S.; Mayor, M.; Mareda, J.; Schalley, C. A.; Matile, S. *Nat Chem* **2010**, *2*, 533-538.
- (41) Ballester, P. *Acc. Chem. Res.* **2013**, *46*, 874-884.
- (42) Cozzi, F.; Cinquini, M.; Annunziata, R.; Dwyer, T.; Siegel, J. S. *J. Am. Chem. Soc.* **1992**, *114*, 5729-5733.
- (43) Cozzi, F.; Cinquini, M.; Annunziata, R.; Siegel, J. S. *J. Am. Chem. Soc.* **1993**, *115*, 5330-5331.
- (44) Annunziata, R.; Benaglia, M.; Cozzi, F.; Mazzanti, A. *Chem. Eur. J.* **2009**, *15*, 4373 - 4381.
- (45) Paliwal, S.; Geib, S.; Wilcox, C. S. *J. Am. Chem. Soc.* **1994**, *116*, 4497-4498.
- (46) Fischer, F. R.; Schweizer, W. B.; Diederich, F. *Chem. Commun.* **2008**, 4031-4033.
- (47) Kim, E.-i.; Paliwal, S.; Wilcox, C. S. *J. Am. Chem. Soc.* **1998**, *120*, 11192-11193.

- (48) Bhayana, B.; Wilcox, C. S. *Angew. Chem., Int. Ed.* **2007**, *46*, 6833-6836.
- (49) Hof, F.; Scofield, D. M.; Schweizer, W. B.; Diederich, F. *Angew. Chem., Int. Ed.* **2004**, *43*, 5056-5059.
- (50) Fischer, F. R.; Schweizer, W. B.; Diederich, F. *Angew. Chem., Int. Ed.* **2007**, *46*, 8270-8273.
- (51) Fischer, F. R.; Wood, P. A.; Allen, F. H.; Diederich, F. *Proc. Natl. Acad. Sci. U. S. A.* **2008**, *105*, 17290-17294.
- (52) McKay, S. L.; Haptonstall, B.; Gellman, S. H. *J. Am. Chem. Soc.* **2001**, *123*, 1244-1245.
- (53) Carroll, W. R.; Pellechia, P.; Shimizu, K. D. *Org. Lett.* **2008**, *10*, 3547-3550.
- (54) Carroll, W. R.; Zhao, C.; Smith, M. D.; Pellechia, P. J.; Shimizu, K. D. *Org. Lett.* **2011**, *13*, 4320-4323.
- (55) Zhao, C.; Parrish, R. M.; Smith, M. D.; Pellechia, P. J.; Sherrill, C. D.; Shimizu, K. D. *J. Am. Chem. Soc.* **2012**, *134*, 14306-14309.
- (56) Oki, M. *Acc. Chem. Res.* **1990**, *23*, 351-356.
- (57) Mati, I. K.; Cockroft, S. L. *Chem. Soc. Rev.* **2010**, *39*, 4195-4205.
- (58) Motherwell, W. B.; Moïse, J.; Aliev, A. E.; Nič, M.; Coles, S. J.; Horton, P. N.; Hursthouse, M. B.; Chessari, G.; Hunter, C. A.; Vinter, J. G. *Angew. Chem., Int. Ed.* **2007**, *46*, 7823-7826.
- (59) Wheeler, S. E.; McNeil, A. J.; Müller, P.; Swager, T. M.; Houk, K. N. *J. Am. Chem. Soc.* **2010**, *132*, 3304-3311.
- (60) Lima, C. F. R. A. C.; Rocha, M. A. A.; Gomes, L. R.; Low, J. N.; Silva, A. M. S.; Santos, L. M. N. B. F. *Chem. Eur. J.* **2012**, *18*, 8934-8943.
- (61) Aradhya, S. V.; Frei, M.; Hybertsen, M. S.; Venkataraman, L. *Nat Mater* **2012**, *11*, 872 - 876.
- (62) Daniel, J. M.; Friess, S. D.; Rajagopalan, S.; Wendt, S.; Zenobi, R. *Int. J. Mass Spectrom.* **2002**, *216*, 1-27.
- (63) McCullough, B. J.; Gaskell, S. J. *Combinatorial Chemistry & High Throughput Screening* **2009**, *12*, 203-211.
- (64) Chong, Y. S.; Carroll, W. R.; Burns, W. G.; Smith, M. D.; Shimizu, K. D. *Chem. Eur. J.* **2009**, *15*, 9117-9126.
- (65) Cook, J. L.; Hunter, C. A.; Low, C. M.; Perez-Velasco, A.; Vinter, J. G. *Angew. Chem., Int. Ed.* **2007**, *46*, 3706-3709.
- (66) Hunter, C. A. *Angew. Chem., Int. Ed.* **2004**, *43*, 5310-5324.
- (67) Cook, J. L.; Hunter, C. A.; Low, C. M.; Perez-Velasco, A.; Vinter, J. G. *Angew. Chem., Int. Ed.* **2008**, *47*, 6275-6277.
- (68) Cabot, R.; Hunter, C. A. *Org. Biomol. Chem.* **2010**, *8*, 1943-1950.
- (69) Cabot, R.; Hunter, C. A.; Varley, L. M. *Org. Biomol. Chem.* **2010**, *8*, 1455-1462.
- (70) Cockroft, S. L.; Hunter, C. A. *Chem. Commun.* **2006**, 3806-3808.
- (71) Cockroft, S. L.; Hunter, C. A. *Chem. Commun.* **2009**, 3961-3963.
- (72) McNaught, A. D.; Wilkinson, A. *IUPAC. Compendium of Chemical Terminology, 2nd ed.* **1997**.

- (73) Wodrich, M. D.; Corminboeuf, C.; Schleyer, P. v. R. *Org. Lett.* **2006**, *8*, 3631-3634.
- (74) Johnson, E. R.; Mackie, I. D.; DiLabio, G. A. *J. Phys. Org. Chem.* **2009**, *22*, 1127-1135.
- (75) Haynes, W. M.; Lide, D. R.; Bruno, T. J. *CRC Handbook of Chemistry and Physics 2012-2013*; 93rd ed.; CRC Press, 2012.
- (76) Hunter, C. A. *Chem. Sci.* **2013**, *4*, 834-848.
- (77) Tsuzuki, S.; Honda, K.; Uchimaru, T.; Mikami, M. *J. Phys. Chem. A* **2004**, *108*, 10311-10316.
- (78) Tsuzuki, S.; Honda, K.; Uchimaru, T.; Mikami, M. *J. Chem. Phys.* **2006**, *124*, 114304-114307.
- (79) Ferrighi, L.; Madsen, G. K. H.; Hammer, B. *Chem. Phys. Lett.* **2010**, *492*, 183-186.
- (80) Echeverria, J.; Aullon, G.; Danovich, D.; Shaik, S.; Alvarez, S. *Nat Chem* **2011**, *3*, 323-330.
- (81) Pitzer, K. S.; Catalano, E. *J. Am. Chem. Soc.* **1956**, *78*, 4844-4846.
- (82) Wodrich, M. D.; Wannere, C. S.; Mo, Y.; Jarowski, P. D.; Houk, K. N.; Schleyer, P. v. R. *Chem. Eur. J.* **2007**, *13*, 7731-7744.
- (83) Wodrich, M. D.; Jana, D. F.; Schleyer, P. R.; Corminboeuf, C. *J. Phys. Chem. A* **2008**, *112*, 11495-11500.
- (84) Schreiner, P. R.; Chernish, L. V.; Gunchenko, P. A.; Tikhonchuk, E. Y.; Hausmann, H.; Serafin, M.; Schlecht, S.; Dahl, J. E. P.; Carlson, R. M. K.; Fokin, A. A. *Nature* **2011**, *477*, 308-311.
- (85) Fokin, A. A.; Chernish, L. V.; Gunchenko, P. A.; Tikhonchuk, E. Y.; Hausmann, H.; Serafin, M.; Dahl, J. E. P.; Carlson, R. M. K.; Schreiner, P. R. *J. Am. Chem. Soc.* **2012**, *134*, 13641-13650.
- (86) Grimme, S.; Schreiner, P. R. *Angew. Chem., Int. Ed.* **2011**, *50*, 12639-12642.
- (87) Rebek, J. J. *Chem. Commun.* **2007**, *0*, 2777-2789.
- (88) Abraham, M. H. *J. Am. Chem. Soc.* **1979**, *101*, 5477-5484.
- (89) Wu, J.; Prausnitz, J. M. *Proc. Natl. Acad. Sci. U. S. A.* **2008**, *105*, 9512-9515.
- (90) Ray, C.; Brown, J. R.; Kirkpatrick, A.; Akhremitchev, B. B. *J. Am. Chem. Soc.* **2008**, *130*, 10008-10018.
- (91) Grimme, S. *Angew. Chem., Int. Ed.* **2008**, *47*, 3430-3434.
- (92) Ringer, A. L.; Sherrill, C. D. *J. Am. Chem. Soc.* **2009**, *131*, 4574-4575.
- (93) Zhao, Y.; Truhlar, D. G. *Acc. Chem. Res.* **2008**, *41*, 157-167.
- (94) Wheeler, S. E. *Acc. Chem. Res.* **2013**, *46*, 1029-1038.
- (95) Sinnokrot, M. O.; Sherrill, C. D. *J. Am. Chem. Soc.* **2004**, *126*, 7690-7697.
- (96) Ringer, A. L.; Sinnokrot, M. O.; Lively, R. P.; Sherrill, C. D. *Chem. Eur. J.* **2006**, *12*, 3821-3828.
- (97) Sherrill, C. D. *Acc. Chem. Res.* **2012**, *46*, 1020-1028.
- (98) Geronimo, I.; Lee, E. C.; Singh, N. J.; Kim, K. S. *J. Chem. Theory Comput.* **2010**, *6*, 1931-1934.
- (99) Watt, M.; Hardebeck, L. K. E.; Kirkpatrick, C. C.; Lewis, M. *J. Am. Chem. Soc.* **2011**, *133*, 3854-3862.
- (100) Piacenza, M.; Grimme, S. *J. Am. Chem. Soc.* **2005**, *127*, 14841-14848.
- (101) Podeszwa, R.; Szalewicz, K. *Phys. Chem. Chem. Phys.* **2008**, *10*, 2735-2746.
- (102) Janowski, T.; Ford, A. R.; Pulay, P. *Molecular Physics* **2009**, *108*, 249-257.

- (103) Janowski, T.; Pulay, P. *J. Am. Chem. Soc.* **2012**, *134*, 17520-17525.
- (104) Mück-lichtenfeld, C.; Grimme, S. *Molecular Physics* **2007**, *105*, 2793-2798.
- (105) Zeinalipour-Yazdi, C. D.; Pullman, D. P. *J. Phys. Chem. B* **2006**, *110*, 24260-24265.
- (106) Cozzi, F.; Annunziata, R.; Benaglia, M.; Baldrige, K. K.; Aguirre, G.; Estrada, J. s.; Sritana-Anantd, Y.; Siegel, J. S. *Phys. Chem. Chem. Phys.* **2008**, *10*, 2686-2694.
- (107) Ehrlich, S.; Moellmann, J.; Grimme, S. *Acc. Chem. Res.* **2012**, *46*, 916-926.
- (108) Kano, K.; Minamizono, H.; Kitae, T.; Negi, S. *J. Phys. Chem. A* **1997**, *101*, 6118-6124.
- (109) Edward, G. H.; Sherrill, C. D. *J. Chem. Phys.* **2010**, *132*, 184111.
- (110) Kim, K. S.; Karthikeyan, S.; Singh, N. J. *J. Chem. Theory Comput.* **2011**, *7*, 3471-3477.
- (111) Fokin, A. A.; Gerbig, D.; Schreiner, P. R. *J. Am. Chem. Soc.* **2011**, *133*, 20036-20039.
- (112) Bloom, J. W. G.; Wheeler, S. E. *Angew. Chem., Int. Ed.* **2011**, *50*, 7847-7849.
- (113) Martinez, C. R.; Iverson, B. L. *Chem. Sci.* **2012**, *3*, 2191-2201.
- (114) Hunter, C. A.; Lawson, K. R.; Perkins, J.; Urch, C. J. *J. Chem. Soc., Perkin Trans. 2* **2001**, 651-669.
- (115) Law, K.; Schauer, M.; Bernstein, E. R. *J. Chem. Phys.* **1984**, *81*, 4871-4882.
- (116) Cockroft, S. L.; Perkins, J.; Zonta, C.; Adams, H.; Spey, S. E.; Low, C. M. R.; Vinter, J. G.; Lawson, K. R.; Urch, C. J.; Hunter, C. A. *Org. Biomol. Chem.* **2007**, *5*, 1062-1080.
- (117) Hunter, C. A.; Low, C. M. R.; Vinter, J. G.; Zonta, C. *J. Am. Chem. Soc.* **2003**, *125*, 9936-9937.
- (118) Gung, B. W.; Xue, X.; Zou, Y. *J. Org. Chem.* **2007**, *72*, 2469-2475.
- (119) Gung, B. W.; Patel, M.; Xue, X. *J. Org. Chem.* **2005**, *70*, 10532-10537.
- (120) Gung, B. W.; Xue, X.; Reich, H. J. *J. Org. Chem.* **2005**, *70*, 3641-3644.
- (121) Newcomb, L. F.; Gellman, S. H. *J. Am. Chem. Soc.* **1994**, *116*, 4993-4994.
- (122) Rotello, V. M.; Viani, E. A.; Deslongchamps, G.; Murray, B. A.; Rebek, J. *J. Am. Chem. Soc.* **1993**, *115*, 797-798.
- (123) Schneider, H.-J.; Wang, M. *J. Org. Chem.* **1994**, *59*, 7464-7472.
- (124) Liu, T.; Schneider, H.-J. *Angew. Chem., Int. Ed.* **2002**, *41*, 1368-1370.
- (125) Nakamura, K.; Houk, K. N. *Org. Lett.* **1999**, *1*, 2049-2051.
- (126) Ribas, J.; Cubero, E.; Luque, F. J.; Orozco, M. *J. Org. Chem.* **2002**, *67*, 7057-7065.
- (127) Lee, E. C.; Hong, B. H.; Lee, J. Y.; Kim, J. C.; Kim, D.; Kim, Y.; Tarakeshwar, P.; Kim, K. *J. Am. Chem. Soc.* **2005**, *127*, 4530-4537.
- (128) Wheeler, S. E.; Houk, K. N. *Molecular Physics* **2009**, *107*, 749-760.

Chapter 2 Measurement of interactions in extended aromatic contacts

Abstract

Aromatic stacking interactions are measured in solution using AAD-DAA H-bonded complexes. Interaction energies between extended aromatics are measured to be less than 3 kJ mol⁻¹ in solution. Quantitative structure property relationships show that aromatic stacking interactions in solution are not governed by a single parameter. Further computational analyses reveal a small but important role of dispersion.

2.1 Introduction

$\pi\cdots\pi$ interactions are common in nucleic acid base stacking and important in protein aggregation.¹⁻² Synthetic chemists have also utilised this interaction to develop new catalysts.³⁻⁴ $\pi\cdots\pi$ interactions are often employed in molecular recognition due to their reversible nature and easy detection in spectroscopy.⁵⁻⁷ Comprehensive studies on this unique non-covalent interaction could lead to further improvements over current applications. Efforts have been invested heavily in the computational study of $\pi\cdots\pi$ interactions.⁸⁻⁹ The total interaction energies are often decomposed into four components, which are electrostatic, induction, exchange and dispersion interactions. While computational chemists come to different conclusions regarding the precise composition of these four interaction components, they agree on importance of dispersion interactions in the gas phase.¹⁰⁻¹³ However, much progress remains to be made before computational approaches are able to accurately to model $\pi\cdots\pi$

interactions in solution. Although many studies have been carried out in solution using unimolecular models or complexes, no agreement has been achieved.^{5,14-17} Cockroft and Hunter suggested that the electrostatic component governs $\pi\cdots\pi$ interactions in solution.¹⁸ Meanwhile, Gung has suggested that the limits where charge transfer interactions might play a role.¹⁴ Furthermore, most previous experiments have focused on interactions between small aromatics, where dispersion effects might be masked by solvent effects. Therefore, further investigations of $\pi\cdots\pi$ interactions in solution, particularly those involving extended aromatic contacts are worthwhile.

2.2 Methodology and initial project design

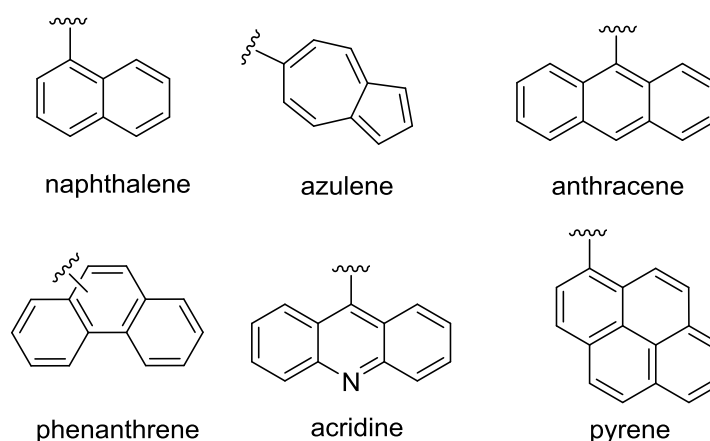


Figure 2.1. Representative polyaromatic hydrocarbons (PAHs).

Although aromatic interactions have been extensively studied in recent years, a knowledge gap still exists concerning interactions in polysubstituted aromatics, particularly those between extended aromatic rings with electron-rich surfaces. Aromatic groups that are able to present large surfaces of contact range from highly

substituted benzenes to polyaromatic rings, including electron-rich and electron-poor rings, and some of those rings that might be of interest for examination in this project are shown above (Fig 2.1). The larger polyaromatic rings should have larger dispersion interactions than benzene rings, which might provide an opportunity for revealing the importance of dispersion in solution. Furthermore, the lack of substituents on these types of polyaromatic rings should mean that additional secondary interactions such as H-bonds and dipole-dipole interactions should not complicate the data analysis. Thus, we have set out to design supramolecular complexes to experimentally determine whether dispersion interactions make important contributions to interactions between extended complementary molecular surfaces in solution.

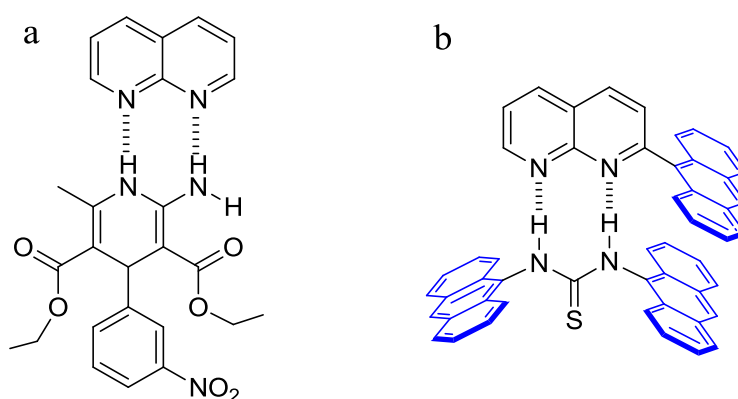


Figure 2.2. AA-DD complex developed by Zimmerman *et al*¹⁹ with $K_a=260 \text{ M}^{-1}$ in CDCl_3 (a) and the initial complex design for this project (b).

The desired geometries are important in studying the aromatic interactions. The complex should be carefully designed to fix the aromatic rings in the geometries of interest. In addition, good solubility is needed for the titration experiments to allow concentrations to fall within the sensitivity regime of NMR, and to allow a large

enough concentration range to be covered for good coverage of the binding isotherm. The complex in Figure 2.2a was previously investigated by Zimmerman *et al*¹⁹ and was found to have an association constant of 240 M^{-1} in CDCl_3 . Inspired by this, we initially designed an AA-DD double H-bond complex with 1,8-naphthyridine as a H-bond acceptor and a disubstituted thiourea as a H-bond donor (Fig 2.2b).

The energy minimised Spartan reference models of naphthyridine derivatives (DFT/B3LYP/6-31G*) show that the dihedral angles of the naphthyridine moiety and aryls increase in sterically bulky aromatics (Fig 2.3). Anthracene is perpendicular to the naphthyridine plane. The steric effect of fluorine twists the phenyl ring out of the plane of naphthyridine compared to an unsubstituted phenyl ring, making the design suitable for the investigation of stacking geometries.

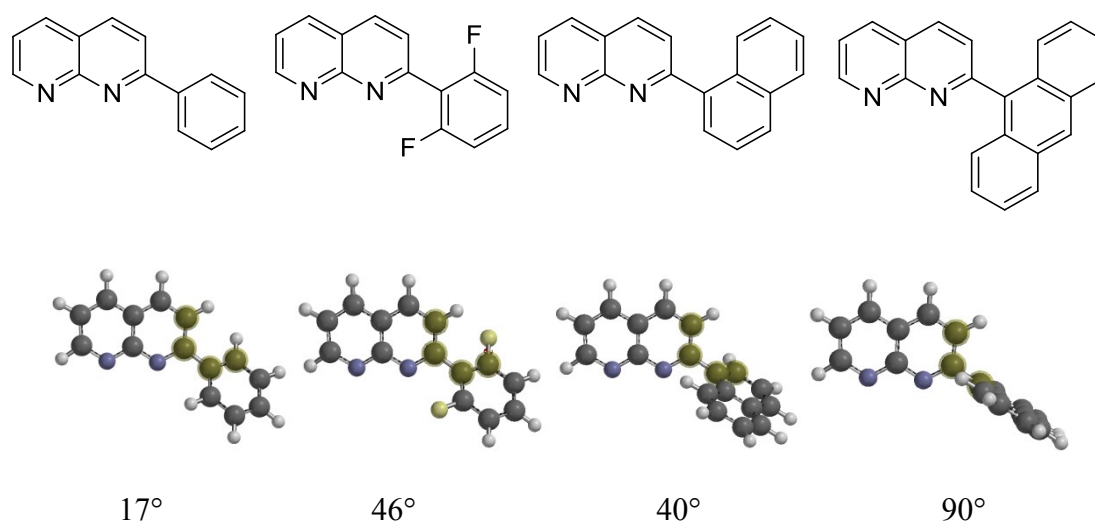


Figure 2.3. Structures of naphthyridine derivatives (top) and energy minimised Spartan models using DFT/B3LYP/6-31G* shown (bottom).

Thermodynamic double-mutant cycles (DMC) provide a convenient means of

dissecting an interaction of interest from the other interactions that contribute to the complexation free energy.²⁰ The approach is widely used in analysing protein structures, in biomolecular recognition studies and for studying cooperativity in synthetic complexes and proteins.²⁰⁻²² As shown to the left in Figure 2.4, the accompanying interactions in complex A complicate the interaction between X and Y. Making a single mutation to the complex by removing one of the interacting aromatic rings (A to B) removes most of the accompanying interactions that contribute to complexation such as the H-bonds. However, latent interactions between X and the other components will also contribute to $\Delta G_A - \Delta G_B$ such as changes in the strengths of the H bonds due to variation in the electronic properties of the adjacent substituents. Thus, control complexes C and D are introduced to quantify the changes in the remaining secondary interactions. $\Delta\Delta G$ represents the net interaction between X and Y. This method is applicable to attractive and repulsive interactions, provided that the anchoring interactions at the core of the complex are more attractive than the repulsive interactions being measured.

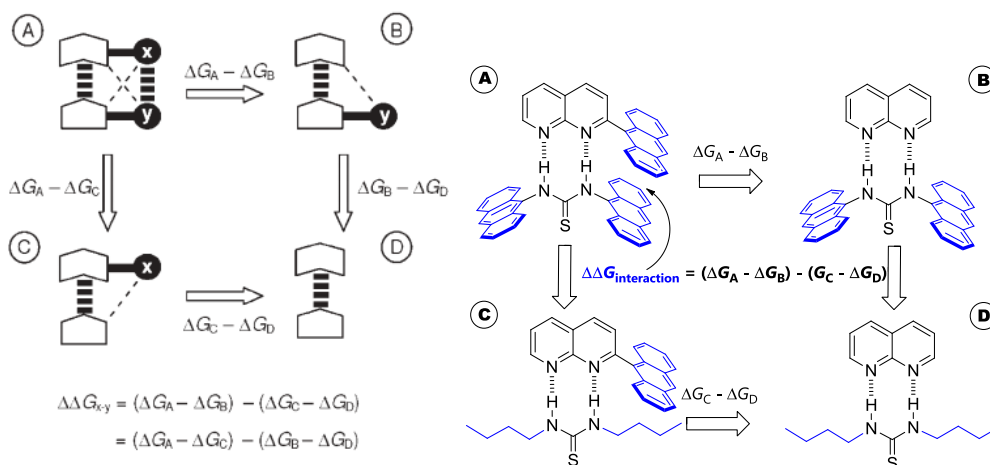


Figure 2.4. (left) Example of a double-mutant cycle that could be used to dissect aromatic stacking interaction energies from the contributions of the H-bonding and secondary effects contributing to the total binding energies, (right) a proposed double-mutant cycle that could be employed in the current project.

Many different methods can be used to determine binding constants in supramolecular complexes, such as fluorescence, UV-Vis, NMR and calorimetric titration. The most suitable method depends on the properties of the complex (*i.e.* the binding constant) and the detection limits of equipment in relation to the solubility of the complexes. NMR titration is the most suitable method for the proposed complexes, since ^1H NMR chemical shifts are sensitive to H bond, and the complexes are expected to have association constants below 10^5 M^{-1} .²³ Dilution and titration data can be fitted to a 1:1 binding isotherm using nonlinear curve fitting procedures to obtain binding constants. Titration data may also be fitted to more complicated models that include dimerisation of the host and guest (as determined by dilution experiments). The free energy of complexation, ΔG can be calculated by the equation below.

$$\Delta G = -RT \ln K_a \quad \text{Equation 2.1}$$

Where R is the gas constant, T is the absolute temperature and K_a is the association constant.

2.3 Synthesis and evolution of the complex design

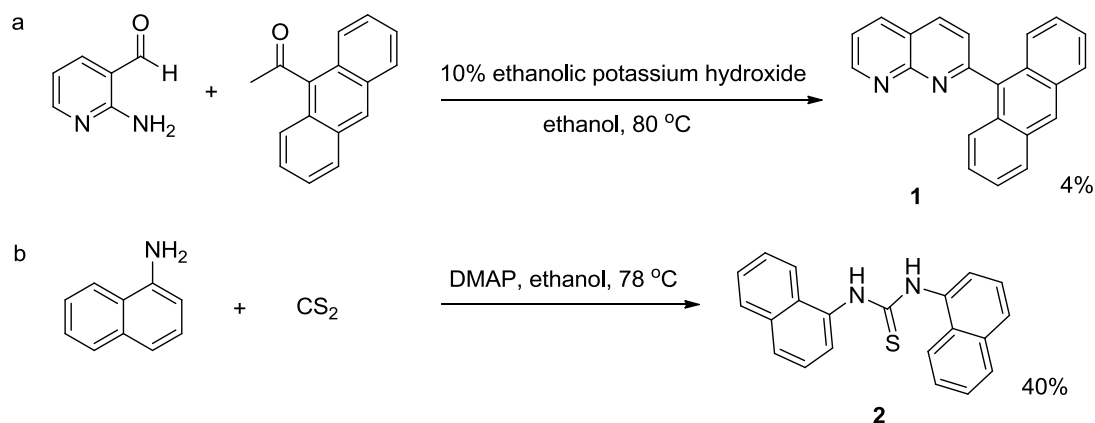


Figure 2.5. Syntheses of an unsymmetrical naphthyridine and a symmetrical thiourea

Syntheses of the initial complex components was straightforward. 2-Substituted 1,8-naphthyridine was obtained by a Friedländer reaction under basic condition. The yield was very low due to the steric hindrance associated with 9-acetylanthracene (Fig 2.5a). A symmetrical thiourea was easily synthesised by reacting the amine with carbon disulfide in the presence of a dimethylaminopyridine (DMAP) catalyst (Fig 2.5b). The product was separated by filtration and was pure enough to use in further experiments.

However, dinaphthyl thiourea had poor solubility in most solvents except for DMSO, and the solubility of the thiourea compounds was seen to decrease dramatically as the aromatic rings became larger. This may not only be due to larger dispersion interactions between the aromatic rings but could perhaps be a result of stronger intermolecular H bonding or weaker solvation. It was suggested that adding solubilising groups to the thioureas could overcome this problem and make NMR titrations possible.

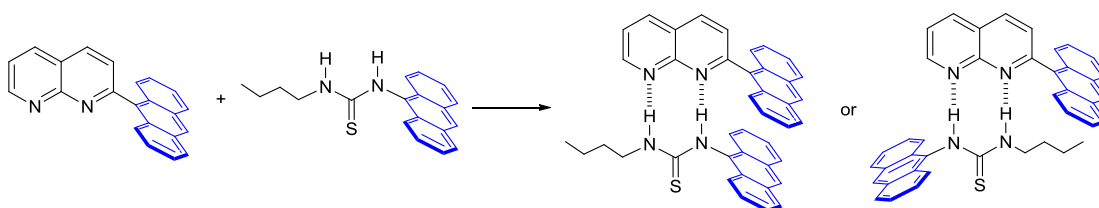


Figure 2.6. Possible complex conformations in the second-generation complex design.

Thus, a second generation model complex was designed. Solubilising groups were introduced into the thioureas to improve solubility (Fig 2.6). However, making the change to unsymmetrical *N*-butyl-*N'*-aryl thioureas introduces a problem with the

complex; two different complexes can be formed upon binding to the naphthyridine (Fig 2.6). One of the complexes contains the desired stacking interaction, but in the other, the two aromatics are on opposite sides of the complex. To overcome this problem the design of the naphthyridine molecules needed to be changed into symmetrical 2,7-diaryl-1,8-naphthyridines (Fig 2.7).

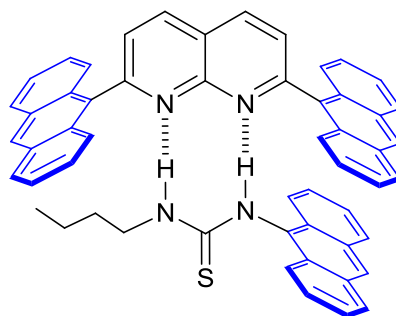


Figure 2.7. Third-generation complex design.

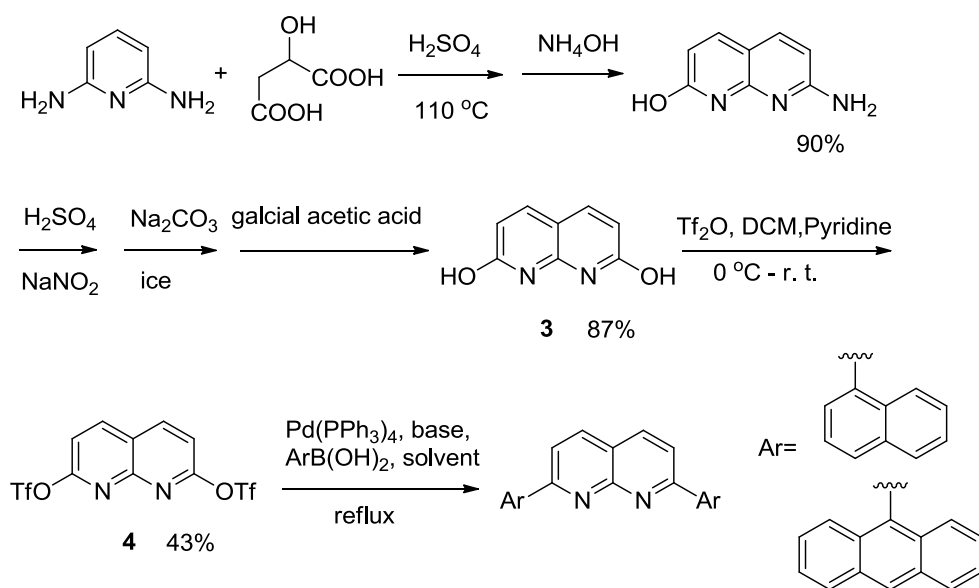


Figure 2.8. Syntheses of symmetrical naphthyridines.

The naphthyridine backbone was obtained in over 90% yield by reaction with the readily available starting materials, 2,6-diaminopyridine and malic acid. The amine was converted to a hydroxyl group through diazotization. Based on the consideration that the reactivity of halides and triflates for the coupling reaction is $I > Br > OTf >> Cl$,²⁴ compound **3** was treated with trifluoromethanesulfonic anhydride to give the corresponding triflate. Boronic acids, which is believed to be more effective than a boronic ester in sterically hindered reactions, was coupled with triflate to give the final product (Fig 2.8). Despite the use of the less hindered boronic acid, the steric hindrance of the large aromatic rings apparently remained, and compound **6** was obtained in a poor yield.

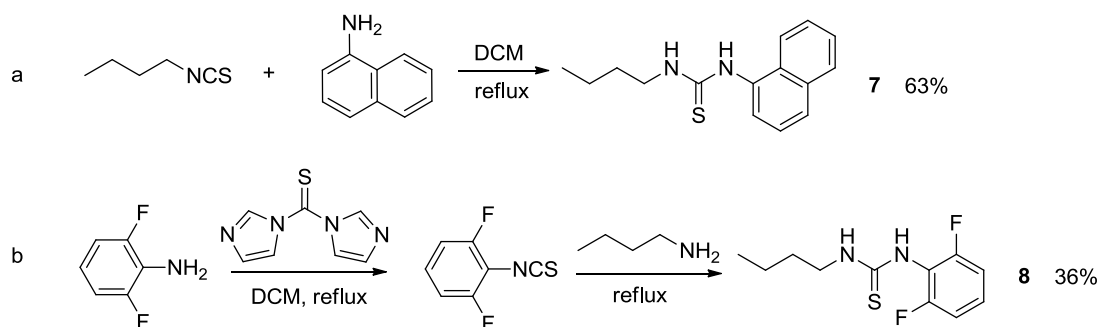


Figure 2.9. Syntheses of unsymmetrical thioureas.

Thiourea was synthesised by refluxing a mixture of butylisothiocyanate and the corresponding amine in DCM overnight (Fig 2.9a). Unfortunately, only compound **7** was successfully made. For the sterically hindered amine, 1,1'-thiocarbonyl diimidazole was employed to convert the bulky amine to isothiocyanate,²⁵ before the butyl amine was added (Fig 2.9b). The solubility of both compounds **7** and **8** was found to be good.

With host and guest in hand, a titration experiment was performed. The limited

solubility of the naphthyridine compound made it hard to cover a large proportion of the binding isotherm. Nonetheless, the binding constant for complex **5•7** was found to be $20\text{-}50\text{ M}^{-1}$, much lower than that of Zimmerman's AA-DD complex (Fig 2.2). Given the similarity of the naphthyridine half of the complex, this suggested that the weak binding may be due to the thiourea. In the solid state, only the *E* conformation was observed by IR spectroscopy in aryl-substituted thioureas.²⁶ Although both *E* and *Z* isomers may exist in the solution, the *E* conformer appears to be more stable due to the presence of an intramolecular hydrogen- π interaction (Fig 2.10). Perhaps one explanation for the low binding constant is that the binding energy upon complexation does not compensate for the energy required to convert the *E* conformer to the *Z* conformer, which is the proper conformation for forming two H bonds to the naphthyridine.

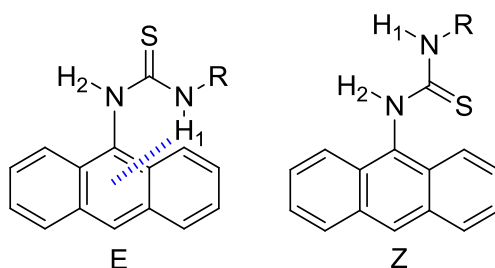


Figure 2.10. *E* and *Z* conformers of *N*-aryl-*N*-butyl thiourea.

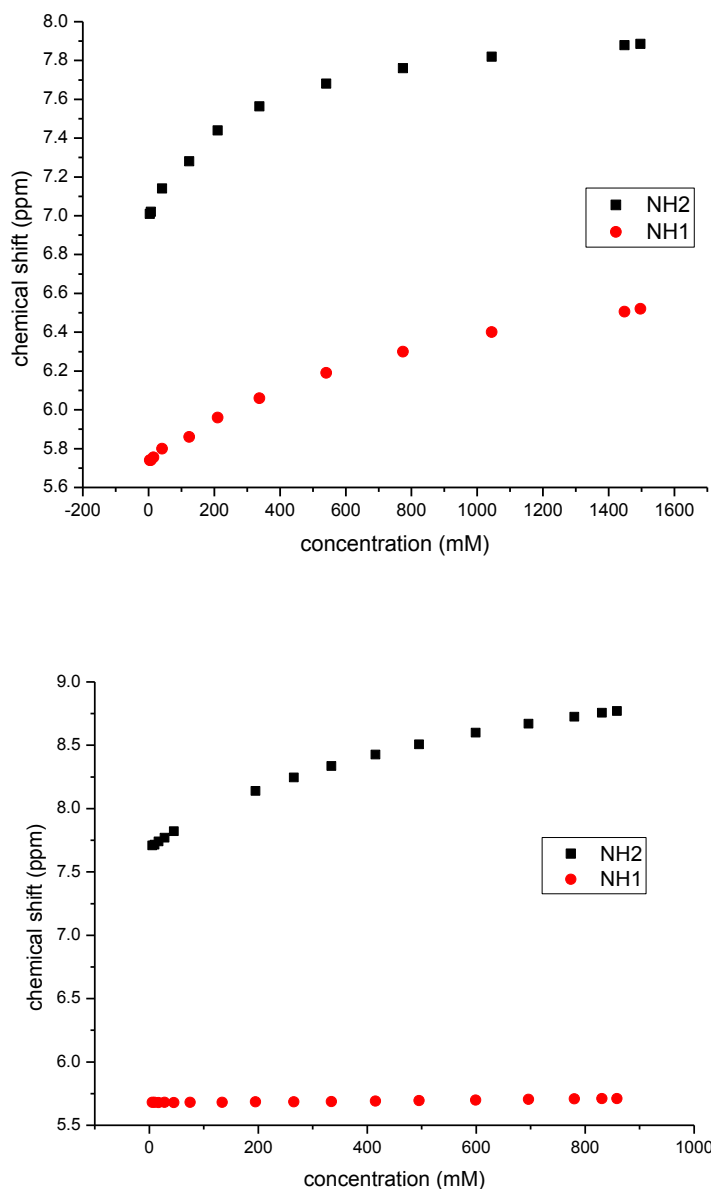


Figure 2.11. NMR dilution of 1-butyl-3-(2,6-difluorophenyl)-2-thiourea **8** (top) and 1-butyl-3-naphthyl-thiourea **7** (bottom).

The NH \cdots π interaction is dominated by electrostatic effects.²⁷ Electrostatic potentials of 2,6-difluorophenyl amine and 1-naphthyl amine were calculated by Spartan to be -45 kJ mol^{-1} and -74 kJ mol^{-1} respectively (DFT/B3LYP/6-31G*). NMR dilution experiments of aryl substituted thioureas showed that NH₁ and NH₂ of

1-butyl-3-(2,6-difluorophenyl)-2-thiourea were shifted upfield as concentration decreases while NH_1 of 1-butyl-3-naphthyl-thiourea was concentration-independent (Fig 2.11). This strongly suggested that the $\text{NH}\cdots\pi$ interaction is stronger in the naphthyl derivative compared to the difluorophenyl derivative, which is consistent with the electrostatic potentials.

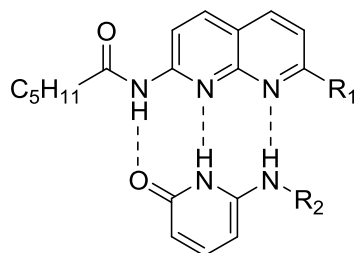


Figure 2.12. Fourth-generation complex design.

In order to cover at least 80% binding isotherm and achieve higher accuracy, complexes with higher binding constant were required for the project. Thus, an additional H-bond was added into the system (Fig 2.12). The upper DAA compound will be referred to a guest compound, and the lower ADD compound as the host from this point on.

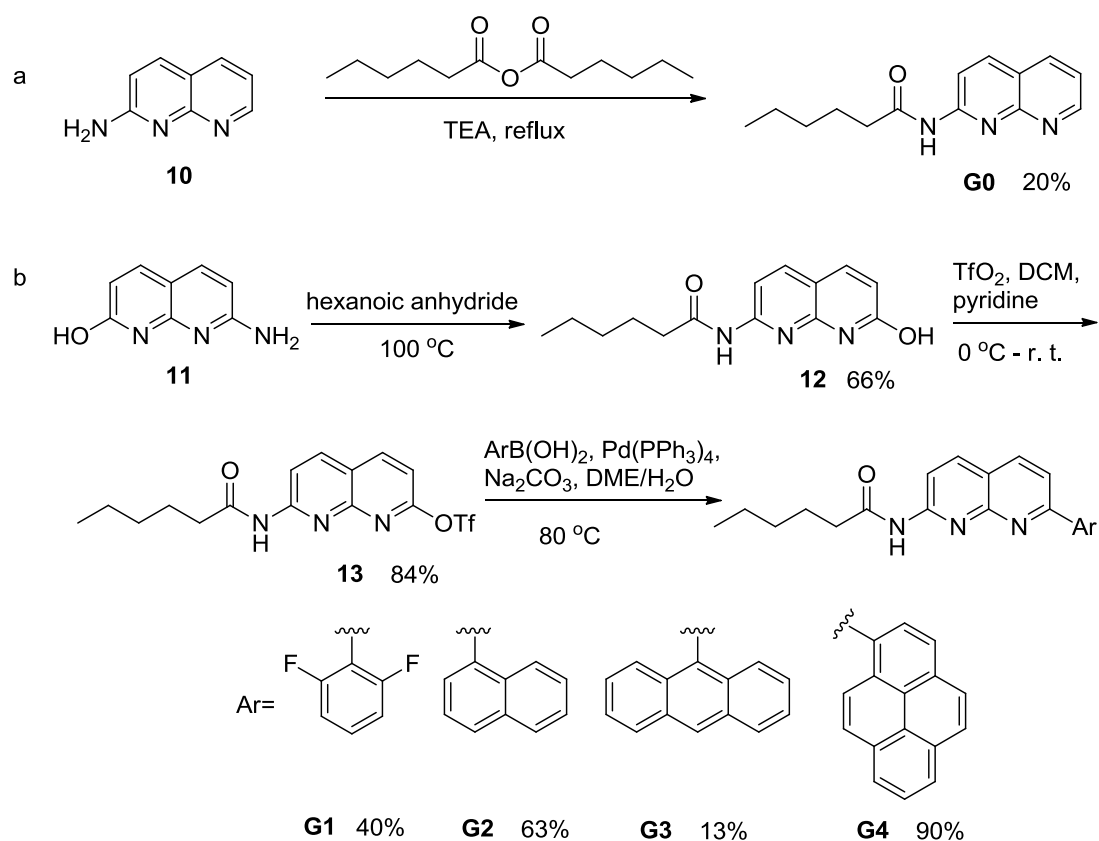


Figure 2.13. Syntheses of (a) control compound **G0** (b) aromatic substituted naphthyridines **G1**, **G2**, **G3**, **G4**.

2-amino-1,8-naphthyridine was refluxed with hexanoic anhydride to give the control compound **G0** (Fig 2.13a). Two steps were involved in making the starting compound **11** following a literature. Then hexanoic anhydride reacts with the amino group to form the amide, this compound is insoluble in most organic solvents, making it easy to purify by filtration. After that the hydroxyl group was converted into the triflate, resulting in a very soluble compound. Finally, a Suzuki reaction was employed to couple the triflate with the corresponding boronic acid (Fig 2.13b). The final products were obtained in moderate to high yield.

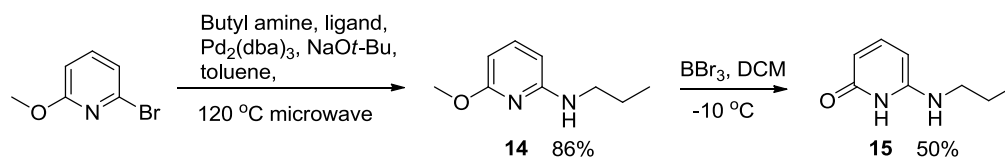


Figure 2.14. Synthesis of compound 15

The ADD host compound is synthesised in two steps; the starting bromide compound was coupled with butyl amine under microwave conditions using Pd catalyst, followed by demethylation using BBr₃. This reaction required an excess of BBr₃ and three days reaction time to achieve just 30% completion (Fig 2.14). The work up was also unpleasant due to the large amount of unreacted BBr₃. This design was abandoned based on the consideration of synthetic challenges and the difficulty in introducing a suitable solubilising group.

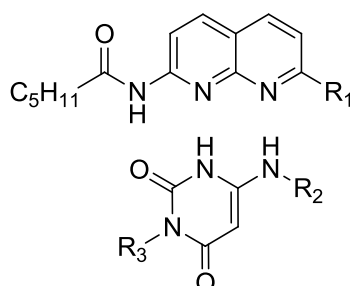


Figure 2.15. Fifth-generation complex design.

Retaining the same guest compound, a uracil host was designed to replace the lower ADD half of the complex. This design keeps three consecutive H-bonds, but adds an alkyl solubilising group (Fig 2.15).

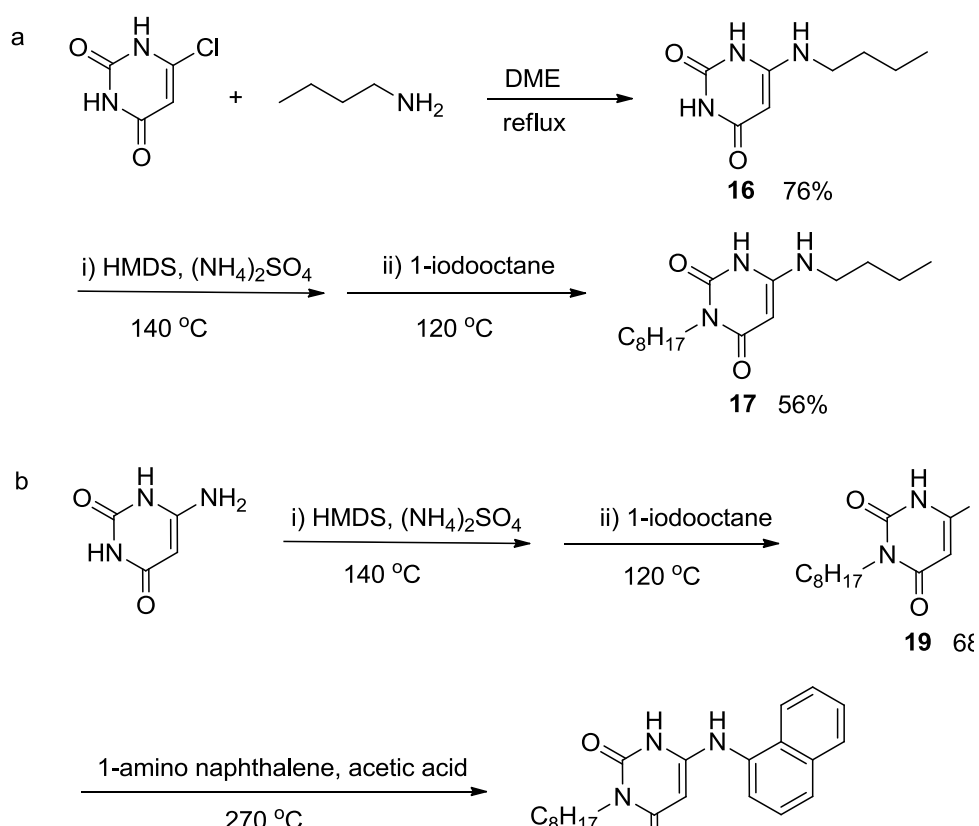


Figure 2.16. Syntheses of uracils.

6-Chlorouracil underwent nucleophilic substitution with the butyl amine, and was then reacted with iodooctane to give the final compound. However, when this route was applied to aminonaphthalene, the reaction was slow and gave a mixture of starting material and product, which was hard to separate (Fig 2.16a). Thus, an alternative route was explored (Fig 2.16b). The solubilising group was added first, and then the product was suspended with aminonaphthalene in acetic acid and refluxed overnight. The precipitate obtained was mostly product which was then recrystallised from hot methanol. The solubility of the compound was still found to be very low despite the long alkyl substituent.

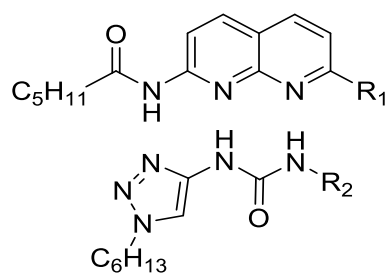


Figure 2.17. The final complex design.

At the same time, another ADD host featuring a five-membered heterocyclic urea was synthesised (Figure 2.17). Previous studies showed that this kind of ADD host were able to form complexes with DAA guests with binding constants in the range of 10^3 - 10^4 M^{-1} .²⁸

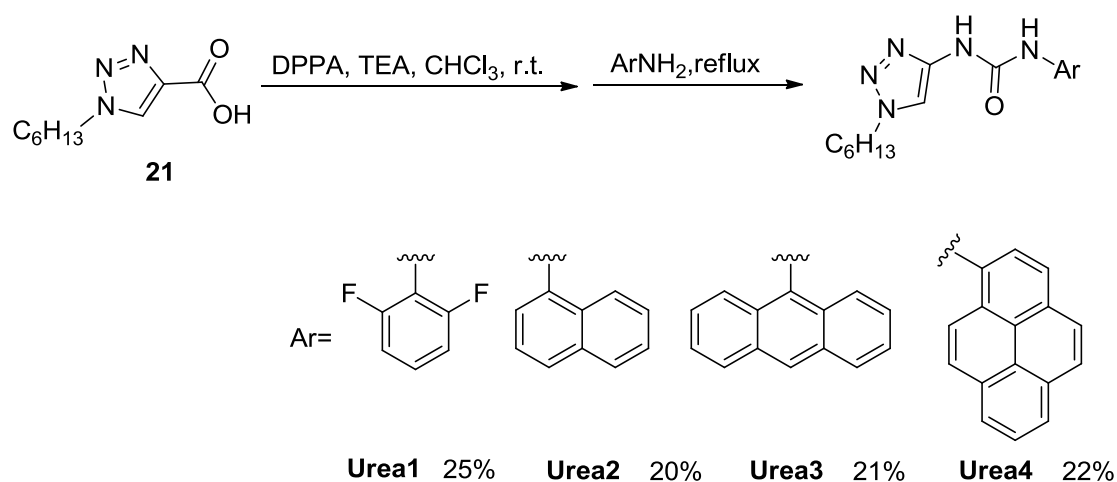


Figure 2.18. Syntheses of five-membered heterocyclic ureas.

The starting compound **21** was synthesised via three steps in high yield. Carboxylic acid was reacted with DPPA to yield carbonyl azide, which was rearranged into the cyanate upon heating before undergoing the reaction with amine. The other urea derivatives were synthesised without difficulty, although the yields were not good over both steps (Fig 2.18). Initial attempts to make the control urea (**Urea0**) via the

same route failed, because the alkyl amine was more reactive than the aromatic amine, it would react with carbonyl azide directly.

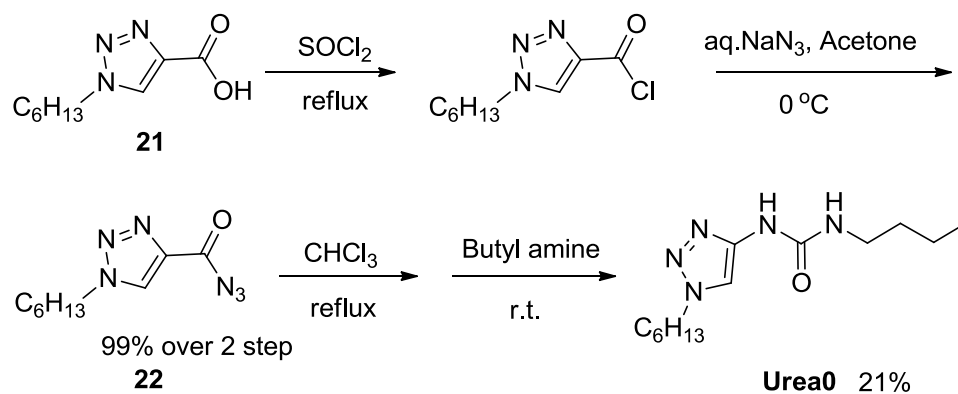


Figure 2.19. Synthesis of control **urea0**

Thus, conditions were required that allowed the carbonyl azide to rearrange before the butyl amine was added to the reaction. Column chromatography was needed to separate the carbonyl azide when using DPPA in the previous method, and the yield was low. Thus, an alternative, but simple and efficient one-pot two-step strategy was applied to make the azide (Fig 2.19). The carbonyl azide was heated in chloroform to give the cyanate, before addition of the butyl amine to yield the final compound.

2.4 Results and Discussion

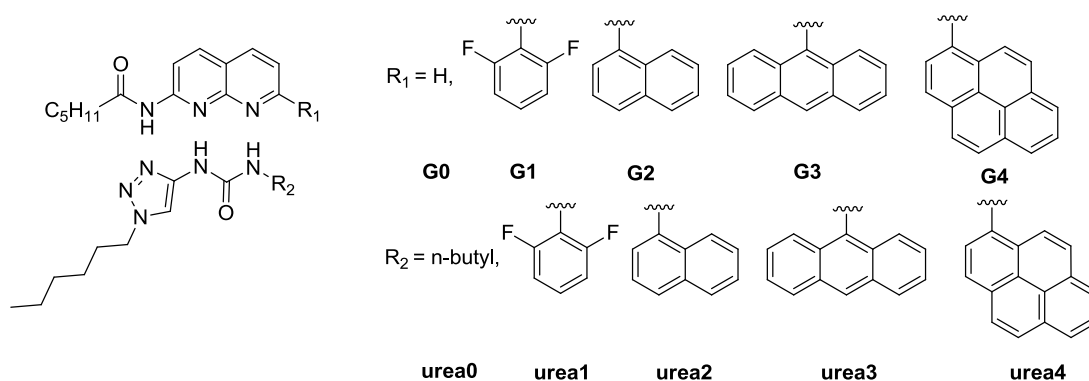


Figure 2.20. Compounds studied in the following section: **G0**, **G1**, **G2**, **G3**, **G4** and **Urea0**, **Urea1**, **Urea 2**, **Urea 3**, **Urea 4**

After several attempts, the complex design shown in Figure 2.20 was chosen for the study of π - π interactions. The synthetic routes provided access to many different combinations of host and guest compounds with varying aromatic surfaces.

2.4.1 Dilution experiments

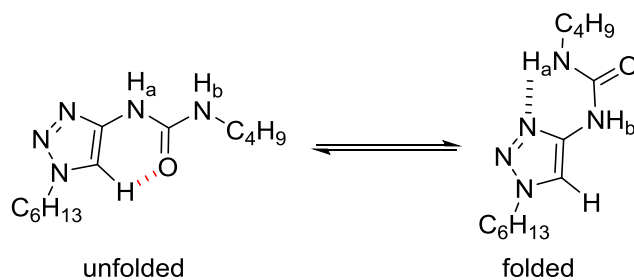


Figure 2.21. Unfolded and folded state of the ureas employed in this study, showing the formation of intramolecular H-bonds.

The six-membered heterocyclic ureas suffer from steric clash between the aromatic CH and the urea O, and prefer the folded state.²⁹ In contrast, the ureas attached to five-membered rings have been shown to favour the unfolded state due to the

intramolecular H-bond between the aromatic CH and urea O (shown in red in Figure 2.21).²⁸ Owing to this pre-organisation, the binding constant of a quadruple H-bond complex has been shown to increase by a factor of 100 when switching from six-membered heterocyclicureas to five-membered heterocyclicureas.²⁹ The ureas adopted in our system have similar properties (Fig 2.22). Computations of the minimised geometries of **ureas0-4** were performed at the B3LYP/6-31G* level using *Spartan*. The planarity of the urea with the heterocyclic ring indicates that the triazole CH does not exert any steric strain against the O atom of the urea (Fig 2.22).

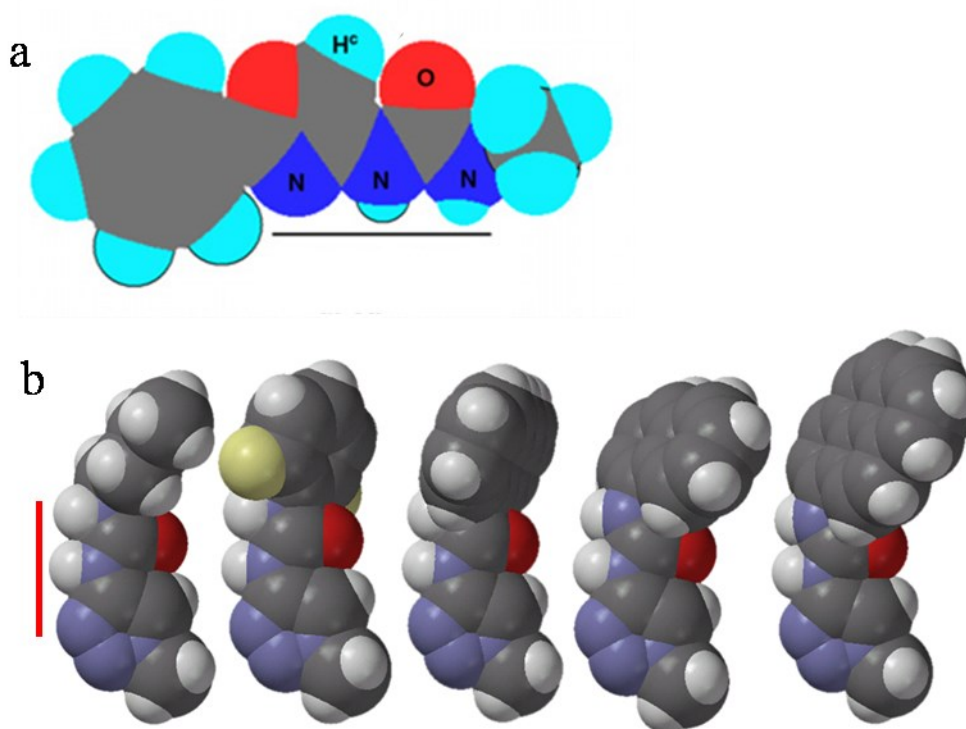
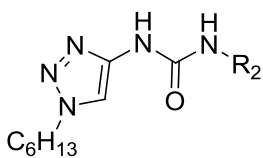
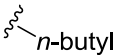
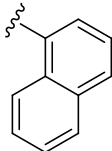
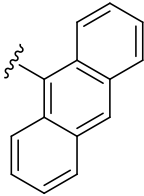


Figure 2.22. a) Structure of the previously reported unfolded 1-Octyl-3-(2-phenyloxazol-4-yl)urea, the octyl group was replaced by methyl group for computational simplicity, and the geometry was calculated with DFT at the B3LYP/6-31G** level.²⁸ b) Optimised Spartan models of **ureas 0-4** employed in our study.

Initially, dilution experiments were performed in CDCl_3 , however the dimerisation constants of the ureas were found to be relatively high. For example, the dimerisation constant of urea **1** was determined to be 622 M^{-1} in CDCl_3 . However, the addition of 5% (v/v) d_3 -MeCN to CDCl_3 , reduced the dimerisation by an order of magnitude (Table 2.1). Therefore, this 5% (v/v) d_3 -MeCN/ CDCl_3 solvent mixture was used in all subsequent studies involving these compounds. The dimerisation constant of **urea 4** could not be determined due to the low solubility of this compound ($< 2\text{mM}$ in CDCl_3).

Table 2.1. Dimerisation constants of ureas obtained from dilution experiments. Dilution experiments in 5% (v/v) d_3 -MeCN/ CDCl_3 were performed twice and errors shown are twice the standard error.

				
	Urea 0	Urea 1	Urea 2	Urea 3
$K_d (\text{M}^{-1})$	60 ± 14	60 ± 6	55 ± 3	234 ± 86

During the dilution experiments, only the chemical shift of NH_a experienced significant downfield shift while the other chemical shifts were only slightly affected. The fact that the NH_b signal was not seen to move upon dilution excluded the folded-folded dimer and unfolded-folded dimers shown in Figure 2.23. This also indicated that the urea preferred the unfolded form as suggested in the earlier discussion.

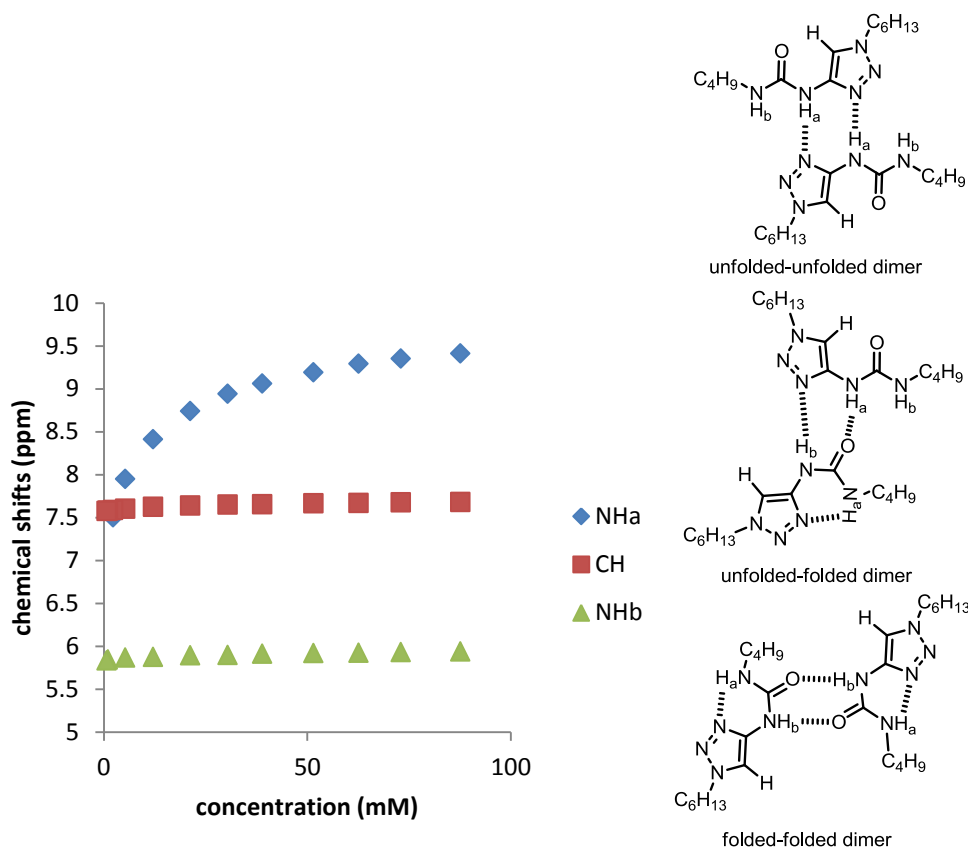


Figure 2.23. Chemical shifts of **urea0** upon dilution in 5% d_3 -MeCN/ $CDCl_3$ mixture (left) and possible dimerisation complexes (right).

Naphthyridine-based guests are frequently used in H-bond complexes.^{19,29-30} Crystal structures in the CCDC database reveal that the amide in the naphthyridine compounds prefer the conformation shown in Fig 2.24. The H-bond donor and acceptors are found to be co-planar, providing a good geometric match with the urea hosts. Dilution of the guest compounds gave very small dimerisation constants, which therefore had a negligible influence on the much larger association constants of the complexes employed in this study (Table 2.2).

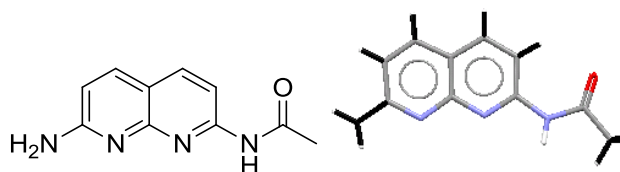


Figure 2.24. Crystal structure of naphthyridine derivatives³¹ (CCDC 236719)

Table 2.2. Dimerisation constants of guest compounds.

	G0	G1	G2	G3	G4
K_d (M ⁻¹)	1.49	0.52	0.84	1.03	0.76

2.4.2 Complex conformation analysis

Compared to Hunter's zipper complexes, which have been previously used to examine aromatic stacking interactions,¹⁸ the complexes of the present study are more rigid and conformationally less complicated. The pre-organisation afforded by the H-bond components of the host and guest compound helps in forming complexes of the desired geometry. To further analyse the conformations of these complexes, M06/6-31G* and DFT/6-31G* calculations were performed on all complexes using Spartan. The three NH...N H bonds had lengths of around 2Å, while the stacked aromatic planes were found in offset or face-to-face stacking with an interplane separation of ~3.5Å. An overlay of these M06-minimised structures shows that the complexes have similar geometries (Fig 2.25), thus, satisfying the structural requirements performing a double-mutant cycle analysis.²⁰

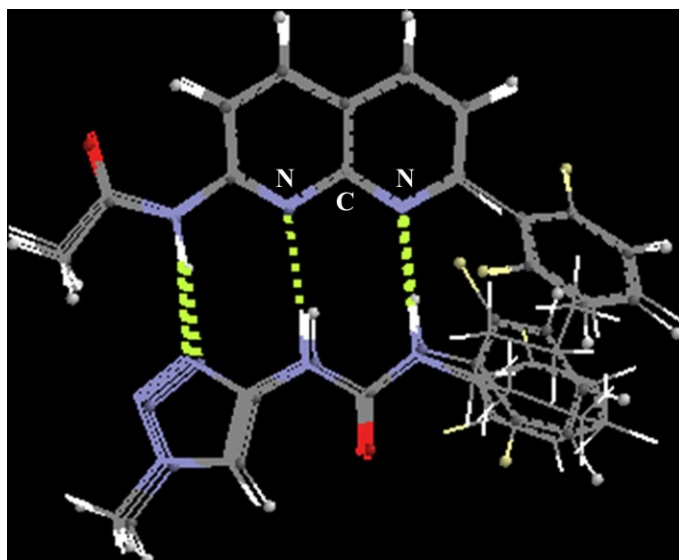


Figure 2.25. Overlapping Spartan calculated complexes (**G0-Urea0**, **G0-Urea1**, **G1-Urea0**, **G1-Urea1**). Structures were aligned using the heavy atoms of N-C-N in parts of the complex (shown in figure)

2.4.3 Physicochemical parameters for analysing aromatic interactions

Electrostatic surface potentials provide a visual and detailed view of any subtle changes in the electrostatic properties of the aromatic surfaces investigated in this study. ESPs of the molecules were calculated at the DFT/B3LYP/6-31G* level. As shown in Figure 2.26, the ESPs were not evenly distributed across the aromatic surfaces, which could complicate the interpretation of the aromatic stacking interactions measured in this study.

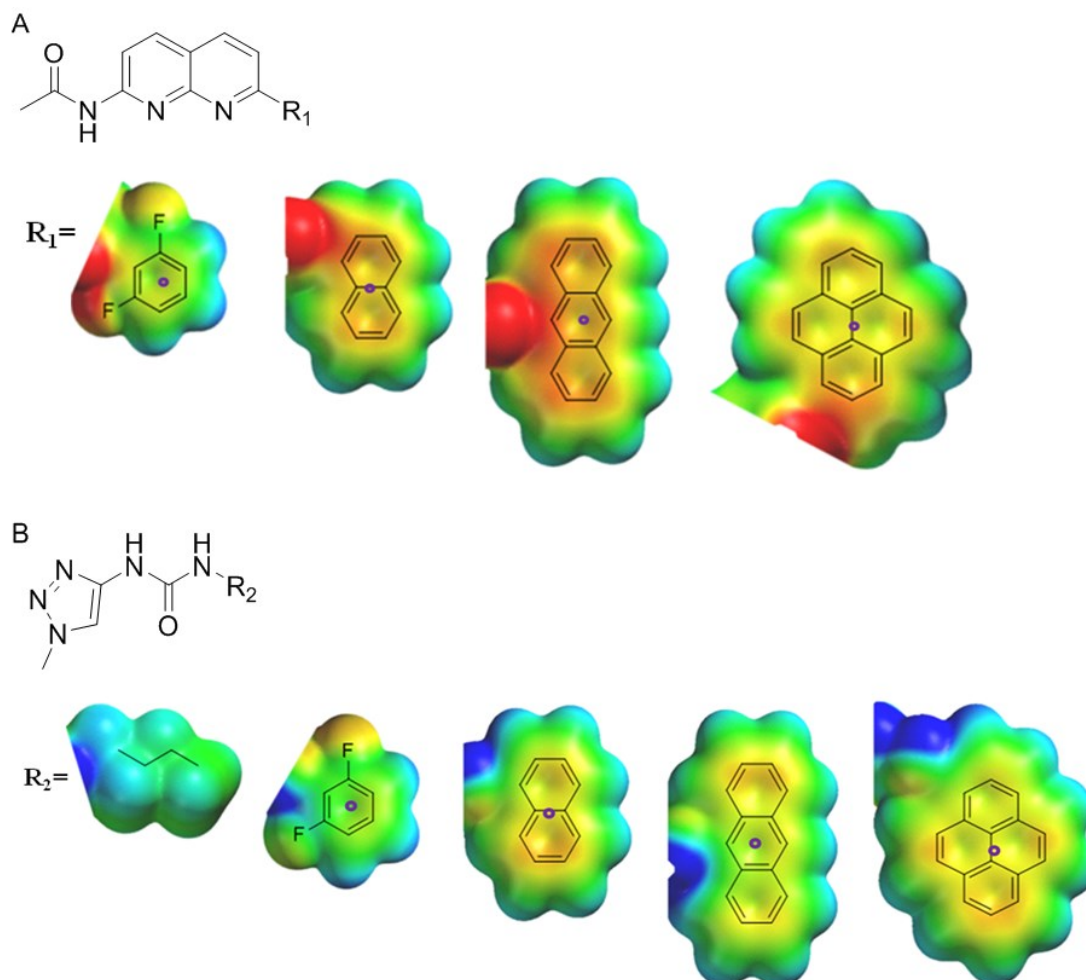


Figure 2.26. ESPs of simplified guest and host molecules (the long alkyl chains were replaced with methyl groups). ESP scales were set to -120 kJ/mol to $+120$ kJ/mol for comparison. Purple dots are the ring center where ESPs are measured as listed in Table 3.

Nonetheless, with the exception of the difluorinated aromatics, the ESPs varied surprisingly little on each half of the complexes (Table 2.3). Other physicochemical properties for these aromatic groups were also calculated using *Spartan*. Polarisability is a parameter for considering dispersion interactions, while differences in surface areas should affect dispersion interactions as well as solvophobic effects.

Table 2.3. Calculated physical properties of guest and host compounds

aromatics	ESP (kJ mol ⁻¹) ^a	Dipole moment (debye) ^b	Polarisability (Å ³) ^b	Surface area (Å ²) ^c
Guest				
Difluorobenzene	-31	0.82	9.25	63
Naphthalene	-68	0.30	14.66	81
Anthracene	-70	0.32	22.19	104
Pyrene	-61	0.42	24.91	110
Host				
Difluorobenzene	-9	0.62	9.31	d
Naphthalene	-58	1.67	14.73	d
Anthracene	n.d.	2.07	22.46	d
Pyrene	-57	2.18	25.42	d

^aESP values are for the ring centre in kJ mol⁻¹ as shown in Figure 26. ^b Dipole moments and polarisability are calculated for the methyl or amino substituted aromatics, depending on whether it is host or guest compound. Polarisabilities are calculated using the AM 1 semiempirical method. ^cHalf of the calculated aromatic surface areas and surface areas are values for the unsubstituted aromatics. ^dthe surface area is the same as in the guest molecule for the corresponding aromatic.

2.4.4 Binding studies

Binding constants were obtained by ¹H-NMR titration experiments. The urea hosts were dissolved in 5% *d*₃-MeCN/CDCl₃ in the concentration range of 0.7-3.8 mM, 500 µl of this solution was transferred into a capped NMR tube. The naphthyridine guest

was dissolved in the stock host solution and titrated into the NMR tube. In this way, the concentration of urea was kept constant during titration. ^1H -NMR spectra were recorded after each addition.

Job plots analyses were performed with all complexes involved in this study. It was confirmed that the DAA-type guest can bind to the ADD-type host in a 1:1 binding stoichiometry (Fig 2.27).

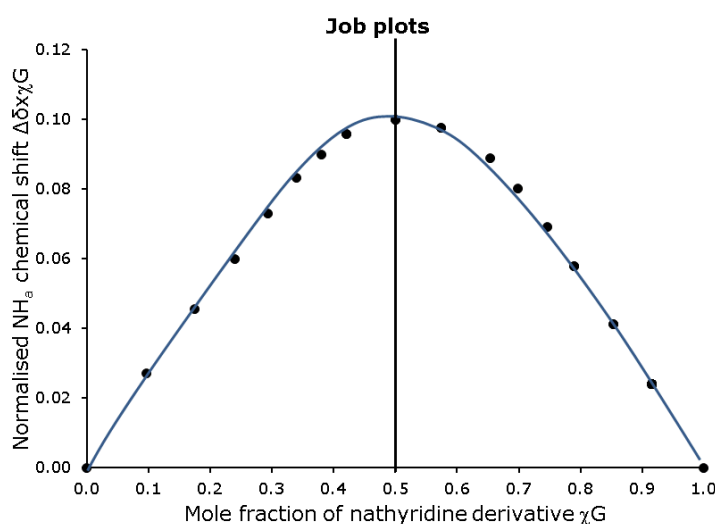
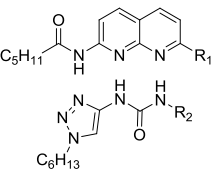
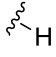
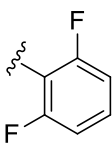
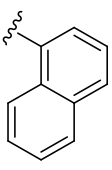
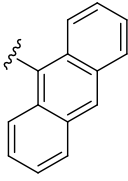
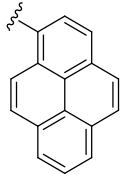
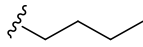
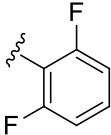
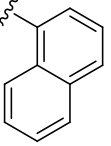
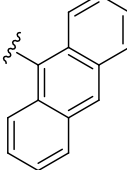
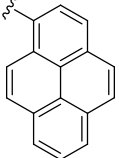


Figure 2.27. Job plot of **G0** with Urea **2** by ^1H -NMR titration experiments in 5% d_3 -MeCN/ CDCl_3 .

During the titration, the chemical shifts of NH_a and NH_b moved downfield, indicating formation of $\text{NH}\cdots\text{N}$ H bonds. The butyl and aromatic signals on the ureas moved upfield due to the shielding of the aromatic rings on the guest. All the NMR observations supported DAA-ADD complexation. Due to the good solubility of the guest compound, all titrations reached saturation, giving higher than 96% binding in all cases, and fitting errors were within 4%.

Table 2.4. Binding constants (K_a in M^{-1}) and free energies (ΔG in $kJ\ mol^{-1}$) measured in 5% (v/v) d_3 -MeCN/ $CDCl_3$.

		Guest 				
	G0	G1	G2	G3	G4	
Host						
Urea0 	2180 ± 340 -19.0 ± 0.4	980 ± 260 -17.0 ± 0.7	4205 ± 50 -20.7 ± 0.0	7005 ± 1190 -21.9 ± 0.4	2810 ± 560 -19.7 ± 0.5	
Urea1 	20700 ± 4200 -24.6 ± 0.5	6060 ± 1100 -21.5 ± 0.5	17150 ± 2100 -24.2 ± 0.3	29100 ± 6200 -25.5 ± 0.5	15100 ± 2800 -23.8 ± 0.5	
Urea2 	5887 ± 1472 -21.5 ± 0.6	3327 ± 1220 -20.0 ± 1.0	4200 ± 580 -20.7 ± 0.3	8873 ± 1437 -22.5 ± 0.4	5265 ± 1230 -21.2 ± 0.6	
Urea3 	n.d.	n.d.	n.d.	n.d.	n.d.	
Urea4 	10510 ± 1180 -22.9 ± 0.3	6647 ± 2110 -21.7 ± 0.8	10220 ± 760 -22.9 ± 0.2	53300 ± 14800 -26.9 ± 0.7	27567 ± 9031 -25.3 ± 0.9	

Titration experiments were repeated at least twice. Errors are twice the standard error .n. d. not determined

Association free energies ranged from $-19.0 \text{ kJ mol}^{-1}$ to $-26.9 \text{ kJ mol}^{-1}$ for all of the complexes, which lie in the energy range of other triple H-bond complexes (Table 2.4).³² Association energies for some **Urea3** complexes could not be determined due to the heavy overlap of NMR spectra. Although other methods like UV-vis spectrometry are attempted, the spectra overlap problem still prevented the extraction of thermodynamic data. Generally, the **G1** complexes were the weakest across all host complexes, this could possibly be due to the partially electronegative fluorine exerting unfavourable $F \cdots \pi$ interactions.

Among the same host series, the patterns of binding energies were found to be very similar, indicating similar conformations in the complexes (Fig 2.28). The largest difference in the binding energies across all π - π stacking complexes are less than 7 kJ mol^{-1} . In stark contrast, high-level computations that take dispersion interactions into account have predicted each 6-membered aromatic stacking interaction to contribute $12\text{-}15 \text{ kJ mol}^{-1}$.^{12,33} This would mean that the pyrene-pyrene complex in our study would have a gas-phase stacking interaction of up to 60 kJ mol^{-1} ! Clearly, the very large favourable dispersion contributions to stacking interactions are mostly washed out by competitive dispersion interactions with the solvent in this experimental study.

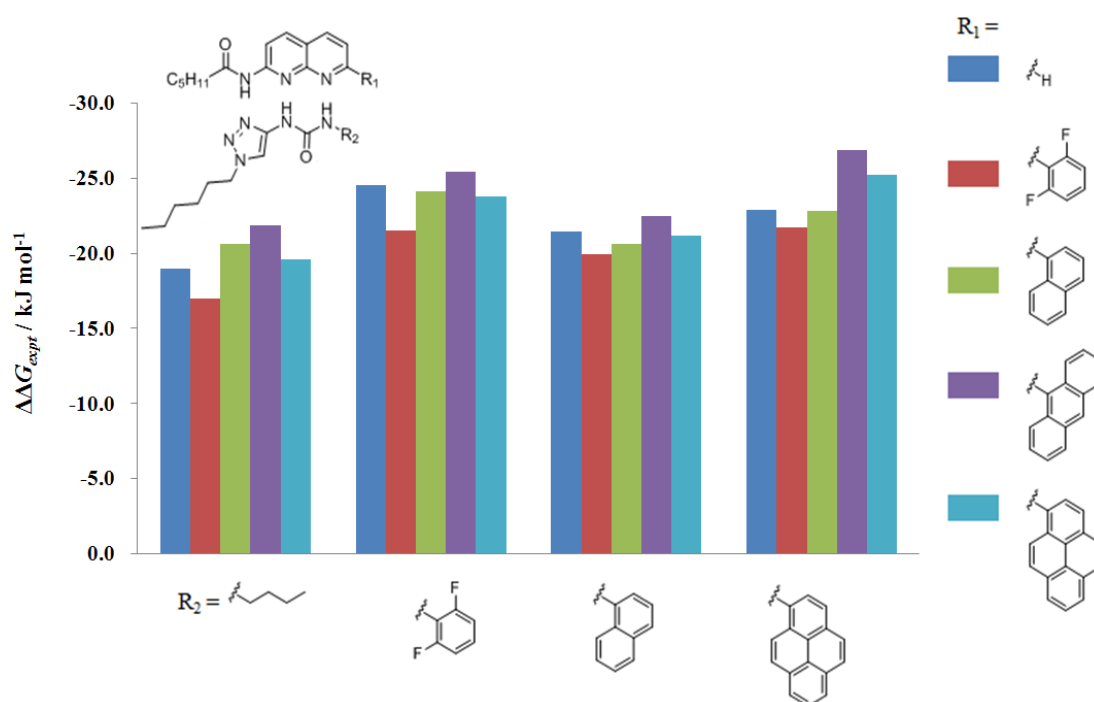


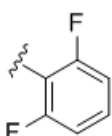
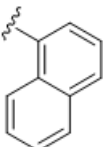
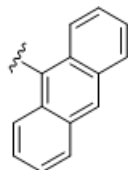
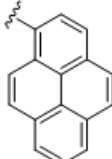
Figure 2.28. Association free energies were shown in bar graph as group of host.

Stacking interactions dissected using the double mutant cycle approach are listed in Table 2.5. The dissected interaction energies are relatively modest and range from -1.7 kJ mol^{-1} to $+2.2 \text{ kJ mol}^{-1}$, and are comparable with interaction energies that have been previously measured for small aromatic stacking interactions.³⁴ For stacking interactions involving small aromatics like 2,6-difluorophenyl (data in the red column in Table 2.5), it is likely that dispersion does not play a large role and electrostatic effects may take control. It was demonstrated by Houk that stacking interactions in small aromatics in solution are not controlled by dispersion,¹⁷ and this is supported by Gung's,^{14,35} and Hunter's experimental studies.^{18,34} With the exception of the data marked in red, $\Delta\Delta G$ becomes more favourable (or less repulsive) as the size of the aromatic group is increased. It can be seen that the difference is small in row 1 where there is only one aromatic ring that can interact with the polyaromatic hydrocarbons (PAH). This difference becomes larger when

naphthalene interacts with PAH. While in the pyrene complexes (row 4), the difference is the most exaggerated, leading to favourable stacking interactions. This observation does not correspond with the ESP changes of the aromatic rings. Naphthalene and pyrene hosts have almost identical ESPs, but have opposite signs for their interaction energies with large aromatics (+1.8 vs -1.1 kJ mol^{-1} , and +0.9 vs -1.7 kJ mol^{-1}). However, the result could possibly be explained by solvophobic or dispersion effects. On one hand, solvophobic driven interactions should increase as the contact areas increase. On the other hand, dispersion interactions depend on both contact surface area and the polarisability of the interacting rings. Within our study, it is very hard to dissect solvophobic and dispersion effects since all measurements have been performed in one solvent. The computed contact surface areas for naphthalene-naphthalene and naphthalene-pyrene interactions are identical (27 \AA^2), however, the naphthalene-pyrene interaction is more favourable than naphthalene-naphthalene. The difference is that pyrene has a larger polarisability, thus, it might be expected that the interaction energy may have a larger contribution from dispersion. However, the difference is just within the error of the experiment. Thus, any contribution from dispersion is likely to be small. Notably, the aromatic stacking energies measured in this study do not show any good correlation with ESPs, polarisability, surface areas or contact surfaces (Fig 2.29).

Table 2.5. Aromatic stacking energies from double mutant cycles are in kJ mol^{-1} . Electrostatic surface potential of aromatic centre are shown beside each aromatic. Quoted errors are calculated as

$$\delta\Delta G_{\text{DMC}} = \sqrt{(\delta\Delta G_{\text{A}})^2 + (\delta\Delta G_{\text{B}})^2 + (\delta\Delta G_{\text{C}})^2 + (\delta\Delta G_{\text{D}})^2}$$

	-31	-68	-70	-61
				
-9	+1.0 ± 1.0	+2.1 ± 0.7	+2.0 ± 0.9	+1.4 ± 0.9
-58	-0.5 ± 1.4	+2.2 ± 0.8	+1.8 ± 0.9	+0.9 ± 1.1
-57	-0.8 ± 1.1	+1.7 ± 0.5	-1.1 ± 0.9	-1.7 ± 1.1

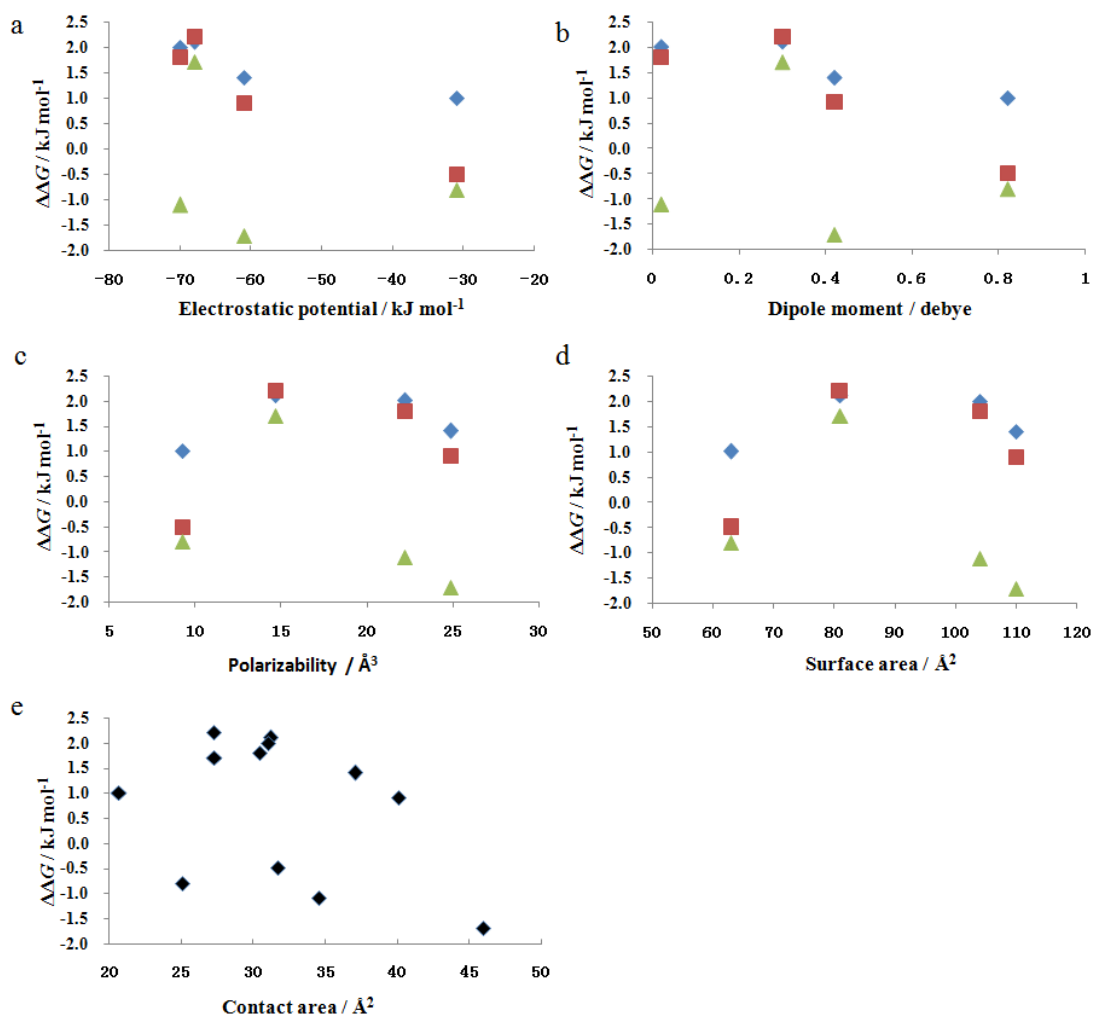


Figure 2.29. Stacking energies correlation with a) ESP, b) dipole moment, c) polarisability and d) surface area. Blue rhombus are **Urea1** series; red square are **Urea2** series; green triangles are **Urea3** series; e) All stacking energies are plotted against contact areas.

Clearly, stacking behaviour in solution is complicated and cannot be characterized by a single parameter, and it seems probable that stacking energies in solution are governed by the interplay of electrostatic, dispersion and solvophobic interactions.

One way in which electrostatic and dispersion effects can be taken into account is to perform calculations on the complexes examined in this study. To reduce the

computational cost of these relatively large complexes, hexyl groups on the host and guest molecules were replaced with methyl groups (Fig 2.30). Complexes were computed with DFT using the M06 and B3LYP methods. Since B3LYP is unable to take dispersion interactions into account,³⁶ it is not recommended for computations on aromatic interactions. Recent research has also pointed out the problems with using B3LYP/6-31G* methods in thermochemical calculations.³⁷ The B3LYP results predict large unfavourable stacking energies and a moderate correlation with the experimental double-mutant cycle results ($R^2=0.71$). M06 method gave a slightly poorer correlation with $R^2=0.62$ (Fig 2.31). However the predictions for attractive or repulsive interactions are almost correct in all cases except for the three stacking energies marked in red in Table 2.6. The key distinction compared to the B3LYP calculations is that the M06 method is able to account for medium-range correlation energy or "dispersion-like" energy.³⁸ Grimme's³³ computational finding that dispersion forces become important for large aromatics, is not obvious in our solution study. Dispersion interaction calculations are dramatically overestimated compared to the experimental results obtained in solution, especially for the large aromatics. A pyrene...pyrene interaction is only worth 1.7 kJ mol^{-1} in our study, while the M06 computations gave 23.0 kJ mol^{-1} . This result further supports our hypothesis that dispersion interactions are largely cancelled in solution.

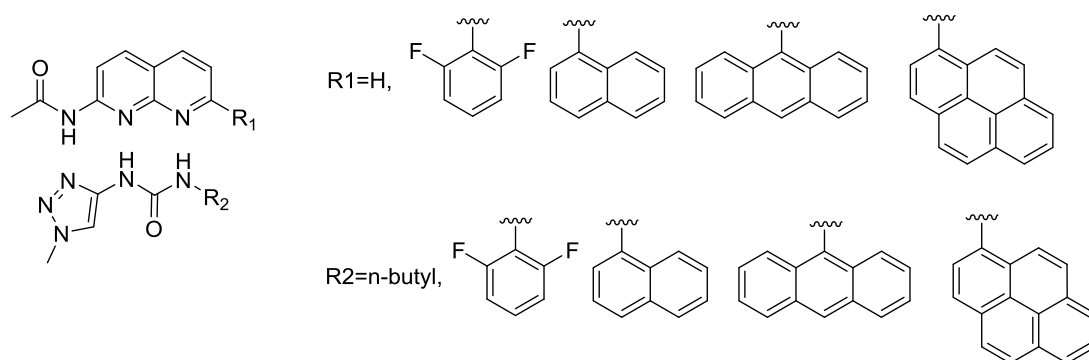
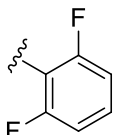
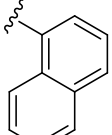
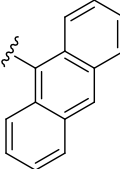
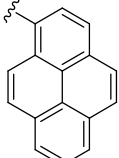
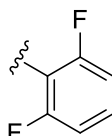
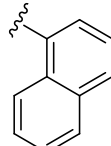
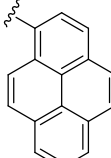


Figure 2.30. Simplified model for Spartan computations on complex energies. The long alkyl chains were replaced by methyl groups.

Table 2.6. Computation double-mutant cycle results. M06 results are shown in roman. B3LYP results are shown in italics. All energies are in kJ mol^{-1} . Aromatic contact areas are shown in parentheses (in \AA^2). Contact area = sum of two individual aromatics surface areas – surface area in the stacked conformation.

				
	3.3 7.5 (21)	3.4 9.9 (31)	2.7 10.7 (31)	0.3 10.5 (37)
	-4.1 1.5 (32)	2.2 6.1 (27)	<i>-2.2</i> 11.8 (30)	<i>-5.9</i> 6.0 (40)
	-3.5 2.1 (25)	<i>-6.2</i> 5.6 (27)	-24.4 3.8 (35)	-23.0 -3.4 (46)

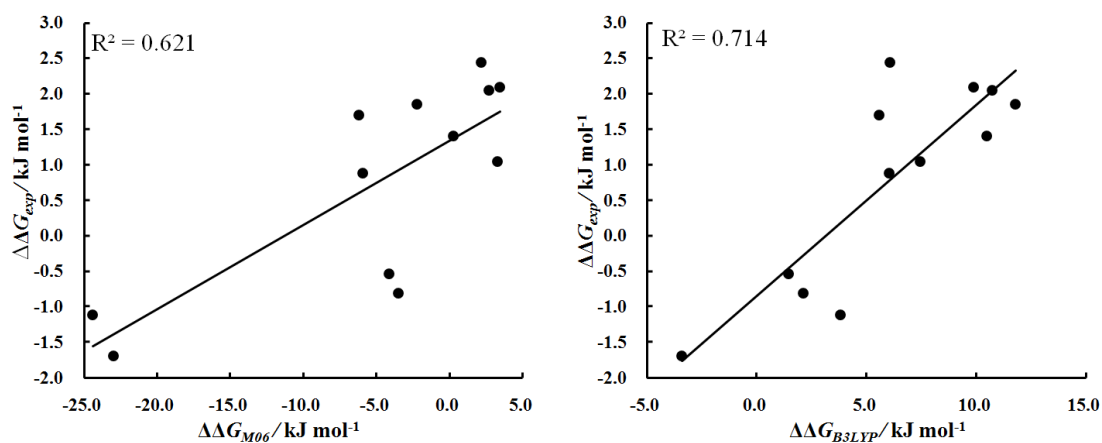


Figure 2.31. M06 (left) and B3LYP (right) computational DMC results correlate against experimental DMC data.

2.5 Conclusion

In summary, a new class of supramolecular complex has been developed for the measurement of π - π interactions in solution. Conformational analysis confirmed that this model is valid for examining stacking geometries. Comprehensive thermodynamic data were obtained for stacking interactions involving polycyclic aromatic rings in solution for the first time. Interaction energies are notably small compared to computational results that take dispersion forces into account. This is the result of the interplay of electrostatic, solvent and dispersion effects. Dispersion is underestimated by B3LYP method while they are overestimated by M06 method.

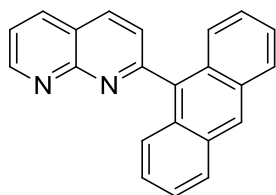
2.6 Experimental Section

All compound numbers refer to compounds exclusively as presented in this chapter.

John Brazier developed the synthetic route to compound **21**. He also tried other synthetic route of some host compounds which are not showed in this thesis. I

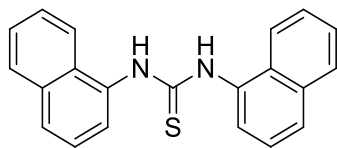
resynthesised compound **21** and synthesised all other compounds, and performed all experiments unless otherwise specified.

All compounds were purchased from *Sigma-Aldrich*, *VWR* or *Fluoro Chem*. Melting points were determined using Stuart melting apparatus and are reported uncorrected. NMR dilution and titration experiments were performed on either a BrukerAvance400 MHz or 600 MHz spectrometers. Mass spectra were obtained by the University of Edinburgh mass spectrometry service. NMR dilutions and titrations were fitted using an Excel spreadsheet provided by Prof. Christopher A. Hunter. Calculations were performed using *Spartan '08*.

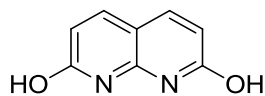


2-Anthracen-9-yl-[1,8]naphthyridine (1).³⁹ A mixture of 2-aminonicotinadehyde (91.5 mg, 0.75 mmol), 9-acetylanthracene (165.1 mg, 0.75 mmol) and a drop of 10% ethanolic potassium hydroxide in ethanol (10 mL) was refluxed until all starting material had disappeared as indicated by TLC. After cooling, the precipitates were collected by filtration and purified by chromatography on silica gel. Product was obtained as red solid (10 mg). Yield 4%. m.p. 180-183°C ¹H NMR (500 MHz, CDCl₃) δ 9.23 (dd, *J* = 4.1, 1.8 Hz, 1H), 8.58 (s, 1H), 8.37 (d, *J* = 8.2 Hz, 1H), 8.34 (dd, *J* = 8.2, 1.9 Hz, 1H), 8.06 (d, *J* = 8.5 Hz, 2H), 7.70 (d, *J* = 8.2 Hz, 1H), 7.66 (d, *J* = 8.8 Hz, 2H), 7.59 (dd, *J* = 8.1, 4.3 Hz, 1H), 7.49 – 7.44 (m, 2H), 7.37 – 7.34 (m, 2H). ¹³C NMR (126 MHz, CDCl₃) δ 162.48, 156.31, 154.11, 137.14, 137.07, 134.57, 131.32,

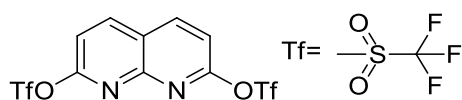
129.89, 128.51, 128.04, 126.07, 126.05, 126.04, 125.22, 122.47, 121.68. MS (EI) m/z 306.1 (M^+)



1,3-di(naphthalen-1-yl)thiourea (2).⁴⁰ A mixture of 1-naphthylamine (3.58 g, 25 mmol), CS_2 (2.4 mL, 40 mmol) and DMAP (0.3 g, 2.5 mmol) in 5 mL dry ethanol was refluxed at 78 °C for 1 day. After cooling, the precipitate was filtered and washed with ethanol. 1.64 g white solid. Yield 40%. Compound was reported in Ref⁴¹ m.p. 205-206°C 1H NMR (360 MHz, d_6 -DMSO: $CDCl_3$ =1:1) δ 9.64 (s, 2H), 8.04 (d, J = 8.2 Hz, 2H), 7.87 (d, J = 8.0 Hz, 2H), 7.78 (d, J = 8.2 Hz, 2H), 7.60 – 7.46 (m, 8H). ^{13}C NMR (63 MHz, DMSO) δ 183.19, 135.63, 134.27, 130.59, 128.46, 127.26, 126.52, 126.47, 126.19, 126.02, 123.54.

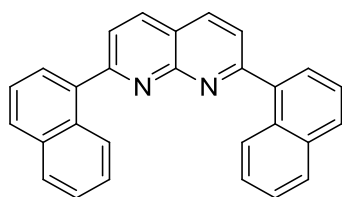


1,8-naphthyridine-2,7-diol (3) was synthesised according to literature.⁴²

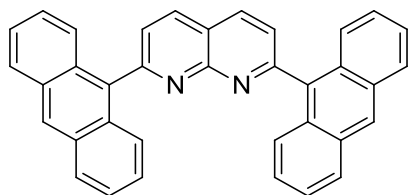


1,8-naphthyridine-2,7-diyl bis(trifluoromethanesulfonate) (4).⁴³ A mixture of trifluoromethanesulfonic anhydride (4.00 mL, 24.0 mmol) in dry CH_2Cl_2 (10.0 mL) was added dropwise to the solution of pyridine (3.23 mL, 40.0 mmol) and 2,7-dihydroxy-1,8-naphthyridine (20.0 mmol) in dry CH_2Cl_2 (20 mL) at 0 °C. After addition, the mixture was warmed to room temperature and stirred for 1 h. 20 mL

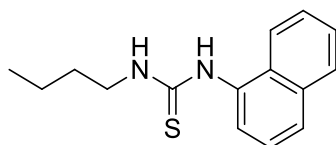
Et₂O was then added. The reaction was quenched with 10 % aq.HCl and washed successively with sat. NaHCO₃ and brine. The solvent was evaporated and the crude product was purified by chromatography on silica gel. 3.66 g white solid. Yield 43%. m.p. 147-149 °C ¹H NMR (500 MHz, CDCl₃) δ 8.55 (d, *J* = 8.7 Hz, 2H), 7.52 (d, *J* = 8.7 Hz, 2H). ¹³C NMR (126 MHz, CDCl₃) δ 157.08, 152.01, 142.42, 122.33, 122.43/119.88/117.33/114.78, 115.91 MS (EI) *m/z* 425.9 (M⁺)



2,7-di(naphthalen-1-yl)-1,8-naphthyridine (5).⁴⁴ The mixture of triflate (51 mg, 0.12 mmol), 1-naphthylboronic acid (82.6 mg, 0.48 mmol), Pd(PPh₃)₄ (27.7 mg, 0.024 mmol) and Ba(OH)₂·8H₂O (174 mg, 0.55 mmol) in 2 mL DME was degassed by sonication several times. The solution was refluxed at 80 °C under N₂. After the reaction was completed as indicated by TLC, the solution was allowed to cool to room temperature, filtered over Celite and extracted with DCM. The crude product was purified by flash chromatography on neutral alumina, followed by recrystallisation in DCM and petroleum ether with slow evaporation. Cubic yellowish crystals were obtained in 53% yield (24 mg). m.p. 230-233 °C ¹H NMR (500 MHz, CDCl₃) δ 8.45 (d, *J* = 8.3 Hz, 2H), 8.30 (d, *J* = 8.4 Hz, 2H), 8.01 – 7.96 (m, 4H), 7.94 – 7.90 (m, 4H), 7.65 – 7.62 (m, 2H), 7.56 – 7.49 (m, 4H). ¹³C NMR (126 MHz, CDCl₃) δ 163.06, 155.97, 137.90, 136.98, 133.89, 131.03, 129.68, 128.75, 128.47, 126.82, 126.00, 125.64, 125.35, 124.50, 120.28. MS (EI) *m/z* 382.0 (M⁺)

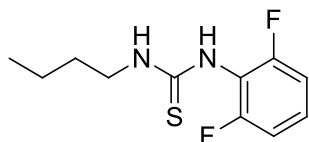


2,7-di(anthracen-9-yl)-1,8-naphthyridine (6).⁴⁴ The mixture of triflate (107 mg, 0.25 mmol), 9-anthracenylboronic acid (220 mg, 1 mmol), Pd(PPh₃)₄ (58 mg, 0.05 mmol) and Cs₂CO₃ (357 mg, 1.08 mmol) in toluene/ethanol/H₂O (2 ml/2 ml/1.5 ml) was degassed by sonication several times. The solution was refluxed at 100 °C under N₂ and protected from light. After the reaction was completed as indicated by TLC, the solution was cooled to room temperature, extracted with DCM. The crude product was purified by flash chromatography on silica gel. 29 mg redish solid Yield 24%. m.p. higher than 300 °C ¹H NMR (500 MHz, CDCl₃) δ 8.61 (s, 2H), 8.59 (d, *J* = 8.2 Hz, 2H), 8.10 (d, *J* = 8.5 Hz, 4H), 7.89 (d, *J* = 8.3 Hz, 2H), 7.84 (dd, *J* = 8.8, 0.9 Hz, 4H), 7.53 – 7.47 (m, 4H), 7.44 – 7.39 (m, 4H). ¹³C NMR (126 MHz, CDCl₃) δ 162.85, 156.35, 136.84, 134.57, 131.31, 129.93, 128.49, 128.11, 126.52, 126.24, 126.08, 125.20, 120.40. MS (EI) *m/z* 482.1 (M⁺)

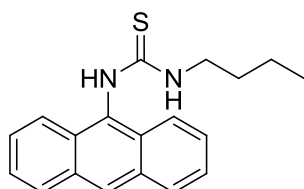


1-butyl-3-(naphthalen-1-yl)thiourea (7). A solution of butylisothiocyanate (0.95 mmol) was added dropwise to the mixture of 1-naphthylamine (0.48 mmol) in 5 ml of DCM. The mixture was refluxed for 2 hours under N₂. The reaction mixture was filtered and the resulting solution was dried with Na₂SO₄. After solvent was evaporated under vacuum, the crude product was purified by flash chromatography to afford the product as 78 mg brownish solid. Yield 63%. m.p. 107-110 °C ¹H NMR

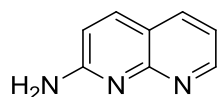
(500 MHz, CDCl_3) δ 8.64 (s, 1H), 8.07 – 7.97 (m, 1H), 7.93 – 7.82 (m, 2H), 7.57 – 7.40 (m, 4H), 5.71 (s, 1H), 3.53 (m, 2H), 1.46 – 1.33 (m, 2H), 1.20 – 1.15 (m, 2H), 0.80 (t, $J = 7.4$ Hz, 3H). ^{13}C NMR (126 MHz, CDCl_3) δ 181.29, 134.69, 131.97, 129.99, 128.86, 128.47, 127.35, 127.05, 125.82, 125.24, 122.78, 45.14, 31.05, 19.90, 13.70. MS (ESI) m/z 281 ($[\text{M}+\text{Na}]^+$)



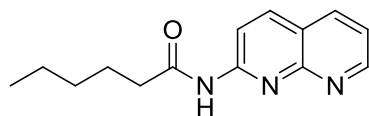
1-butyl-3-(2,6-difluorophenyl)thiourea (8).²⁵ The mixture of 2,6-difluoroaniline (215 ml, 2mmol) and butyl isothiocyanate (241 ml, 2mmol) in 5ml dry DCM was refluxed overnight. TLC shows no product formed. So 1,1'-thiocarbonyldiimidazole (315 mg, 1.77 mmol) was added, refluxed overnight. The isothiocyanate was formed, monitored by TLC. Butyl amine (0.4 ml, 4 mmol) was added, refluxed for 5h. The solvent was removed by rotary evaporation. The crude product was purified by chromatography on silica gel. 176 mg white solid. Yield 36%. m.p. 82-85°C ^1H NMR (500 MHz, CDCl_3) δ 7.68 (s, 1H), 7.32 – 7.26 (m, 1H), 6.99 (t, $J = 8.1$ Hz, 2H), 6.20 (s, 1H), 3.72 – 3.44 (br, 2H), 1.67 – 1.44 (m, 2H), 1.36 – 1.31 (m, 2H), 0.91 (t, $J = 7.4$ Hz, 3H). ^{13}C NMR (126 MHz, CDCl_3) δ 181.46, 159.35, 157.35, 129.21/129.13/129.06(t), 114.00, 112.42, 112.26, 45.56, 30.89, 19.94, 13.73. ^{19}F NMR (376 MHz, CDCl_3) δ -116.70. MS (ESI) m/z 267 ($[\text{M}+\text{Na}]^+$)



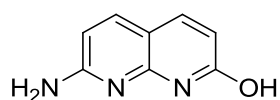
1-(anthracen-9-yl)-3-butylthiourea (9) was synthesised as reported.²⁶



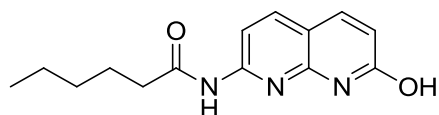
1,8-naphthyridin-2-amine (10) was made according to literature.⁴⁵



N-(1,8-naphthyridin-2-yl)hexanamide (G0).³⁰ The mixture of 1,8-naphthyridin-2-amine (218 mg, 2 mmol), 2 ml hexanoic anhydride and 0.3 ml triethylamine was heated to reflux at 100 °C overnight. After cooling down, the solution was diluted with DCM and washed with sat. NaHCO₃ three times. Then the solvent was removed. The crude product was purified by column chromatography. 97 mg brownish solid. Yield 20%. m.p. 148-150°C ¹H NMR (500 MHz, CDCl₃) δ 9.82 (s, 1H), 9.00 (dd, *J* = 4.3, 1.9 Hz, 1H), 8.59 (d, *J* = 8.9 Hz, 1H), 8.20 (d, *J* = 8.9 Hz, 1H), 8.13 (dd, *J* = 8.0, 1.9 Hz, 1H), 7.39 (dd, *J* = 8.0, 4.3 Hz, 1H), 2.49 (t, *J* = 7.6 Hz, 2H), 1.79 – 1.62 (m, 2H), 1.31 – 1.18 (m, 4H), 0.84 (t, *J* = 7.1 Hz, 3H). ¹³C NMR (126 MHz, CDCl₃) δ 173.28, 154.86, 154.36, 153.60, 139.40, 136.58, 120.73, 120.55, 115.94, 37.69, 31.25, 24.91, 22.32, 13.87. MS (EI) *m/z* 243.1 (M⁺)

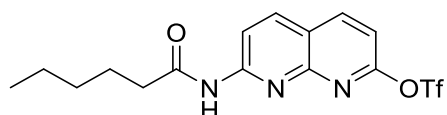


7-amino-1,8-naphthyridin-2-ol (11) was made according to literature.⁴²



N-(7-hydroxy-1,8-naphthyridin-2-yl)hexanamide (12).³⁰

2-amino-7-hydroxyl-1,8-naphthyridine (495 mg, 3 mmol) and 10 ml hexanoic anhydride was heated at 100°C for 2 days until TLC shows the completion of reaction. The precipitate was collected by filtration and washed with diethyl ether. The crude product was used without further purification. 513 mg white solid. Yield 66%. ¹H NMR (500 MHz, DMSO) δ 11.86 (s, 1H), 10.50 (s, 1H), 8.05 (d, J = 8.5 Hz, 1H), 7.95 (d, J = 8.5 Hz, 1H), 7.85 (d, J = 9.4 Hz, 1H), 6.43 (d, J = 9.4 Hz, 1H), 2.44 (t, J = 7.4 Hz, 2H), 1.62 – 1.56 (m, 2H), 1.40 – 1.22 (m, 4H), 0.88 (t, J = 6.9 Hz, 3H). ¹³C NMR (126 MHz, DMSO) δ 172.96, 163.39, 152.55, 148.89, 138.98, 138.50, 120.41, 110.58, 108.55, 36.18, 30.87, 24.64, 21.93, 13.91. MS (EI) m/z 259.1 (M⁺) HRMS (EI) m/z 259.131263(M⁺, C₁₄H₁₇N₃O₂⁺, calc. 259.13153)

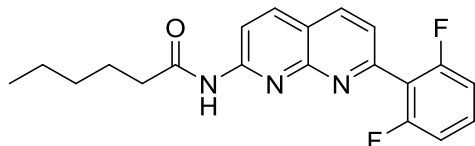


7-hexanamido-1,8-naphthyridin-2-yl trifluoromethanesulfonate (13).⁴³ Triflic anhydride (0.28 ml, 1.64 mmol) in 10 ml dry DCM was added dropwise to the phenol (354 mg 1.37 mmol) and 0.22 ml pyridine in 40 ml dry DCM at 0°C. Then solution was stirred for 2h at room temperature before it was diluted with diethyl ether, quenched with 10% aq. HCl solution, washed with sat. NaHCO₃ and brine. The organic layer was dried over MgSO₄. Solvent was removed. The product was purified by column chromatography. 450 mg white/yellowish solid. Yield 84%. m.p. 103-105°C ¹H NMR (400 MHz, CDCl₃) δ 8.89 (s, 1H), 8.68 (d, J = 8.9 Hz, 1H), 8.35

(d, $J = 8.5$ Hz, 1H), 8.29 (d, $J = 8.9$ Hz, 1H), 7.27 (d, $J = 8.5$ Hz, 1H), 2.50 (t, $J = 7.5$ Hz, 2H), 1.86 – 1.66 (m, 2H), 1.48 – 1.21 (m, 4H), 0.91 (t, $J = 7.1$ Hz, 3H). ^{13}C NMR (101 MHz, CDCl_3) δ 172.81, 156.30, 155.28, 152.95, 142.02, 139.23, 123.37/120.18/116.99/113.80 (CF_3), 120.25, 116.27, 112.63, 37.90, 31.24, 24.86, 22.36, 13.86. ^{19}F -NMR (376 MHz, CDCl_3) -73.1 MS (EI) m/z 391.1 (M^+)

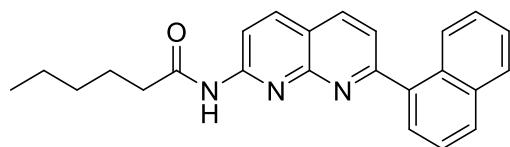
General procedure for Suzuki coupling

Triflate (1mmol), the corresponding boronic acid (1.05 mmol), sodium carbonate (137 mg, 1.3 mmol) and $\text{Pd}(\text{PPh}_3)_4$ was added into the solution of 25 ml dimethoxyethane (DME) and 5 ml H_2O . The mixture was degassed, protected from light and stirred at 80°C under N_2 overnight. After cooling down, the mixture was quenched with H_2O , extracted with DCM and washed with brine. The organic layer was dried over MgSO_4 . Solvent was removed. The residue was purified by column chromatography.

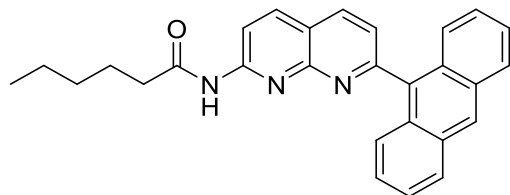


N-(7-(2,6-difluorophenyl)-1,8-naphthyridin-2-yl)hexanamide (G1). White solid. Yield 40%. m.p. $167\text{-}169^\circ\text{C}$ ^1H NMR (400 MHz, CDCl_3) δ 8.62 (d, $J = 8.9$ Hz, 1H), 8.49 (s, 1H), 8.20 (t, $J = 9.1$ Hz, 2H), 7.63 (d, $J = 8.2$ Hz, 1H), 7.44 – 7.31 (m, 1H), 7.07 (t, $J = 8.0$ Hz, 2H), 2.49 (t, $J = 7.5$ Hz, 2H), 1.91 – 1.71 (m, 2H), 1.45 – 1.31 (m, 4H), 0.94 (t, $J = 7.0$ Hz, 3H). ^{13}C NMR (101 MHz, CDCl_3) δ 173.35, 161.73, 159.19, 154.59, 153.26, 139.10, 136.67, 130.66, 122.93, 119.66, 116.32, 111.94, 111.69,

37.60, 31.16, 24.98, 22.32, 13.83. ^{19}F NMR (376 MHz, CDCl_3) δ -113.86 (t, $J = 6.4$ Hz). MS (EI) m/z 355.1 (M^+)

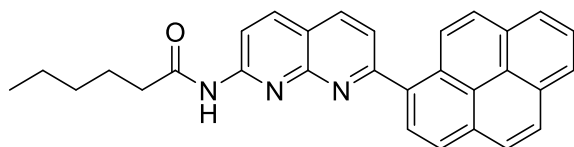


N-(7-(naphthalen-1-yl)-1,8-naphthyridin-2-yl)hexanamide (G2). White solid. Yield 63%. m.p. 138-140°C ^1H NMR (500 MHz, CDCl_3) δ 8.68 (s, 1H), 8.62 (d, $J = 8.8$ Hz, 1H), 8.30 – 8.25 (m, 3H), 7.979 – 7.95 (m, 2H), 7.82 (dd, $J = 7.1, 1.0$ Hz, 1H), 7.76 (d, $J = 8.2$ Hz, 1H), 7.62 (dd, $J = 8.1, 7.2$ Hz, 1H), 7.56 – 7.79 (m, 2H), 2.50 (t, $J = 7.6$ Hz, 2H), 1.80 – 1.67 (m, 2H), 1.42 – 1.30 (m, 4H), 0.92 (t, $J = 6.9$ Hz, 3H). ^{13}C NMR (126 MHz, CDCl_3) δ 172.63, 162.87, 154.85, 153.97, 139.19, 138.02, 136.55, 133.90, 130.98, 129.58, 128.47, 128.39, 126.79, 125.98, 125.56, 125.29, 122.99, 119.28, 115.18, 38.00, 31.28, 24.96, 22.40, 13.90. MS (EI) m/z 369.2 (M^+)

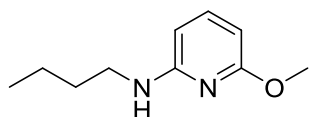


N-(7-(anthracen-9-yl)-1,8-naphthyridin-2-yl)hexanamide (G3). Yellowish solid. Yield 13%. m.p. 253-255°C ^1H NMR (500 MHz, CDCl_3) δ 8.67 (d, $J = 8.9$ Hz, 1H), 8.58 (s, 1H), 8.37 – 8.34 (m, 3H), 8.08 (d, $J = 8.5$ Hz, 2H), 7.68 – 7.62 (m, 3H), 7.53 – 7.42 (m, 2H), 7.39 – 7.31 (m, 2H), 2.47 (t, $J = 7.5$ Hz, 2H), 1.83 – 1.68 (m, 2H), 1.41 – 1.31 (m, 4H), 0.91 (t, $J = 7.0$ Hz, 3H). ^{13}C NMR (126 MHz, CDCl_3) δ 172.49, 162.72, 155.00, 153.92, 139.36, 136.54, 134.64, 131.29, 129.82, 128.49, 127.95, 126.05, 126.01, 125.19, 124.64, 119.44, 115.42, 77.28, 77.03, 76.77, 38.08, 31.28,

24.99, 22.41, 13.90. MS (EI) m/z 419.1 (M^+) HRMS (EI) m/z 419.199792(M^+ , $C_{28}H_{25}N_3O^+$, calc. 419.19921)

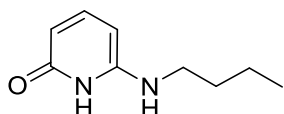


N-(7-(pyren-1-yl)-1,8-naphthyridin-2-yl)hexanamide (G4). Yellow solid. Yield 90%. m.p. 129-132 °C 1H NMR (500 MHz, $CDCl_3$) δ 8.70 (s, 1H), 8.63 (d, $J = 8.8$ Hz, 1H), 8.55 (d, $J = 9.3$ Hz, 1H), 8.38 (d, $J = 7.9$ Hz, 1H), 8.35 – 8.20 (m, 5H), 8.18 – 8.10 (m, 3H), 8.06 (t, $J = 7.6$ Hz, 1H), 7.89 (d, $J = 8.2$ Hz, 1H), 2.51 (t, $J = 7.5$ Hz, 2H), 1.76 (dd, $J = 15.0, 7.4$ Hz, 2H), 1.43 – 1.30 (m, 4H), 0.91 (t, $J = 7.1$ Hz, 3H). ^{13}C NMR (126 MHz, $CDCl_3$) δ 172.62, 163.14, 155.01, 154.00, 139.22, 136.49, 135.14, 131.90, 131.39, 130.86, 128.72, 128.40, 128.26, 128.23, 127.43, 126.12, 125.60, 125.29, 125.01, 124.80, 124.74, 123.60, 119.17, 115.18, 38.03, 31.30, 24.99, 22.40, 13.90. MS (EI) m/z 443.1 (M^+) HRMS (EI) m/z 443.198947(M^+ , $C_{30}H_{25}N_3O^+$, calc. 443.19921)

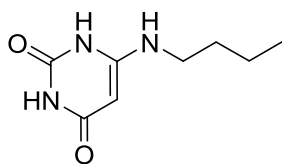


N-butyl-6-methoxypyridin-2-amine (14).⁴⁶ Bromopyridine (5 mmol, 1eq), $Pd_2(dba)_3$ (0.05 mmol, 1 mol%), 2-dicyclohexylphosphino-2'-(*N,N*-dimethylamino) biphenyl (0.075 mmol, 1.5 mol%), amine (6 mmol, 1.2eq) and Na^t-OBu (7 mmol, 1.4 mol%) was mixed in 12 ml toluene in the vial. The vial was sealed. The mixture was degassed three times and placed in the microwave reactor at 120 °C for certain minutes. After the mixture was cooled down, it was diluted with ethyl acetate. The

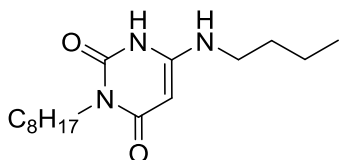
solution was filtered through Celite. The filtrate was concentrated under reduced vacuum. The crude product was purified by chromatography on silica gel. 774 mg brown solid. Yield 86%. ^1H NMR (400 MHz, CDCl_3) δ 7.36 (t, $J = 7.9$ Hz, 1H), 6.03(d, $J = 7.6$ Hz, 1H), 5.95 (d, $J = 7.8$ Hz, 1H), 4.40 (s, 1H), 3.87 (s, 3H), 3.28 – 3.23 (m, 2H), 1.70 – 1.56 (m, 2H), 1.55 – 1.38 (m, 2H), 0.98 (t, $J = 7.3$ Hz, 3H). ^{13}C NMR (101 MHz, CDCl_3) δ 163.65, 158.00, 139.99, 97.24, 97.02, 53.06, 42.06, 31.74, 20.25, 13.89.



6-(butylamino)pyridin-2(1H)-one (15). Methoxy pyridine (2.3 mmol, 1eq) was dissolved in dry DCM. The solution was cooled to -10°C in an ice-brine bath. BBr_3 (4.6 mmol, 2 eq) was added. After addition, the solution was warmed to room temperature overnight. Then the reaction was quenched by H_2O . The resulting mixture was neutralised with sat. NaHCO_3 , extracted with ether. The organic layer was washed with H_2O and brine, dried over MgSO_4 and purified by chromatography on silica gel. 246 mg purple solid. Yield 50%. m.p. $85\text{--}87^\circ\text{C}$ ^1H NMR (400 MHz, CDCl_3) δ 7.33 (t, $J = 8.2$ Hz, 1H), 6.13 (s, 1H), 5.72 (d, $J = 8.6$ Hz, 1H), 5.37 (d, $J = 7.9$ Hz, 1H), 3.11 (br, 2H), 1.68 – 1.60 (m, 2H), 1.53 – 1.35 (m, 2H), 0.97 (t, $J = 7.3$ Hz, 3H). ^{13}C NMR (101 MHz, CDCl_3) δ 164.27, 151.97, 143.98, 102.28, 86.28, 42.12, 30.96, 20.14, 13.77. MS(EI) m/z 166.0 (M^+)

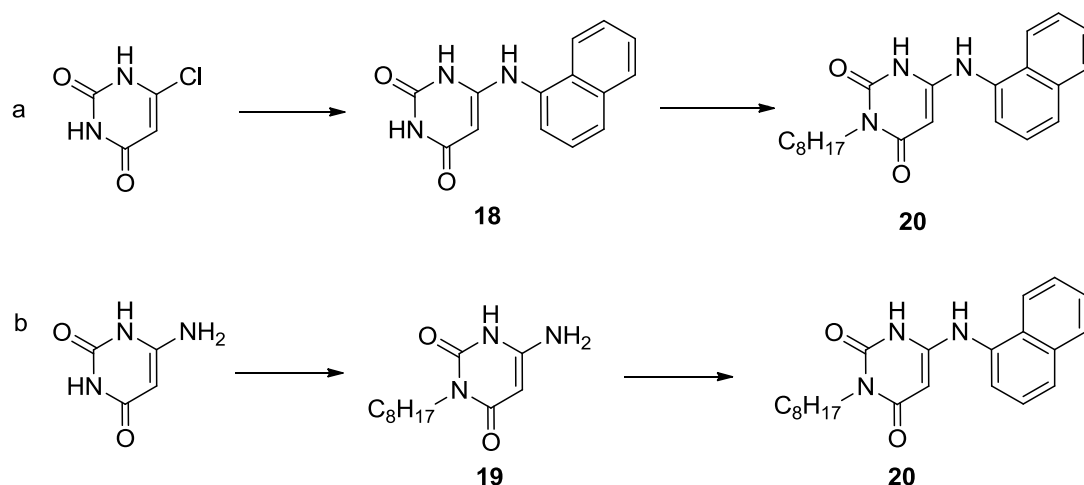


6-(butylamino)pyrimidine-2,4(1H,3H)-dione (16) was reported.⁴⁷⁻⁴⁸

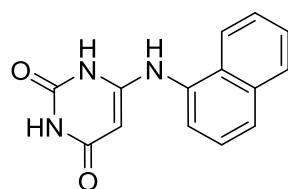


6-(butylamino)-3-octylpyrimidine-2,4(1H,3H)-dione (17).⁴⁹ A mixture of Uracil**16** (236 mg, 1.3 mmol), hexamethyldisilazane (1ml, 4.8 mmol) and $(\text{NH}_4)_2\text{SO}_4$ (9 mg, 0.07 mmol) was heated to 140 °C for 2h. Then the solution was cooled down, 1-iodoactane (0.25 ml, 1.4 mmol) was added. The solution was heated to 120°C for 2.5h. Cooling in an iced bath, sat. NaHCO_3 was added. The mixture was extracted with DCM. The organic layer was dried over MgSO_4 . Solvent was removed. The crude product was purified by column chromatography. 215 mg white solid. Yield 56%. m.p. 199-200°C ^1H NMR (400 MHz, CDCl_3) δ 10.46 (s, 1H), 5.33 (s, 1H), 4.87 (s, 1H), 3.89 – 3.80 (m, 2H), 3.12 – 3.08 (m, 2H), 1.71 – 1.52 (m, 4H), 1.51 – 1.19 (m, 12H), 0.97 (t, $J = 7.3$ Hz 3H), 0.88 (t, $J = 6.9$ Hz 3H). ^{13}C NMR (126 MHz, CDCl_3) δ 164.77, 152.62, 152.34, 74.41, 41.92, 40.24, 31.85, 30.75, 29.41, 29.28, 28.21, 27.05, 22.65, 20.00, 14.09, 13.68. MS (ESI) m/z 294.25 $[\text{M-H}]^+$

Synthesis of compound 20 was attempted by two methods.



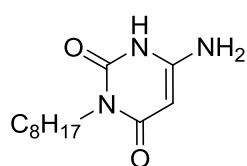
Method 1



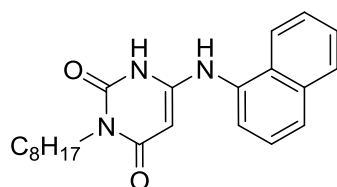
6-(naphthalen-1-ylamino)pyrimidine-2,4(1H,3H)-dione (18).⁵⁰ 6-chlorouracil (146 mg, 1 mmol) and 1-aminonaphthalene (168 mg, 1.2 mmol) was ground together. The oil bath was preheated to 180 °C, and then the mixture was heated at the same temperature under N₂ for 1 h. After cooling down, the mixture was suspended in ether and filtered. The solid was recrystallised from ethanol. 169 mg white solid. Yield 67%. m.p. higher than 300°C ¹H NMR (500 MHz, DMSO) δ 10.45 (s, 1H), 10.35 (s, 1H), 8.46 (s, 1H), 8.03 – 7.98 (m, 1H), 7.98 – 7.93 (m, 1H), 7.89 (d, *J* = 8.2 Hz, 1H), 7.64 – 7.52 (m, 3H), 7.48 (d, *J* = 7.2 Hz, 1H), 4.22 (s, 1H). ¹³C NMR (126 MHz, DMSO) δ 164.79, 154.29, 151.35, 134.53, 133.60, 129.43, 128.89, 127.32, 127.17, 127.03, 126.38, 123.99, 122.78, 76.14. MS(EI) *m/z* 253.1 (M⁺)

Uracil 18^{49} (254 mg, 1 mmol), hexamethyldisilazane (1.4 ml, 6.7 mmol) and $(\text{NH}_4)_2\text{SO}_4$ (3.3 mg, 0.02 mmol) was heated to 140 °C until a clear solution was obtained. Then the solution was cooled to 65°C, 1-iodooctane (1.2 ml, 6.7 mmol) was added. The solution was heated to 120°C for 12h. Cooling in iced bath, 5 ml sat. NaHCO_3 was added with vigorous stirring. The precipitate was filtered and washed with H_2O and ether. The crude product was hard to purify.

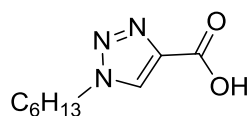
Method 2



6-amino-3-octylpyrimidine-2,4(1H,3H)-dione (19).⁴⁹ 1-aminouracil (1.9 g, 15 mmol), hexamethyldisilazane (5.3 ml, 25.5 mmol) and $(\text{NH}_4)_2\text{SO}_4$ (50 mg, 0.38 mmol) was heated to 140 °C for 3h. After cooled down to 65 °C, 1-iodooctane (2.9 ml, 16 mmol) was added. The solution was heated at 120 °C for 2h. Cooling in the ice bath, sat. NaHCO_3 was added and the mixture was stirred overnight. The precipitate was filtered and washed with H_2O and ether. 2.4 g white solid. Yield 68%. m.p. 246-249°C ^1H NMR (400 MHz, DMSO) δ 10.35 (s, 1H), 6.19 (s, 2H), 4.54 (s, 1H), 3.62 – 3.60 (m, 2H), 1.53 – 1.37 (m, 2H), 1.34 – 1.11 (m, 10H), 0.86 (t, J = 6.8 Hz, 3H). ^{13}C NMR (126 MHz, DMSO) δ 163.52, 154.15, 151.56, 74.65, 39.13, 31.68, 29.20, 29.07, 28.12, 26.83, 22.54, 14.41. MS(EI) m/z 239.2 (M^+)



6-(naphthalen-1-ylamino)-3-octylpyrimidine-2,4(1H,3H)-dione(20).⁵¹ The mixture of uracil (2.39 g, 10 mmol), 1-aminonaphthalene (4.3 g, 30 mmol) and 0.6 ml acetic acid was heated at 207 °C for 6 h. After cooled down, 9 ml ethanol was added and further stirred for 15 min. The precipitate was filtered and recrystallised from methanol. 1.06 g brownish needle-like crystal. Yield 29%. m.p. 171-173 °C ¹H NMR (400 MHz, DMSO) δ 10.59 (s, 1H), 8.42 (s, 1H), 8.07 – 7.92 (m, 2H), 7.90 (d, *J* = 8.2 Hz, 1H), 7.66 – 7.53 (m, 3H), 7.48 (dd, *J* = 7.3, 1.0 Hz, 1H), 4.34 (s, 1H), 3.77 – 3.60 (m, 2H), 1.54 – 1.41 (m, 2H), 1.37 – 1.12 (m, 10H), 0.86 (t, *J* = 6.9 Hz, 3H). ¹³C NMR (101 MHz, DMSO) δ 163.41, 152.64, 151.28, 134.54, 133.61, 129.42, 128.89, 127.25, 127.14, 127.02, 126.38, 123.87, 122.78, 76.12, 31.69, 29.18, 29.07, 28.03, 26.85, 22.54, 14.42. one C peak is in the DMSO residual MS (EI) *m/z* 365.1 (*M*⁺)

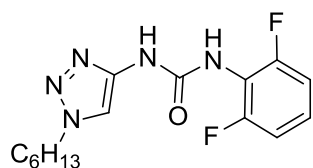


1-hexyl-1H-1,2,3-triazole-4-carboxylic acid(21) was made according to literature.²⁹

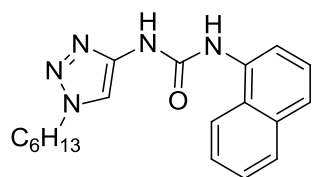
General procedure for the synthesis of urea compounds²⁸

Et₃N (350 μl, 1.75 mmol), diphenylphosphoryl azide (DPPA) (355 μl, 1.65 mmol) was added successively into the carboxylic acid **21** (197 mg, 1 mmol) in 25 ml dry chloroform. The mixture was protected from light and stirred at room temperature under N₂ for 10h. Then the corresponding amine (5.5 mmol) was added. After that, the mixture was heated to reflux overnight. The mixture was cooled down and

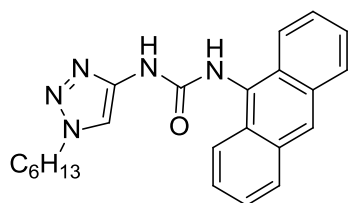
solvent was removed under vacuum. The crude product was purified by column chromatography.



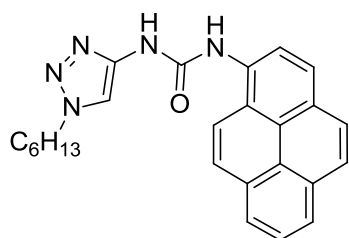
1-(2,6-difluorophenyl)-3-(1-hexyl-1H-1,2,3-triazol-4-yl)urea Urea1. White solid. Yield 25%. m.p. 160-161°C ^1H NMR (400 MHz, CDCl_3) δ 10.39 (s, 1H), 7.96 (s, 1H), 7.43 (br, 1H), 7.02 – 6.84 (m, 2H), 4.32 (t, $J = 7.2$ Hz, 2H), 2.07 – 1.76 (m, 2H), 1.40 – 1.22 (m, 6H), 0.87 (t, $J = 7.0$ Hz, 3H). ^{13}C NMR (126 MHz, CDCl_3) δ 159.09(d), 157.13(d), 152.59, 144.87, 126.78(t), 114.53(t), 112.14, 111.63(d), 111.44(d), 50.97, 31.12, 30.00, 26.07, 22.38, 13.93. ^{19}F NMR (376 MHz, CDCl_3) δ -118.62. MS (ESI) m/z 346.20 $[\text{M}+\text{Na}]^+$



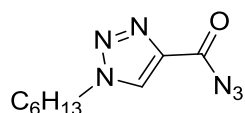
1-(1-hexyl-1H-1,2,3-triazol-4-yl)-3-(naphthalen-1-yl)urea Urea2. White solid. Yield 20%. m.p. 127-130°C ^1H NMR (400 MHz, CDCl_3) δ 10.40 (s, 1H), 8.62 – 7.62 (m, 5H), 7.58 (d, $J = 8.1$ Hz, 1H), 7.46 – 7.34 (m, 3H), 4.29 (t, $J = 7.2$ Hz, 2H), 2.01 – 1.78 (m, 2H), 1.42 – 1.17 (m, 6H), 0.89 (t, $J = 6.8$ Hz, 3H). ^{13}C NMR (101 MHz, CDCl_3) δ 153.49, 145.40, 134.14, 133.04, 128.41, 127.57, 126.07, 125.89, 125.67, 125.00, 121.39, 120.20, 111.66, 51.00, 31.14, 30.03, 26.14, 22.42, 13.97. MS (ESI) m/z 360.94 $[\text{M}+\text{Na}]^+$



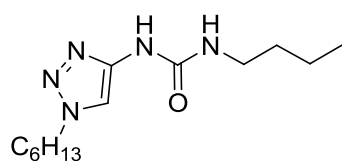
1-(anthracen-9-yl)-3-(1-hexyl-1H-1,2,3-triazol-4-yl)urea Urea3. Yellowish solid. Yield 21%. No obvious melting over 300°C, compound turned black. ¹H NMR (500 MHz, DMSO) δ 9.57 (s, 1H), 8.87 (s, 1H), 8.60 (s, 1H), 8.24 – 8.06 (m, 4H), 7.86 (s, 1H), 7.63 – 7.47 (m, 4H), 4.30 (t, *J* = 7.0 Hz, 2H), 1.86 – 1.69 (m, 2H), 1.37 – 1.10 (m, 6H), 0.85 (t, *J* = 6.9 Hz, 3H). ¹³C NMR (126 MHz, DMSO) δ 153.84, 144.94, 131.83, 129.76, 129.07, 128.86, 126.47, 126.02, 125.96, 124.21, 112.38, 50.10, 31.05, 30.07, 25.96, 22.40, 14.32. MS (ESI) *m/z* 410.18 [M+Na]⁺



1-(1-hexyl-1H-1,2,3-triazol-4-yl)-3-(pyren-1-yl)urea Urea4. White/yellowish solid. Yield 22%. No obvious melting over 300°C, compound turned black. ¹H NMR (500 MHz, DMSO) δ 9.69 (s, 1H), 9.34 (s, 1H), 8.66 (d, *J* = 8.4 Hz, 1H), 8.35 (d, *J* = 9.4 Hz, 1H), 8.29 – 8.27 (m, 3H), 8.18 – 8.03 (m, 3H), 4.36 (t, *J* = 7.0 Hz, 2H), 1.92 – 1.73 (m, 2H), 1.45 – 1.07 (m, 6H), 0.87 (t, *J* = 6.9 Hz, 3H). ¹³C NMR (126 MHz, DMSO) δ 152.50, 144.58, 133.24, 131.57, 131.04, 127.82, 127.64, 127.14, 126.90, 126.22, 125.84, 125.53, 125.04, 124.97, 124.63, 121.38, 121.24, 120.02, 112.41, 50.20, 31.07, 30.09, 25.98, 22.42, 14.34. MS (ESI) *m/z* 434.51 [M+Na]⁺



1-hexyl-1H-1,2,3-triazole-4-carbonyl azide (22).²⁸ **21** (250 mg, 1.3 mmol) and SOCl₂ (4 mL) was refluxed overnight. Excess SOCl₂ was evaporated to give dry acid chloride. Then the acid chloride was dissolved in 7 ml dry acetone at 0°C. Sodium azide (300 mg, 4.6 mmol) in 15 ml H₂O was added to the solution. The mixture was stirred at 0°C for 30min and further stirred at room temperature for 4 h. The mixture was filtered and washed with H₂O to give the azide. The product was dried thoroughly and used in the next step without further purification. 289 mg white solid. Yield 99%. ¹H NMR (400 MHz, CDCl₃) δ 8.18 (s, 1H), 4.40 (t, *J* = 7.3 Hz, 2H), 1.92 – 1.86 (m, 2H), 1.44 – 1.09 (m, 6H), 0.82 (t, *J* = 7.0 Hz, 3H). ¹³C NMR (126 MHz, CDCl₃) δ 165.66, 140.51, 128.09, 50.81, 30.96, 29.99, 25.91, 22.29, 13.81.



1-butyl-3-(1-hexyl-1H-1,2,3-triazol-4-yl)urea Urea0. Azide **22** (222 mg, 1 mmol) was dissolved in 5 ml dry CHCl₃ and heated to reflux for 10 h under N₂. The solution was cooled down to room temperature. Then butyl amine (400 μl, 4 mmol) was added and the solution was kept stirring overnight. Then solvent was removed under reduced pressure. The crude product was purified by column chromatography. 56 mg white solid. Yield 21%. m.p. 83-85°C ¹H NMR (400 MHz, CDCl₃) δ 9.63 (s, 1H), 7.62 (s, 1H), 5.96 (s, 1H), 4.31 (t, *J* = 7.2 Hz, 2H), 3.35 – 3.31 (m, 2H), 1.99 – 1.84 (m, 2H), 1.63 – 1.51 (m, 2H), 1.49 – 1.23 (m, 8H), 0.98 – 0.90 (m, 6H). ¹³C NMR

(126 MHz, CDCl₃) δ 154.94, 145.76, 110.65, 50.88, 40.08, 32.17, 31.16, 30.03,
26.13, 22.42, 20.04, 13.96, 13.80. MS (ESI) m/z 290.47 [M+Na]⁺

References

- (1) Marcey, L. W. *Peptide Science* **2004**, *76*, 435-445.
- (2) Riley, K. E.; Hobza, P. *Acc. Chem. Res.* **2012**, *46*, 927-936.
- (3) Xu, H.; Zuend, S. J.; Woll, M. G.; Tao, Y.; Jacobsen, E. N. *Science* **2010**, *327*, 986-990.
- (4) Krenske, E. H.; Houk, K. N. *Acc. Chem. Res.* **2012**, *46*, 979-989.
- (5) Salonen, L. M.; Ellermann, M.; Diederich, F. *Angew. Chem., Int. Ed.* **2011**, *50*, 4808-4842.
- (6) Emmanuel, A. M.; Ronald, K. C.; François, D. *Angew. Chem., Int. Ed.* **2003**, *42*, 1210-1250.
- (7) Nandwana, V.; Samuel, I.; Cooke, G.; Rotello, V. M. *Acc. Chem. Res.* **2012**, *46*, 1000-1009.
- (8) Ehrlich, S.; Moellmann, J.; Grimme, S. *Acc. Chem. Res.* **2012**, *46*, 916-926.
- (9) Wheeler, S. E. *Acc. Chem. Res.* **2013**, *46*, 1029-1038.
- (10) Ringer, A. L.; Sherrill, C. D. *J. Am. Chem. Soc.* **2009**, *131*, 4574-4575.
- (11) Watt, M.; Hardebeck, L. K. E.; Kirkpatrick, C. C.; Lewis, M. *J. Am. Chem. Soc.* **2011**, *133*, 3854-3862.
- (12) Podeszwa, R.; Szalewicz, K. *Phys. Chem. Chem. Phys.* **2008**, *10*, 2735-2746.
- (13) Sherrill, C. D. *Acc. Chem. Res.* **2012**, *46*, 1020-1028.
- (14) Gung, B. W.; Xue, X.; Zou, Y. *J. Org. Chem.* **2007**, *72*, 2469-2475.
- (15) Newcomb, L. F.; Gellman, S. H. *J. Am. Chem. Soc.* **1994**, *116*, 4993-4994.
- (16) McKay, S. L.; Haptonstall, B.; Gellman, S. H. *J. Am. Chem. Soc.* **2001**, *123*, 1244-1245.
- (17) Wheeler, S. E.; McNeil, A. J.; Müller, P.; Swager, T. M.; Houk, K. N. *J. Am. Chem. Soc.* **2010**, *132*, 3304-3311.
- (18) Scott L. Cockroft; Christopher A. Hunter; Kevin R. Lawson; Julie Perkins; Urch, C. J. *J. Am. Chem. Soc.* **2005**, *127*, 8594-8595.
- (19) Zimmerman, S. C.; Murray, T. J. *Tetrahedron Lett.* **1994**, *35*, 4077-4080.
- (20) Cockroft, S. L.; Hunter, C. A. *Chem. Soc. Rev.* **2007**, *36*, 172-188.
- (21) Hunter, C. A.; Jones, P. S.; Tiger, P.; Tomas, S. *Chem. Eur. J.* **2002**, *8*, 5435-5446.
- (22) Schreiber, G.; Fersht, A. R. *J. Mol. Biol.* **1995**, *248*, 478-486.
- (23) Blight, B. A.; Camara-Campos, A.; Djurdjevic, S.; Kaller, M.; Leigh, D. A.; McMillan, F. M.; McNab, H.; Slawin, A. M. Z. *J. Am. Chem. Soc.* **2009**, *131*, 14116-14122.
- (24) Miyaura, N.; Suzuki, A. *Chem. Rev.* **1995**, *95*, 2457-2483.
- (25) Yang, D.; Chen, Y.-C.; Zhu, N.-Y. *Org. Lett.* **2004**, *6*, 1577-1580.
- (26) Janovec, L.; Suchar, G.; Imrich, J.; Kristian, P.; Sasinkova, V.; Alfoldi, J.; Sedlak, E. *ChemInform* **2002**, *33*, 96-96.
- (27) Plevin, M. J.; Bryce, D. L.; Boisbouvier, J. *Nat. Chem.* **2010**, *2*, 466-471.
- (28) Hisamatsu, Y.; Fukumi, Y.; Shirai, N.; Ikeda, S.-i.; Odashima, K. *Tetrahedron Lett.* **2008**, *49*, 2005-2009.
- (29) Hisamatsu, Y.; Shirai, N.; Ikeda, S. I.; Odashima, K. *Org. Lett.* **2010**, *12*, 1776-1779.

- (30) Corbin, P. S.; Zimmerman, S. C.; Thiessen, P. A.; Hawryluk, N. A.; Murray, T. J. *J. Am. Chem. Soc.* **2001**, *123*, 10475-10488.
- (31) Alvarez-Rua, C.; Garcia-Granda, S.; Goswami, S.; Mukherjee, R.; Dey, S.; Claramunt, R. M.; Santa Maria, M. D.; Rozas, I.; Jagerovic, N.; Alkorta, I.; Elguero, J. *New J. Chem.* **2004**, *28*, 700-707.
- (32) Murray, T. J.; Zimmerman, S. C. *J. Am. Chem. Soc.* **1992**, *114*, 4010-4011.
- (33) Grimme, S. *Angew. Chem., Int. Ed.* **2008**, *47*, 3430-3434.
- (34) Cockroft, S. L.; Perkins, J.; Zonta, C.; Adams, H.; Spey, S. E.; Low, C. M. R.; Vinter, J. G.; Lawson, K. R.; Urhc, C. J.; Hunter, C. A. *Org. Biomol. Chem.* **2007**, *5*, 1062-1080.
- (35) Gung, B. W.; Xue, X.; Reich, H. J. *J. Org. Chem.* **2005**, *70*, 3641-3644.
- (36) Zhao, Y.; Truhlar, D. G. *Acc. Chem. Res.* **2008**, *41*, 157-167.
- (37) Kruse, H.; Goerigk, L.; Grimme, S. *J. Org. Chem.* **2012**, *77*, 10824-10834.
- (38) Zhao, Y.; Truhlar, D. G. *Theor. Chem. Account.* **2008**, *120*, 215-241.
- (39) Fernández-Mato, A.; Blanco, G.; Quintela, J. M.; Peinador, C. *Tetrahedron* **2008**, *64*, 3446-3456.
- (40) Bollini, M.; Casal, J. J.; Alvarez, D. E.; Boiani, L.; González, M.; Cerecetto, H.; Bruno, A. M. *Bioorg. Med. Chem.* **2009**, *17*, 1437-1444.
- (41) Ranu, B. C.; Dey, S. S.; Bag, S. *ARKIVOC* **2003**, 14-20.
- (42) Newkome, G. R.; Garbis, S. J.; Majestic, V. K.; Fronczek, F. R.; Chiari, G. *J. Org. Chem.* **1981**, *46*, 833-839.
- (43) Goossen, L. J.; Rodríguez, N.; Linder, C. *J. Am. Chem. Soc.* **2008**, *130*, 15248-15249.
- (44) Carreño, M. C.; González-López, M.; Latorre, A.; Urbano, A. *J. Org. Chem.* **2006**, *71*, 4956-4964.
- (45) Gueiffier, A.; Viols, H.; Blache, Y.; Chapat, J. P.; Chavignon, O.; Teulade, J. C.; Fauvelle, F.; Grassy, G.; Dauphin, G. *J. Heterocyclic Chem.* **1997**, *34*, 765-771.
- (46) Heo, J.-N.; Song, Y. S.; Kim, B. T. *Tetrahedron Lett.* **2005**, *46*, 4621-4625.
- (47) Fang, W.-P.; Cheng, Y.-T.; Cheng, Y.-R.; Cherg, Y.-J. *Tetrahedron* **2005**, *61*, 3107-3113.
- (48) Wright, G. E.; Brown, N. C. *J. Med. Chem.* **1980**, *23*, 34-38.
- (49) Hockemeyer, J.; Burbiel, J. C.; Müller, C. E. *J. Org. Chem.* **2004**, *69*, 3308-3318.
- (50) Wilson, J. M.; Henderson, G.; Black, F.; Sutherland, A.; Ludwig, R. L.; Vousden, K. H.; Robins, D. J. *Bioorg. Med. Chem.* **2007**, *15*, 77-86.
- (51) Cowden, W. B.; Clark, I. A.; Hunt, N. H. *J. Med. Chem.* **1988**, *31*, 799-801.

Chapter 3 Solvent effects on alkyl dispersion interactions

Abstract

Weak alkyl-alkyl interactions are examined using delicately designed Wilcox torsion balances. The variety of solvents examined in this study allow full analyses of solvent effects on alkyl-alkyl interactions. The dispersion between alkyl-alkyl chains is largely washed out by the competitive cohesive solvent effects. Density functional theory computations suggest HF or DFT/B3LYP methods are better at estimating non-covalent interactions in solution than the DFT-D method.

3.1 Introduction

Dispersion, part of van der Waals forces, are weak non-covalent interaction between induced instantaneous dipole/multipoles.¹ Dispersion forces are found widely in Nature, from protein folding² to gecko adhesion,³ and have been exploited in biologically inspired robot systems.⁴⁻⁵ It has been calculated that dispersion energy in one C-H...H-C contact is 1.3 kJ mol⁻¹ in the gas-phase and that they may provide significant stabilising forces when they are totalled over extended molecular contacts.^{6,7} Owing to this interaction, fully extended alkanes (C_nH_{2n+1}) do not exist for n > 17.⁸ Dispersion forces are known to stabilise branched alkanes⁹ and these cumulative alkane-alkane interactions are also responsible for stabilising long C-C bonds.¹⁰⁻¹¹ However, the question remains, how strong are dispersion forces in solution? Here we present our study on dispersion interactions in a wide range of

solvents using modified Wilcox torsion balances and the double-mutant cycle method.

3.2 Project design and methodology

Alkanes are a good subject for the investigation of dispersion forces in solution. The apolar nature of alkanes means that they can only form dispersion interactions and only weak, or negligible polar interactions such as hydrogen bonds (H-bond). Thus, the enthalpy of vaporisation (ΔH_{vap}), which is the energy required to break intermolecular interactions during the transition from liquid to gas, can be used as a measure of dispersion forces in alkanes. Table 3.1 lists a series of alkanes showing that vaporisation energies increase by around 4 kJ mol^{-1} per CH_2 from methane to hexane. This energy is equivalent to a H bond between amides in chloroform.¹² However, it is not fully understood how solvent competition affects the apparent strength of alkane-alkane dispersion interactions in solution.

Table 3.1. Boiling points and enthalpies of vaporisation for alkanes (ΔH_{vap}) reported to the nearest unit.¹³

	Boiling point, $t_b/^\circ\text{C}$	ΔH_{vap} at t_b / kJ mol^{-1}
methane	-164	+8
ethane	-89	+15
propane	-45	+19
<i>n</i> -butane	-1	+22
<i>n</i> -pentane	36	+26
<i>n</i> -hexane	69	+29

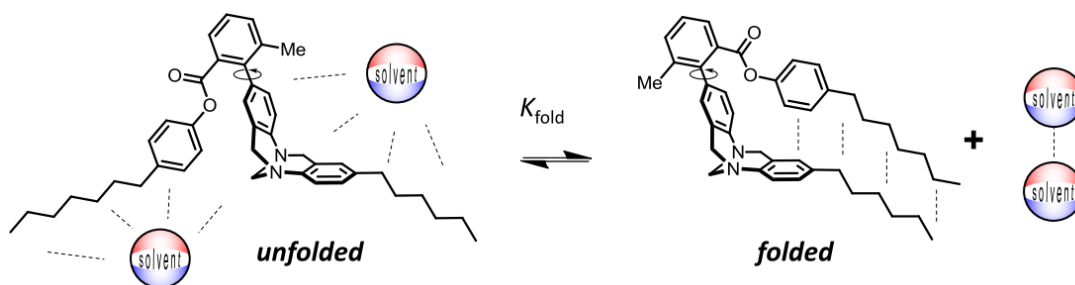


Figure 3.1. Unfolded and folded conformations of a Wilcox balance in equilibrium in solution.

A new Wilcox torsion balance was designed to study alkane-alkane interactions (Fig 3.1). The Wilcox balance backbone is very well-defined and features two conformations at room temperature on the NMR time scale.¹⁴⁻¹⁵ In the unfolded state, the ester arm rests outside the pocket formed by the Tröger's base, keeping the two alkyl substituted aromatic rings apart. In the folded state, the ester arm is located inside the pocket of the Tröger's base, and the aromatic rings come into contact in an edge-to-face configuration. The two long alkyl chains are also brought into contact in this folded conformation (Fig 3.1). According to Hunter's solvation theory,¹² in the unfolded state, the alkyl chains should be fully solvated by the surrounding solvent molecules. In the folded state, the alkyl chains are close to each other, excluding solvent molecules where the chains come into contact. As a result, the folded/unfolded ratio at equilibrium is the result of competition between solvent-solute interactions, solute-solute interactions and solvent-solvent interactions (Fig 3.1).

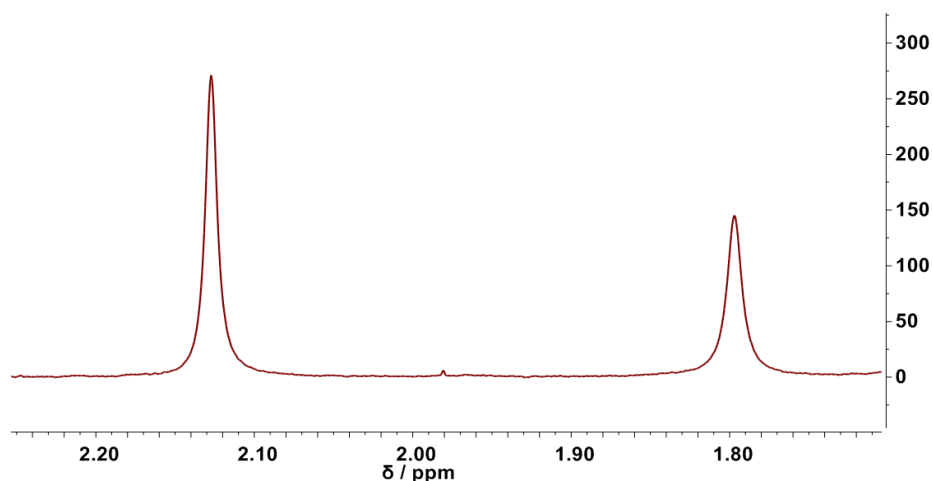


Figure 3.2. ^1H NMR spectra showing two peaks corresponding to the methyl protons in the unfolded and folded conformations.

In these two states, the methyl group gives two distinct NMR signals due to different magnetic environments provided by the aromatic ring in the Tröger's base (Fig 3.2). By integrating these two peaks separately, one can work out the folded/unfolded ratio and the folding free energy is given by:

$$\Delta G = -RT \ln (c_{\text{folded}}/c_{\text{unfolded}}) \quad \text{Equation 3.1}$$

where R is the gas constant.

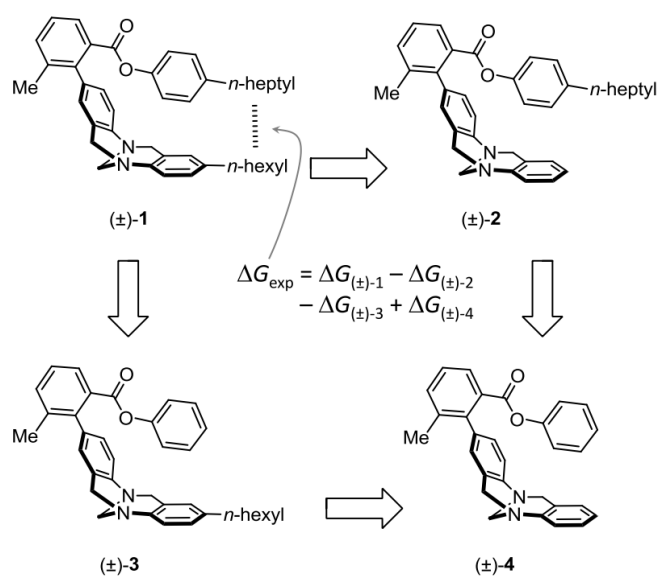


Figure 3.3. Double mutant cycle for dissecting alkyl-alkyl interactions.

As mentioned above, there is an aromatic edge-to-face interaction formed in the folded state in addition to the alkyl-alkyl interaction of interest. Figure 3.3 shows how it is possible to extract the free energy of the alkyl-alkyl interaction using the double mutant cycle approach.¹⁶ A control balance (\pm)-**2** which lacks the *n*-hexyl group on the Tröger's base is introduced. Going from balance (\pm)-**1** to balance (\pm)-**2**, the energy of the edge-to-face aromatic interaction is subtracted from the folding free energy of (\pm)-**1**. However, other secondary interactions such as the interaction between the hexyl group and the Tröger's base backbone may also contribute to the folding free energies. Therefore, two further control balances (\pm)-**3** and (\pm)-**4** can be synthesised. The secondary interaction energies are given by the difference going from balance (\pm)-**3** to balance (\pm)-**4**. Thus, a full double mutant cycle gives the net interaction between the alkyl chains (including any effects of the solvent).

$$\Delta G_{\text{alkyl-alkyl}} = (\Delta G_{(\pm)\text{-1}} - \Delta G_{(\pm)\text{-3}}) - (\Delta G_{(\pm)\text{-3}} - \Delta G_{(\pm)\text{-4}}) \quad \text{Equation 3.2}$$

To gain more understanding of dispersion interactions in solution, we thus examined balances (\pm)-**1** to (\pm)-**4** in a large range of organic solvents and solvent mixtures.

3.3 Synthesis

The esters **7a** and **7b** were obtained in good yield using *N,N'*-dicyclohexylcarbodiimide (DCC) as a coupling reagent in esterification reactions. However, in the step to make the Tröger's base, a yield of only 19% was achieved due to the formation of two other self-coupling products. Next, the iodo compound was converted to boronic esters (\pm)-**5a** or **5b** using a palladium catalyst.

These boronic esters were then incorporated into the previously made bromide **7a** or **7b** to form Wilcox balances (\pm)-**1-4** (Fig 3.4).

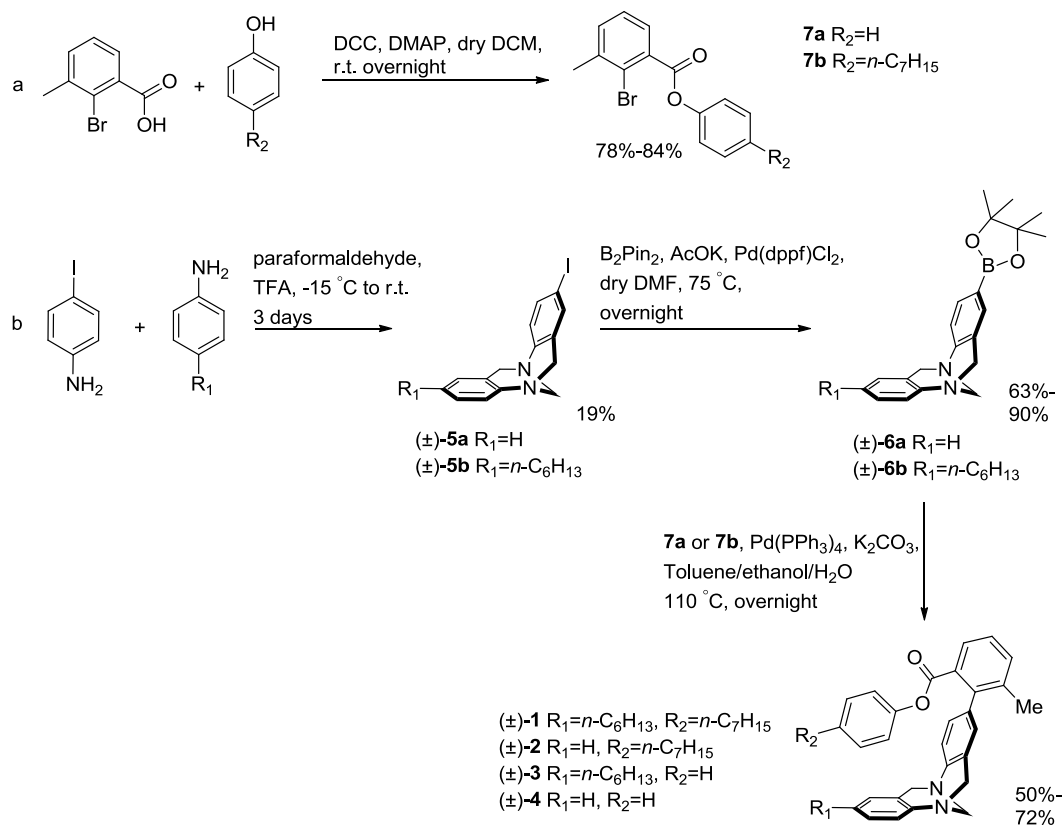


Figure 3.4. Syntheses of Wilcox balances.

3.4 Results and Discussion

3.4.1 Structure determination

Due to the two conformations being in equilibrium on the NMR time scale, 1H NMR and ^{13}C NMR spectra of balances (\pm)-**1** to (\pm)-**4** were quite complicated with most of the proton environments exhibiting two signals. However, the peaks could be assigned using COSY, HSQC, DEPT and HMBC. To confirm that the alkyl-alkyl come into contact in the folded state, a 1D-NOE spectrum was taken (Fig 3.5). The

methylene signal indicated in Figure 3.5 was irradiated in the folded state. The NOE signals marked with a star correspond to H_a and H_b which were close to the excited proton in space. For the other protons on the alkyl chain, the NOE cannot be distinguished due to overlapping signals.

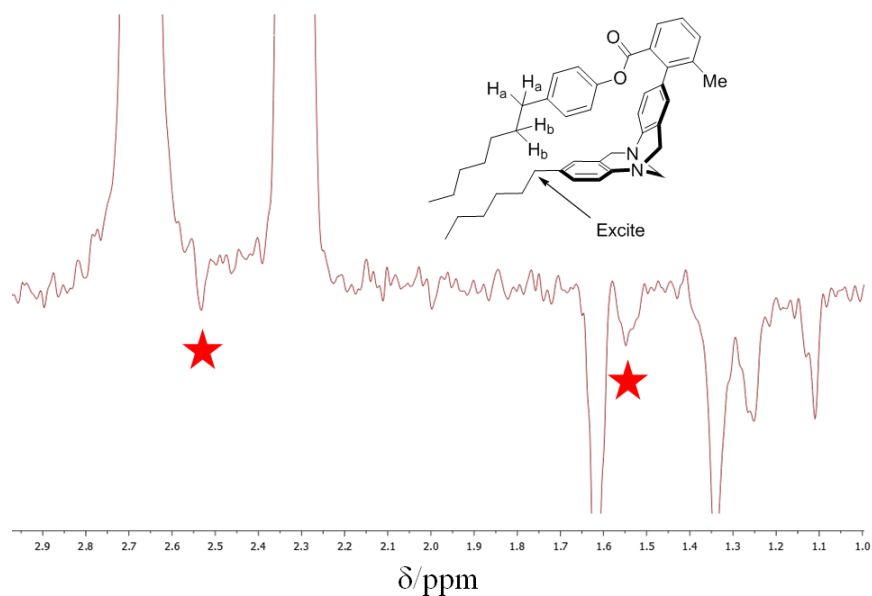


Figure 3.5. Partial 1D-NOE spectrum of balance (±)-1 in *d*₅-pyridine.

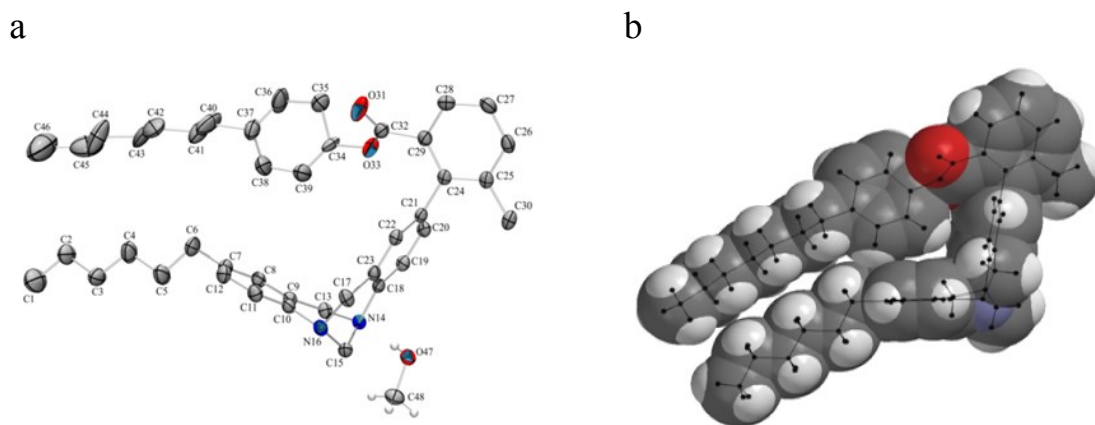


Figure 3.6. (a) The asymmetric unit of balance (±)-1 (CCDC deposition number 898520). Displacement ellipsoids are at the 50% probability level; most H atoms and all disorder are omitted. (b) Spacefilling model of the crystal structure determined in this study.

Luckily, we were able to crystallise balance (\pm)-**1** from a saturated methanol solution. The X-ray crystal structure shows the balance is in its folded state with two alkyl chains lying together. The space-filling model suggests that there is no severe steric clash between these two alkyl chains. Although the solid state does not necessarily represent the structure in solution, it implies that this conformation is one of the energy minimum states (Fig 3.6).

3.4.2 Solvent studies

Various solvents with a range of interaction properties were examined in subsequent studies (Table 3.2). THF has low H-bond donor ability ($\alpha_s = 0.9$), while methanol and ethanol have higher H-bond donor abilities ($\alpha_s = 2.7$). DMSO is a good H-bond acceptor ($\beta_s = 8.7$) while alkane solvents and carbon tetrachloride are very poor H-bond acceptors. Solvents with different polarisability ranging from methanol ($\alpha_{\text{pol}} = 3.3$) to hexane ($\alpha_{\text{pol}} = 11.9$) are included. Dielectric constants^{13,17} and E_T30 ¹⁸ provide alternative measures of polarity, with ϵ_r ranging from 1.9 to 47.2, and E_T30 from 30.9 to 55.5. The wide range of solvents covered in this study allows us to explore the factors contributing to alkyl-alkyl interactions in solution in depth.

Table 3.2. Solvent properties. Molecular polarisabilities (α_{pol}),¹⁹ H-bond donor constants (α_s), H-bond acceptor constants (β_s),^{12,20} E_{T30} values, enthalpies of vaporisation at the solvent boiling point (ΔH_{vap}) and relative permittivities (ϵ_r), molecular surface area per volume (A_{vol})^a

	$\alpha_{\text{pol}} / \text{\AA}^3$	α_s	β_s	E_{T30} /kcal mol ⁻¹	ΔH_{vap} /kJ mol ⁻¹	ϵ_r	A_{vol} / km ² dm ⁻³
Cyclohexane	11.0	1.2	0.6	30.9	29.97	2.0	7.24
n-Hexane	11.9	1.2	0.6	31	28.85	1.9	7.01
Carbon disulfide	8.5	1.0	0.1	32.60	26.76	2.6	7.24
Dichloromethane	6.5	1.9	1.1	40.7	28.06	8.9	7.91
Chloroform	8.5	2.2	0.9	39.1	29.29	4.8	7.51
Carbon tetrachloride	10.5	1.4	0.6	32.4	29.82	2.2	7.24
Benzene	10.4	1.1	2.1	34.3	30.72	2.3	7.77
Tetrahydrofuran	8.0	0.9	5.9	37.4	29.81	7.5	7.85
Pyridine	9.6	1.4	7.0	40.5	35.09	13.3	8.19
Acetone	6.5	1.5	5.8	42.20	29.10	21.01	7.85
Acetonitrile	4.4	1.7	5.1	46	29.75	36.6	8.47
Ethanol	5.1	2.7	5.3	52	38.56	25.3	8.46
Methanol	3.3	2.7	5.3	55.5	35.21	33.0	9.10
Dimethylsulfoxide	8.0	2.2	8.7	45.1	43.10	47.2	8.81
THF/9% D ₂ O	-	-	-	-	-	18.1	8.29
THF/15% D ₂ O	-	-	-	-	-	22.8	8.60
THF/20% D ₂ O	-	-	-	-	-	26.7	8.85
THF/25% D ₂ O	-	-	-	-	-	30.7	9.10
THF/30% D ₂ O	-	-	-	-	-	34.8	9.34
THF/35% D ₂ O	-	-	-	-	-	38.9	9.58
THF/40% D ₂ O	-	-	-	-	-	43.0	9.81
1-iodoperfluoro- <i>n</i> -hexane	-	-	-	-	-	-	6.80
Hexafluorobenzene	10.6	1.6	0.7	34.2 ²⁰	31.66	2.0	7.78
Pentafluoropyridine	10.2	1.9	2.9	36.3 ²⁰	36.3 ²¹	-	7.55

a. A_{vol} = molecular surface area / (density/ molecular weight)

Table 3.3. Experimental folding free energies for Wilcox balances (\pm)-1 to (\pm)-4, errors are within 0.12 kJ mol⁻¹.²¹ ΔG_{exp} is the value of the alkyl-alkyl interaction (including solvent effects) calculated using the double-mutant cycle, errors are within 0.25 kJ mol⁻¹.²¹ Solvents used are all deuterated solvent except fluorinated solvents.

	$\Delta G_{(\pm)-1}$ /kJ mol ⁻¹	$\Delta G_{(\pm)-2}$ /kJ mol ⁻¹	$\Delta G_{(\pm)-3}$ /kJ mol ⁻¹	$\Delta G_{(\pm)-4}$ /kJ mol ⁻¹	ΔG_{exp} /kJ mol ⁻¹
Cyclohexane	-2.05	-2.09	-2.31	-2.00	+0.36
<i>n</i> -Hexane	-1.48	-1.58	-1.54	-1.31	+0.34
Carbon disulfide	+0.14	-0.34	-0.08	-0.34	+0.21
Dichloromethane	-0.85	-1.00	-0.91	-0.87	+0.21
Chloroform	-0.86	-1.02	-0.93	-0.93	+0.16
Carbon tetrachloride	-1.06	-1.21	-1.18	-1.22	+0.11
Benzene	-1.22	-1.41	-1.28	-1.40	+0.07
Tetrahydrofuran	-1.19	-1.33	-1.07	-1.11	+0.11
Pyridine	-0.89	-1.07	-0.88	-1.09	-0.03
Acetone	-1.03	-1.02	-0.87	-0.78	+0.09
Acetonitrile	-1.19	-1.06	-0.71	-0.72	-0.14
Ethanol	-1.94	-1.63	-1.38	-1.33	-0.26
Methanol	-1.64	-1.41	-1.22	-1.28	-0.29
DMSO	-2.02	-1.34	-1.10	-1.05	-0.63
THF/9% D ₂ O	-1.44	-1.22	-0.99	-0.99	-0.21
THF/15% D ₂ O	-2.03	-1.75	-1.22	-1.19	-0.25
THF/20% D ₂ O	-2.32	-1.83	-1.36	-1.33	-0.45
THF/25% D ₂ O	-2.61	-1.95	-1.39	-1.33	-0.60
THF/30% D ₂ O	-2.91	-2.03	-1.58	-1.46	-0.75
THF/35% D ₂ O	-3.25	-2.18	-1.66	-1.49	-0.89
THF/40% D ₂ O	-3.60	-2.34	-1.77	-1.60	-1.09
1-iodoperfluorohexane	-1.47	-1.27	-1.34	-1.23	-0.10
Hexafluorobenzene	-2.61	-2.53	-2.47	-2.27	+0.11
Pentafluoropyridine	-2.83	-2.59	-2.63	-2.10	+0.28

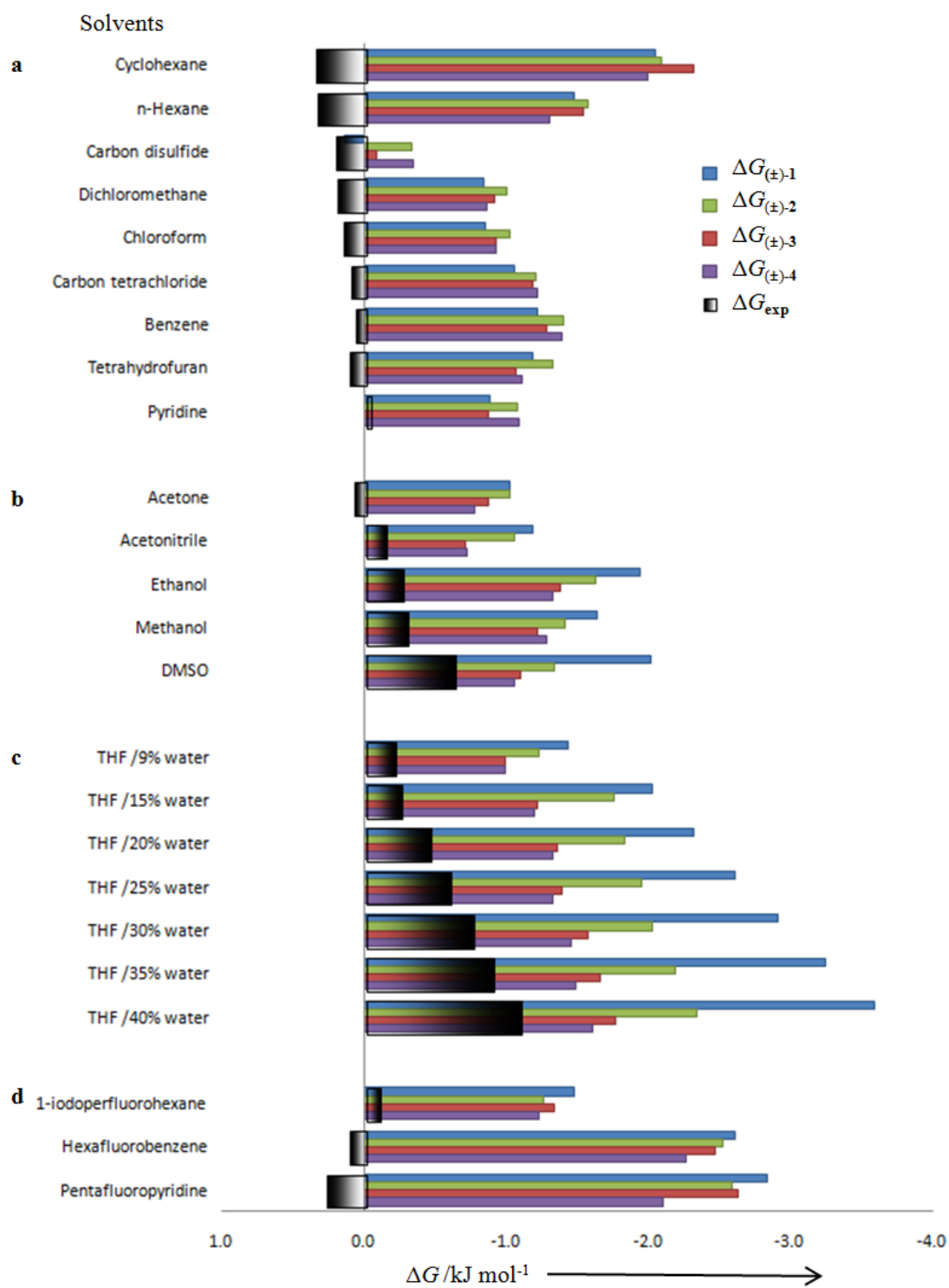


Figure 3.7. Experimental free energies (ΔG) of folding for compounds (\pm)-1 to (\pm)-4 (coloured bars) and alkyl-alkyl interaction energies dissected using the chemical double-mutant cycle. Errors are discussed in Table 3.3. Solvents used are all deuterated solvent except fluorinated solvents.

To gain more insight from the solvent study, all data are shown in a bar graph for comparison (Fig 3.7).

Folding free energies for balance (\pm)-**1** in apolar (group a) solvents are similar to the other three control balances, with CS₂ being an exception (Table 3.3). The DMC results are listed in Table 3.3. In more polar solvents (group b), $\Delta G_{(\pm)\text{-1}}$ values become more significant and alkyl-alkyl interactions become favourable. This finding implies that the interaction is mostly driven by a solvophobic effect. Thus, further measurements were carried out in THF/D₂O mixtures. As the water content increased, the folding free energy of balance (\pm)-**1** increased dramatically, while the others see little change. This result strongly points to a contribution from solvophobic effect. Nonetheless, the most important observation is that even in the most polar solvents the interaction energies are very small compared to the computed *n*-hexane dimer interaction, which has been reported to be as high as 19 kJ mol⁻¹ in the gas-phase.²² Thus, the large dispersion forces present in alkyl-alkyl interactions in the gas phase appear to be very much reduced in solution.

Given the large amount of data collected, the question may then arise: when do alkyl-solvent dispersion interactions win over alkyl-alkyl dispersion interactions? No obvious correlation was seen between the experimental alkyl-alkyl interaction results against the experimental molecular polarisability (α_{pol}) of the solvents (Fig 3.8). Correlations against E_T30 and solvent H-bond donor (α_{s}) and acceptor abilities (β_{s}) were also poor. Better correlations were obtained with dielectric constants ($R^2 = 0.80$) and enthalpies of vaporisation ($R^2 = 0.78$). However, these correlations are not very satisfying (Fig 3.8). Surprisingly, ΔG_{exp} values were highly dependent on the solvent

molecular surface area per unit volume ($R^2 = 0.94$, Fig 3.9). Solvents with greater accessible areas can develop larger solvent cohesive interactions. In other words, this observation is consistent with favourable alkane-alkane interactions been driven by stronger solvent-solvent (solvophobic) interactions, however further dissection of whether solvent cohesion is driven by cohesive electrostatic interactions or dispersion interactions is difficult. Nonetheless, some interesting results are seen in the perfluorinated solvents and CS_2 . Notably, the perfluorocarbon solvents are slight outliers on the correlation in Figure 3.9. Perfluorocarbon solvents possess lower polarisabilities than their non-fluorinated equivalents. For example, a small increase in the preference for folding is seen in 1-iodoperfluorohexane and perfluorobenzene. Although perfluorobezene and perfluorohexane are nonpolar solvents, 1-iodoperfluorohexane exhibits halogen bond donor ability with its σ -hole which may complicate the interpretation of these subtle interaction trends.²³⁻²⁴

Interesting results are also seen in the folding ratios determined in CS_2 , which were significantly smaller for all four balances than in other solvents (the opposite to that observed in CS_2). This phenomenon was also observed in Motherwell's balances (unpublished result). The reason might be that CS_2 is a very good solvent for aromatics, even for carbon nanotubes and buckyballs²⁵ i.e. the balances are better solvated by CS_2 . It has also been demonstrated in a recent study that large binding between CS_2 and aromatics was arising from dispersion interactions.²⁶ CS_2 is a very apolar solvent ($\alpha_s = 1.0$ and $\beta_s = 0.1$), thus these interesting results are likely due to the high polarisability of sulfur compared to hydrocarbons, but once again the energy differences are small, consistent with a small, but measurable influence from differences in dispersion interactions.

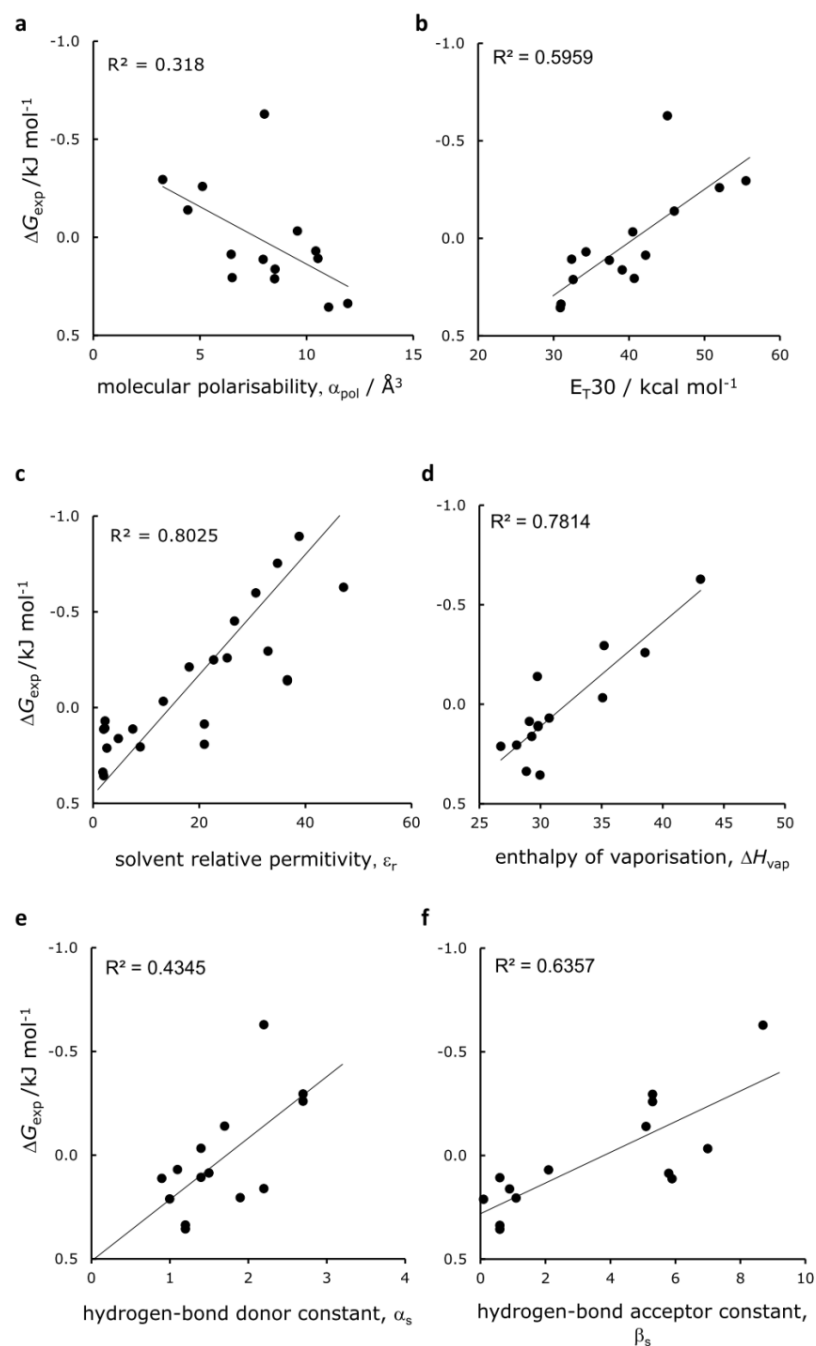


Figure 3.8. Experimental double-mutant cycle alkyl-alkyl interaction free energies (ΔG_{exp}) measured in a range of solvents (except fluorinated solvents and solvent mixtures) plotted against a range of solvent properties (Table 3.2).

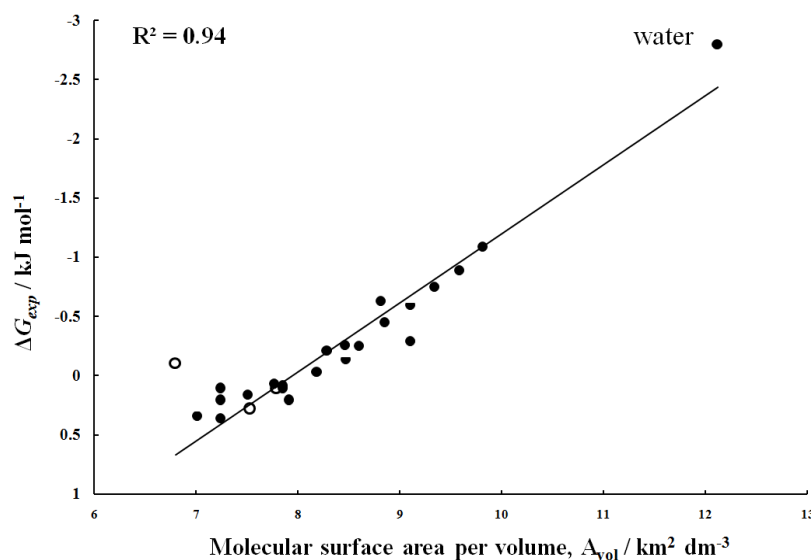


Figure 3.9. Experimental double-mutant cycle alkyl-alkyl interaction free energies (ΔG_{exp}) measured in a range of solvents (except fluorinated solvents and solvent mixtures) plotted against molecular surface area per unit volume. Hollow dots are energies in fluorinated solvents and are excluded from the fitting. The energy in water is extrapolated from data obtained in THF/D₂O mixtures.

An alternative approach for dissecting the measured alkyl-alkyl interactions can make use of Hunter's simple solvation model.¹² Using this model, the alkyl-alkyl folding process can be considered as being made up of solute-solute interactions ($\Delta G_{\text{alkyl-alkyl}}$), solute-solvent interactions ($\Delta G_{\alpha\text{s}} + \Delta G_{\beta\text{s}}$, which correspond to the desolvation energy of the alkyl chains by H-bond donors and H-bond acceptors, respectively) and solvent-solvent interactions ($\Delta G_{\alpha\text{s}\beta\text{s}}$). Thus, the experimental interaction energy in solution can be divided into four components as expressed in the following equation:

$$\Delta G_{\text{exp}} = \Delta G_{\text{alkyl-alkyl}} + \Delta G_{\alpha\text{s}} + \Delta G_{\beta\text{s}} + \Delta G_{\alpha\text{s}\beta\text{s}} \quad \text{Equation 3.3}$$

Derived from the above equation, the interaction energy can also be expressed as:

$$\Delta G_{\text{calc}} = a + b\alpha_{\text{s}} + c\beta_{\text{s}} + d\alpha_{\text{s}}\beta_{\text{s}} \quad \text{Equation 3.4}$$

Where α_s and β_s are the H-bond donor and acceptor ability of solvents, a , b , c , d are constants. The a term represents the solvent-independent solute-solute interaction $\Delta G_{\text{alkyl-alkyl}}$ plus any constant energy contribution from other components such as entropy.

The data were fitted into equation 3.4 with solver function in Excel, and the results are shown in Table 3.4. The positive a value implies there is no favourable dispersion contribution to the overall interaction energy. The positive b and c values suggest the desolvation processes are associated with a small energy cost as might be expected. The only negative value, d suggests that a favourable interaction energy comes from the stronger solvent-solvent interaction/solvophobic effect, consistent with earlier discussion.

Table 3.4. Calculated energies shown in 4 components.

a	0.183				
b	0.056				
c	0.035				
d	-0.060				
	$b\alpha_s$	$c\beta_s$	$d\alpha_s\beta_s$	ΔG_{calc}	ΔG_{exp}
	/kJ mol ⁻¹	/kJ mol ⁻¹	/kJ mol ⁻¹	/kJ mol ⁻¹	/kJ mol ⁻¹
Cyclohexane	0.067	0.021	-0.043	0.23	0.36
<i>n</i> -Hexane	0.067	0.021	-0.043	0.23	0.34
Carbon disulfide	0.056	0.004	-0.006	0.24	0.21
Dichloromethane	0.106	0.039	-0.125	0.20	0.21
Chloroform	0.123	0.032	-0.119	0.22	0.16
Carbon tetrachloride	0.078	0.021	-0.050	0.23	0.11
Benzene	0.062	0.074	-0.139	0.18	0.07
Tetrahydrofuran	0.050	0.207	-0.319	0.12	0.11
Pyridine	0.078	0.245	-0.588	-0.08	-0.03
Acetone	0.084	0.203	-0.522	-0.05	0.09
Acetonitrile	0.095	0.179	-0.520	-0.06	-0.14
Ethanol	0.151	0.186	-0.859	-0.34	-0.26
Methanol	0.151	0.186	-0.859	-0.34	-0.29
DMSO	0.123	0.305	-1.148	-0.54	-0.63

The calculated interaction energies determined from this fitting process were plotted against the experimental results, and gave a good correlation ($R^2 = 0.89$) (Fig 3.10a). Indeed, solvophobic term $d\alpha_s\beta_s$, is so dominant, that it alone correlates well with the experimental interaction energies ($R^2 = 0.88$) (Fig 3.10b). This again confirmed that alkyl-alkyl interactions are dominated by solvophobic effects. The same analysis was applied to calculated energies with added polarisability term (Fig 3.11). However, no improvement in the correlation was seen, and polarisability coefficient e was determined to be very small. This further confirmed that dispersion forces between alkyl and solvent are subtle.

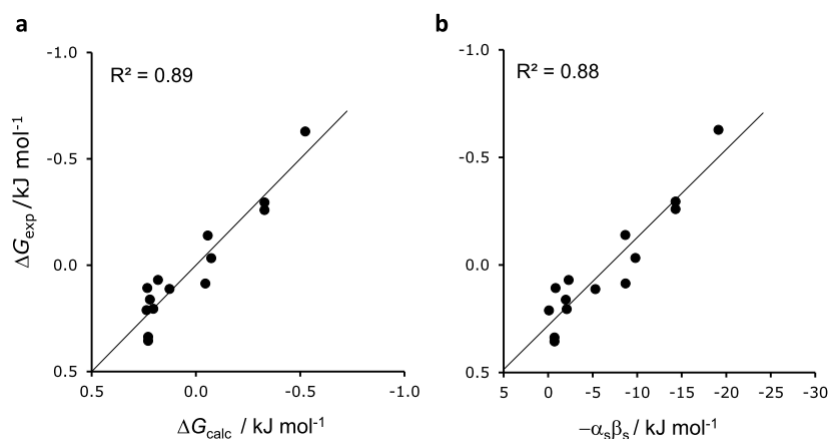


Figure 3.10. Experimental double-mutant cycle alkyl-alkyl interaction free energies (ΔG_{exp}) measured in a range of solvents vs. (a) ΔG_{calc} calculated using Equation 3.4, and (b) the product of solvent H-bond parameters α_s and β_s , which provides a measure of solvent cohesive interactions.

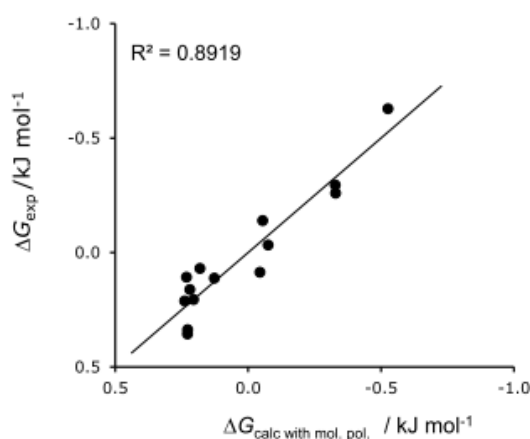


Figure 3.11. Experimental double-mutant cycle alkyl-alkyl interaction free energies (ΔG_{exp}) measured in a range of solvents plotted against $\Delta G_{\text{calc}} = a + b\alpha_s + c\beta_s + d\alpha_s\beta_s + e\alpha_{\text{pol}}$. Where the empirically derived coefficients were determined to be $a = 0.19$, $b = 0.053$, $c = 0.035$, $d = -0.059$, $e = -0.001$.

3.4.3 Enthalpy and entropy determination

The folding free energy consists of enthalpic and entropic components. Thus, to dissect these contributions to folding, variable-temperature NMR experiments were

performed in *d*₆-ethanol. NMR spectra were recorded from 283K to 303K. As the temperature increased, the equilibrium shifted towards the unfolded state. A Van't Hoff plot was obtained based on the data (Fig 3.12). According to the Van't Hoff equation,

$$\ln K = \frac{-\Delta H}{RT} + \frac{\Delta S}{R}$$

Equation 3.5

Where *R* is the gas constant. Thus, the slope of the graph plotted in Figure 3.12 is equal to $-\Delta H$ and the intercept is equal to ΔS . Generally, the fitting was good with $R^2 = 0.88$ for balance (±)-3 and all the others exceeded 0.94.

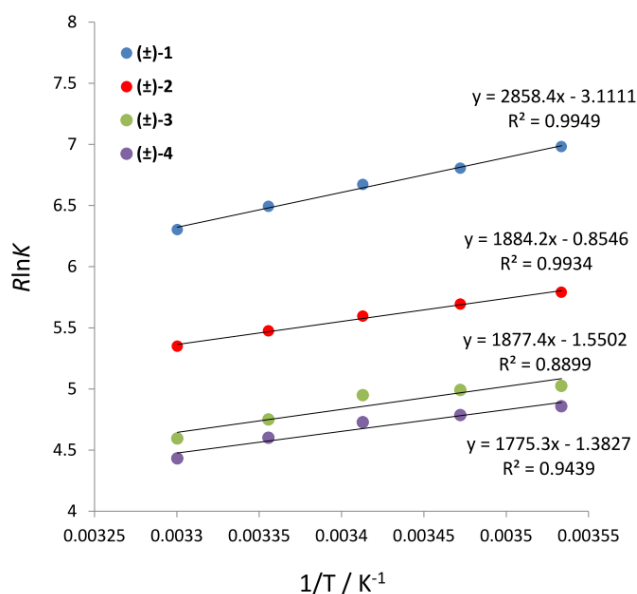


Figure 3.12. Van't Hoff plot of balances (±)-1-4. $R \ln K$ was plotted against $1/T$.

The determined enthalpy and entropy values are summarised in Table 3.5 along with the experimental DMC results. It reveals that the folding for all four balances is enthalpy driven, which is similar to previous findings.²¹ The alkyl-alkyl interaction dissected by the DMC approach was also found to be enthalpy driven. Basically, the

folding enthalpies for balances (±)-2, (±)-3 and (±)-4 are very similar and ~1 kJ/mol higher than for balance (±)-1. The net gain in enthalpy for balance (±)-1 can be attributed to the extra (mostly solvophobic driven) alkyl-alkyl interaction which is absent in the other balances. The same pattern is seen in entropy. The entropy decreases more in balance (±)-1 in accordance with enthalpy-entropy compensation.²⁷ The enthalpy ($\Delta H = -0.87$ kJ/mol) gained in forming the alkyl-alkyl interaction is almost cancelled by the large entropic term ($-T\Delta S = +0.62$ kJ/mol), leaving only a small favourable interaction free energy ($\Delta G = -0.25$ kJ/mol).

Table 3.5. Folding enthalpies (ΔH) and entropies (ΔS) in d_6 -ethanol determined from Van't Hoff plot, and alkyl-alkyl interaction enthalpy and entropy determined by double mutant cycle

	ΔH /kJ mol ⁻¹	ΔS /J mol ⁻¹ K ⁻¹	$-T\Delta S^{298K}$ /kJ mol ⁻¹
(±)-1	-2.86	-3.11	+0.93
(±)-2	-1.88	-0.85	+0.25
(±)-3	-1.88	-1.55	+0.46
(±)-4	-1.78	-1.38	+0.41
Double-mutant cycle	-0.87	-2.09	+0.62

The classic hydrophobic effect is driven by entropy, because disorder increases upon liberation of solvent molecules upon the association of two solutes.²⁸ This conclusion is true in many cases for small species. However, solvophobic effects are a multifaceted phenomenon complicated by the nature of the solvent, and the size of the solute, and sometimes solvophobic binding is found to be enthalpy driven.²⁹ A non-classical hydrophobic effect was reported previously for folding molecules.³⁰ Analogously, in our case, the solvophobic effects is enthalpy driven, which means that it is thus categorised as a non-classical solvophobic effect.

3.4.4 Computation studies

Computations were performed using the Hartree-Fock (HF), and DFT methods using B3LYP, ω B97X-D and M06 functionals as indicated in Table 3.6. The minimised folded and unfolded configurations were calculated for all four balances. The computed folded configurations for balance (\pm)-1 are similar to the crystal structure (Fig 3.6). The HF and B3LYP method do not provide complete electron correlation.³¹ B3LYP functional cannot accurately describe medium range exchange correlation,³² which is crucial to dispersion interactions. Without dispersion, balance (\pm)-4 (which contains no alkyl substituents) is predicted to be most stable in the folded conformation, whilst folding in balance (\pm)-1 is predicted to be less favourable in the gas phase (Table 3.6). The alkyl-alkyl interaction as dissected using an *in silico* DMC is predicted to be slightly favourable ($\Delta G_{\text{calc}} = -1.9$ and -3 kJ/mol) using the 6-31G* basis set with B3LYP and HF. ω B97X-D³³ and M06³² both take dispersion into account. In these calculations, folding free energy estimates for balance (\pm)-1 are dramatically more favourable than the other balances (over 20 kJ mol⁻¹ difference). The dissected DMC alkyl-alkyl interaction is now predicted to be very favourable ($\Delta G_{\text{calc}} = -13.4$ and -14.7 kJ mol⁻¹). In contrast, the folding energies for balance (\pm)-1 calculated using HF and B3LYP functional are very small compared to the ω B97X-D and M06 energies. Given the differences between these computational approaches discussed above, the energy differences can be attributed to large calculated dispersion forces between the alkyl chains in the M06 and ω B97X-D methods. Although HF and B3LYP method are blamed for their systematic errors in estimating dispersion in alkanes in the gas phase,³⁴ the data calculated by these methods appeared to be closer to the experimental results obtained in solution; while the ω B97X-D and M06 results overestimate the interaction by a considerable margin.

This further supports the view that dispersion interactions are almost negligible in solution. This suggests that one should never use ω B97X-D and M06 methods, when considering dispersion interaction in solution.

Table 3.6. Gas-phase folding free energy differences calculated from the minimised folded and unfolded structures of compounds (\pm)-1 to (\pm)-4 using Density Functional Theory at the levels of theory shown. ΔG_{calc} is the value of the alkyl-alkyl interaction calculated using the double-mutant cycle.

	Dispersion-corrected method?	$\Delta G_{(\pm)-1}$ /kJ mol ⁻¹	$\Delta G_{(\pm)-2}$ /kJ mol ⁻¹	$\Delta G_{(\pm)-3}$ /kJ mol ⁻¹	$\Delta G_{(\pm)-4}$ /kJ mol ⁻¹	ΔG_{calc} /kJ mol ⁻¹
HF/6-31G*	No	-1.8	-2.0	+1.0	-2.2	-3.0
B3LYP/6-31G*	No	-1.5	-1.5	0.0	-1.9	-1.9
ω B97X-D/6-31G*	Yes	-41.9	-19.9	-18.8	-10.2	-13.4
M06/6-31G*	Yes	-36.7	-15.0	-15.7	-8.7	-14.7

3.5 Conclusion

In conclusion, a Wilcox torsion balance featuring in intramolecular alkane-alkane interaction was carefully designed and synthesised. Systematic evaluation of the alkyl-alkyl interaction was carried out in a variety of solvents. The experimentally determined interaction energies, ΔG_{exp} correlated with molecular surface area per unit volume of solvent, and other measures of cohesive solvent interactions. This points to a major contribution to apolar alkyl associate from solvophobic effects. Further decomposition of the interaction energy by Hunter's theory, combined with enthalpy-entropy analyses and computational results, led to a conclusion that dispersion plays minor role in molecular recognition in solution. Very small contributions to alkyl-alkyl interactions (<0.5 kJ mol⁻¹) from dispersion differences

were seen in very highly polarisable solvents (e.g. CS₂), and those with low polarisability (perfluorinated solvents).

3.6 Experimental Section

All compound numbers refer to compounds exclusively as presented in this chapter.

Hayat P. H. Saifuddin assisted in developing the synthetic routes to balances (±)-**1** and (±)-**4**, and carried out a preliminary solvent study on these two balances. Gary S. Nichol performed X-ray crystal analyses.

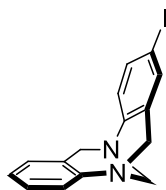
General Synthetic Methods and Materials

Unless otherwise stated, all chemicals were purchased for *Sigma-Aldrich*, *VWR* or *FluoroChem* and used without further purification. Dry solvents were obtained from a *PureSolv* solvent purification system. Unless stated otherwise, all reactions were carried out under an atmosphere of nitrogen. All ¹H, ¹³C NMR were recorded using either a 400 MHz *Bruker AV 400* spectrometer or a 500 MHz *Bruker Avance III* spectrometer. ¹H and ¹³C NMR spectra were referenced to residual solvent peaks and reference to tetramethylsilane. Mass spectra recorded by the Mass Spectrometry Service at the University of Edinburgh. Melting points were determined using Stuart melting point apparatus and are uncorrected. Column chromatography was performed on *GeduranSi 60* silica gel. Preparative TLC was performed on molecular balances (±)-**1** to **4** using 2.0 mm thick *Uniplate* Silica gel plates, and observed under UV light.

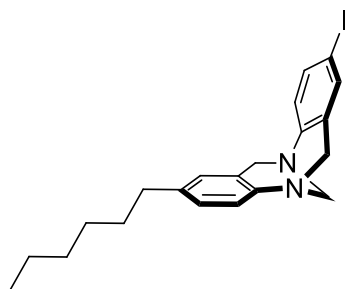
General procedure for the synthesis of Tröger's base ((±)-5a, b)³⁵

4-iodoaniline (1.3 g, 6 mmol), aniline (6 mmol) and paraformaldehyde (580 mg, 19.2 mmol) were successively dissolved 30 mL TFA in -15°C ice/salt bath. The mixture was warmed to room temperature and stirred for 3 days under N_2 and protected from light. Then the mixture was basified with 90 mL ammonium solution (30 mL 36% ammonium and 60 mL water), 100 mL sat. NaHCO_3 aqueous solution. The mixture was extracted with DCM and washed with brine. The organic layer was dried over MgSO_4 , filtered and the solvent was removed under vacuum. The crude product was purified by column chromatography.

2-iodo-6*H*,12*H*-5,11-methanodibenzo[*b,f*][1,5]diazocine ((±)-5a) was synthesised by a previously reported route.³⁵



2-hexyl-8-iodo-6*H*,12*H*-5,11-methanodibenzo[*b,f*][1,5]diazocine ((±)-5b).



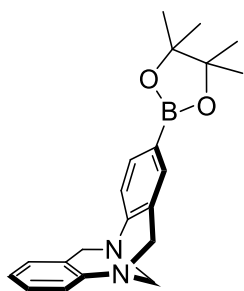
Brown solid. Yield 19%. m.p. $112\text{-}114^{\circ}\text{C}$ ^1H NMR (400 MHz, CDCl_3) δ 7.47 (dd, $J = 8.5, 2.0$ Hz, 1H), 7.26 (d, $J = 1.9$ Hz, 1H), 7.02 (m, 2H), 6.92 (d, $J = 8.5$ Hz, 1H), 6.73 (s, 1H), 4.69 (d, $J = 16.7$ Hz, 1H), 4.64 (d, $J = 16.8$ Hz, 1H), 4.35 – 4.25 (m, 2H), 4.15 (d, $J = 5.8$ Hz, 1H), 4.11 (d, $J = 5.6$ Hz, 1H), 2.50 (t, $J = 7.8$ Hz, 2H), 1.62

– 1.48 (m, 2H), 1.36 – 1.26 (m, 6H), 0.90 (t, $J = 6.9$ Hz, 3H). ^{13}C NMR (101 MHz, CDCl_3) δ 148.13, 145.19, 138.96, 136.19, 135.79, 130.70, 127.69, 127.11, 126.52, 124.79, 87.32, 66.77, 58.77, 58.08, 35.46, 31.71, 31.46, 29.08, 22.60, 14.11. MS (ESI) m/z 433.27 ($[\text{M}+\text{H}]^+$).

General procedure for the synthesis of boronic ester ((±)-6a, b)³⁶

The corresponding iodide compound (1.05 mmol), bis(pinacolato)diboron (300 mg, 1.19 mmol), AcOK (309 mg, 3.15 mmol), and $[\text{Pd}(\text{dppf})\text{Cl}_2] \cdot \text{CH}_2\text{Cl}_2$ (19 mg, 0.025 mmol) were mixed in 10 mL dry DMF. The mixture was degassed, flushed with N_2 and heated to 70 °C overnight. Then the reaction was cooled to room temperature, diluted with DCM, washed with brine and water. The organic layer was dried over MgSO_4 , filtered and the solvent was removed under reduced pressure. The crude product was purified by column chromatography.

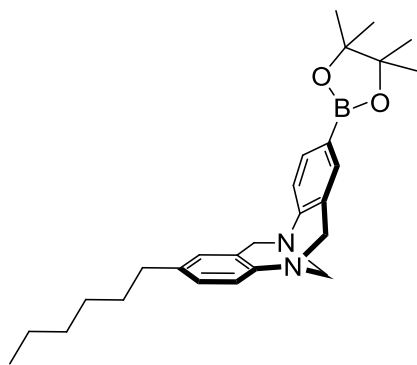
2-(4,4,5,5-tetramethyl-1,3,2-dioxaborolan-2-yl)-6*H*,12*H*-5,11-methanodibenzo[*b*,*f*][1,5]diazocine ((±)-6a).



White Solid. Yield 63%. m.p. 166-168°C ^1H NMR (500 MHz, CDCl_3) δ 7.63 (d, $J = 8.0$ Hz, 1H), 7.43 (s, 1H), 7.22 – 7.10 (m, 3H), 6.98 (m, 1H), 6.91 (d, $J = 7.6$ Hz, 1H), 4.74 (d, $J = 16.6$ Hz, 1H), 4.71 (d, $J = 16.6$ Hz, 1H) 4.37 (s, 2H), 4.23 (d, $J = 16.6$ Hz, 2H), 1.32 (s, 12H). ^{13}C NMR (126 MHz, CDCl_3) δ 151.03, 147.67, 133.93,

133.74, 127.74, 127.44, 127.09, 126.96, 125.05, 124.38, 124.11, 83.71, 66.83, 58.73, 58.61, 24.83. MS (ESI) m/z 349.29 ($[M+H]^+$).

2-hexyl-8-(4,4,5,5-tetramethyl-1,3,2-dioxaborolan-2-yl)-6*H*,12*H*-5,11-methanodibenzo[*b,f*][1,5] diazocine (\pm)-6b).



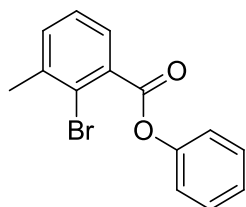
Dark/brown oil. Yield 90%. ^1H NMR (400 MHz, CDCl_3) δ 7.65 (dd, $J = 8.0, 0.9$ Hz, 1H), 7.44 (s, 1H), 7.17 (d, $J = 8.0$ Hz, 1H), 7.06 (d, $J = 8.2$ Hz, 1H), 6.99 (dd, $J = 8.2, 1.7$ Hz, 1H), 6.72 (s, 1H), 4.72 (d, $J = 16.6$ Hz, 1H), 4.71 (d, $J = 16.6$ Hz, 1H), 4.35 (s, 2H), 4.21 (d, $J = 16.6$ Hz, 2H), 1.64 – 1.45 (m, 2H), 1.39 – 1.24 (m, 18H), 0.91 (t, $J = 6.8$ Hz, 3H). ^{13}C NMR (126 MHz, CDCl_3) δ 151.40, 145.46, 138.64, 134.00, 133.64, 127.55, 127.37, 126.52, 124.81, 124.41, 83.67, 66.94, 58.82, 58.57, 35.46, 31.74, 31.48, 29.08, 24.85, 22.62, 14.14. MS (ESI) m/z 433.38 ($[M+H]^+$)

General procedure for the esterification (7a, b).

2-bromo-3-methylbenzoic acid (2 mmol, 430 mg), the corresponding phenol (2 mmol), dicyclohexylcarbodiimide (2.2 mmol, 454 mg) and 4-dimethylaminopyridine (0.2 mmol, 25 mg) were dissolved in 20 mL dry DCM. The mixture was stirred at room temperature overnight. Then the mixture was filtered, the filtrate was

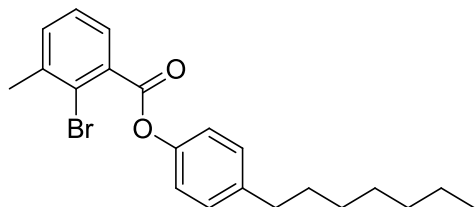
concentrated under reduced pressure. The crude product was purified by column chromatography.

phenyl 2-bromo-3-methylbenzoate (7a).



White solid. Yield 84%. m.p. 62-65°C ^1H NMR (500 MHz, CDCl_3) δ 7.72 (dd, $J = 7.6, 1.1$ Hz, 1H), 7.52 – 7.41 (m, 3H), 7.39 – 7.26 (m, 4H), 2.54 (s, 3H). ^{13}C NMR (126 MHz, CDCl_3) δ 165.68, 150.80, 140.05, 133.69, 133.29, 129.55, 128.37, 127.00, 126.12, 123.57, 121.57, 23.84. MS (EI) m/z 290.0 (M^+).

4-heptylphenyl 2-bromo-3-methylbenzoate (7b).

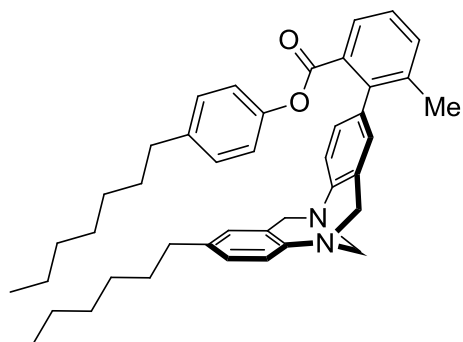


Obtained as colourless oil. Yield 78%. ^1H NMR (400 MHz, CDCl_3) δ 7.70 (dd, $J = 7.6, 1.3$ Hz, 1H), 7.46 – 7.42 (m, 1H), 7.35 (t, $J = 7.6$ Hz, 1H), 7.30 – 7.24 (m, 2H), 7.23 – 7.17 (m, 2H), 2.66 (t, $J = 7.7$ Hz, 2H), 2.54 (s, 3H), 1.74 – 1.59 (m, 2H), 1.45 – 1.23 (m, 8H), 0.94 (t, $J = 6.9$ Hz, 3H). ^{13}C NMR (101 MHz, CDCl_3) δ 165.88, 148.70, 140.83, 139.99, 133.59, 133.48, 129.39, 128.33, 126.98, 123.53, 121.18, 35.43, 31.85, 31.54, 29.27, 29.21, 23.83, 22.70, 14.14. MS (ESI) m/z 389.06 ($[\text{M}+\text{H}]^+$)

General procedure for Suzuki coupling ((±)-1, (±)-2, (±)-3, (±)-4).

Boronic ester (0.22 mmol), corresponding bromide (0.22 mmol), and Pd(PPh₃)₄ (0.02 mmol, 23 mg) were mixed in 10 mL toluene and 2 mL ethanol. K₂CO₃ (0.66 mmol, 91 mg) in 1 mL water was added. The mixture was degassed and heated to 110 °C under N₂ overnight. Then the reaction was cooled to room temperature, diluted with DCM and washed with water. The organic layer was dried over MgSO₄, filtered and solvent was removed under reduced pressure. The crude product was purified by column chromatography.

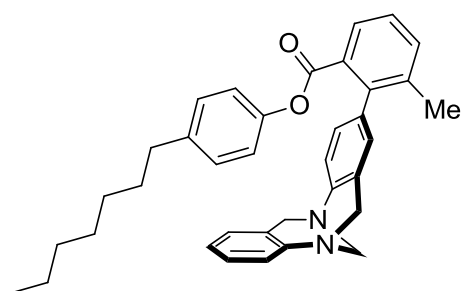
4-heptylphenyl 2-(8-hexyl-6*H*,12*H*-5,11-methanodibenzo[*b*,*f*][1,5]diazocin-2-yl)-3-methylbenzoate ((±)-1).



White solid/colourless crystal. Yield 63%. m.p. 103-105°C ¹H NMR (500 MHz, CDCl₃) δ 7.76/7.70 (2d, *J* = 7.5 Hz, 1H), 7.45 – 7.35 (m, 2H), 7.25 – 7.04 (m, 5H), 6.90 – 6.77 (m, 2H), 6.71-6.67 (m, 2H), 6.09 (d, *J* = 8.3 Hz, 1H), 4.89 – 4.58 (m, 2H), 4.48 – 4.06 (m, 4H), 2.69 – 2.37 (m, 4H), 2.18/2.12 (2s, 3H), 1.72 – 1.48 (m, 4H), 1.48 – 1.10 (m, 14H), 1.00 – 0.82 (m, 6H). ¹³C NMR (126 MHz, CDCl₃) δ 168.15/167.66, 148.54/148.06, 147.09, 145.40, 140.91/140.50, 140.41/139.96, 138.85/138.73, 137.47/137.35, 136.07/135.80, 133.27/133.12, 132.14, 129.12, 129.02, 128.47/128.15, 127.75/127.50, 127.39 (2C), 127.28/127.23, 127.15/127.07,

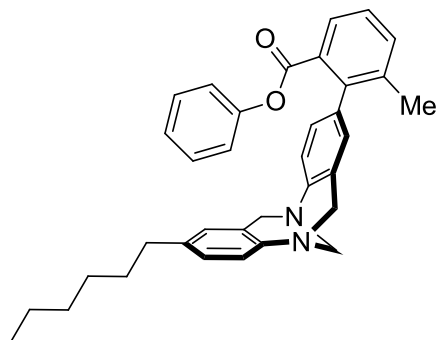
126.98/126.87, 126.56/126.51, 125.16/125.01, 124.86, 120.89, 120.62, 66.89/66.77, 58.43/58.37/58.34/58.16 (2C), 35.77/35.53/35.51/35.35 (2C), 31.89/31.83/31.76/31.72 (2C), 31.47, 31.45, 29.46/29.29/29.26/29.17/29.06 (3C), 22.70/22.66/22.60 (2C), 20.81/20.75, 14.13, 14.12. MS (EI) m/z 614.3 (M^+). HRMS (EI) m/z 614.386860 (M^+ , $C_{42}H_{50}N_2O_2^+$, calc. 614.38668)

4-heptylphenyl 2-(6*H*,12*H*-5,11-methanodibenzo[*b,f*][1,5]diazocin-2-yl)-3-methyl benzoate(±)-2).



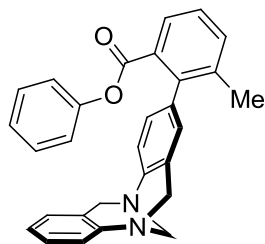
Obtained as a waxy colourless solid. Yield 61%. 1H NMR (500 MHz, $CDCl_3$) δ 7.77/7.69 (2d, $J = 7.5$ Hz, 1H), 7.45 – 7.35 (m, 2H), 7.28 – 6.95 (m, 7H), 6.86/6.84 (2s, 1H), 6.70 – 6.68 (m, 2H), 6.06 (d, $J = 8.3$ Hz, 1H), 4.88 – 4.64 (m, 2H), 4.50 – 4.12 (m, 4H), 2.65 – 2.39 (m, 2H), 2.17/2.11 (2s, 3H), 1.60 – 1.53 (m, 2H), 1.39 – 1.25 (m, 8H), 0.97 – 0.84 (m, 3H). ^{13}C NMR (126 MHz, $CDCl_3$) δ 168.15/167.60, 148.54/148.04, 147.84, 146.83, 140.90/140.47, 140.42/139.90, 137.45/137.39, 136.27/135.94, 133.29/133.12, 132.15/132.06, 129.12, 129.06, 128.54/128.22, 127.92, 127.61/127.40, 127.29, 127.27/127.24, 127.17/127.09, 127.03, 126.96/126.90, 125.44/125.29, 124.85, 124.34/124.14, 120.89, 120.44, 66.80/66.70, 58.47/58.42/58.34/58.26 (2C), 35.35/35.27, 31.85/31.83, 31.49/31.41, 29.26/29.22/29.17 (2C), 22.71/22.69, 20.82/20.73, 14.14/14.13. MS (EI) m/z 530.2 (M^+). HRMS (EI) m/z 530.292729 (M^+ , $C_{36}H_{38}N_2O_2^+$, calc. 530.29278)

phenyl 2-(8-hexyl-6*H*,12*H*-5,11-methanodibenzo[*b*,*f*][1,5]diazocin-2-yl)-3-methyl benzoate ((±)-3).



White solid/colourless crystal. Yield 72%. m.p. 134-136°C ¹H NMR (500 MHz, CDCl₃) δ 7.77/7.70 (2d, *J* = 7.5 Hz, 1H), 7.46 – 7.31 (m, 3H), 7.28 – 6.95 (m, 5H), 6.78 – 6.91 (m, 4H), 6.23 (d, *J* = 7.7 Hz, 1H), 4.91 – 4.59 (m, 2H), 4.54 – 4.07 (m, 4H), 2.66 – 2.44 (m, 2H), 2.17/2.12 (2s 3H), 1.66 – 1.56 (m, 2H), 1.45 – 1.20 (m, 6H), 0.99 – 0.82 (m, 3H). ¹³C NMR (126 MHz, CDCl₃) δ 167.97/167.46, 150.69/150.21, 147.18, 145.41, 140.98/140.60, 138.83, 137.52/137.41, 136.02/135.73, 133.36/133.22, 132.01/131.99, 129.28, 129.13, 128.40/128.11, 127.71, 127.51, 127.47, 127.26, 127.17/127.00, 127.11/126.92, 126.53, 125.72/125.19, 125.11/125.01, 124.89, 121.27, 120.90, 66.88/66.76, 58.45/58.38/58.18 (2C), 35.64/35.50, 31.78/31.72, 31.49, 29.29/29.06, 22.63, 20.81/20.75, 14.13/14.10. MS (EI) *m/z* 516.2 (M⁺). HRMS (EI) *m/z* 516.277583 (M⁺, C₃₅H₃₆N₂O₂⁺, calc. 516.27713)

phenyl 2-(6*H*,12*H*-5,11-methanodibenzo[*b,f*][1,5]diazocin-2-yl)-3-methyl benzoate(±)-4).



White solid. Yield 50%. m.p. 63-65 °C ^1H NMR (500 MHz, CDCl_3) δ 7.77/7.74 (2d, $J = 7.5$ Hz, 1H), 7.48 – 7.30 (m, 3H), 7.27 – 6.73 (m, 10H), 6.19 (d, $J = 7.8$ Hz, 1H), 4.88 – 4.64 (m, 2H), 4.51 – 4.14 (m, 4H), 2.24/2.08 (2s, 3H). ^{13}C NMR (126 MHz, CDCl_3) δ 167.93/167.39, 150.69/150.20, 147.77, 146.91, 140.97/140.55, 137.50/137.45, 136.20/135.90, 133.40/133.24, 131.98/131.90, 129.29, 129.21, 128.50/128.20, 127.62, 127.51, 127.40, 127.29/127.23, 127.19/127.14, 127.03/127.01, 126.97, 125.73/125.32, 125.29, 124.84, 124.38/124.14, 121.27, 120.82, 66.79/66.74, 58.46/58.41/58.34 (2C), 20.83/20.75. MS (EI) m/z 432.2 (M^+). HRMS (EI) m/z 432.183059(M^+ , $\text{C}_{29}\text{H}_{24}\text{N}_2\text{O}_2^+$, calc. 432.18323)

Solvent study

All four balances were prepared as 10mM solutions in deuterated or fluorinated solvents, except in d_{12} -cyclohexane where solubilities were lower, saturated solutions were used instead. As for nondeuterated solvents, internal standards filled with D_2O were used. Folding ratios were determined by integration of the folded/unfolded NMR signals (methyl signal in most cases, ArCH signal in acetone and acetonitrile where methyl signals overlap with solvent residual signal or water). The integrated regions were fitted with Gaussian/Lorentzian=1:1 function incorporated in MestReNova software.

VT experiments

All 4 balances were prepared as 10mM solutions in d_6 -ethanol. Spectra were taken every 5°C elevated from 278K to 323K.

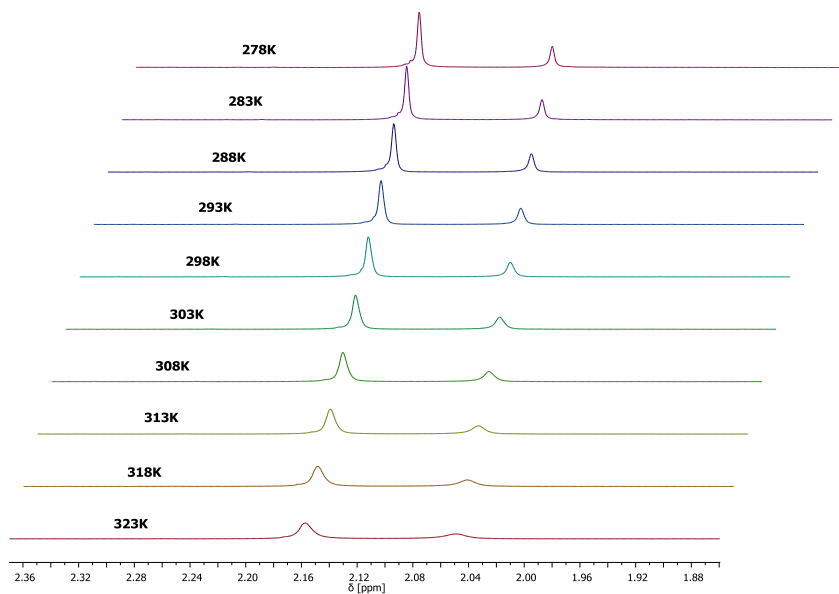


Figure S3.1. ^1H NMR spectra of (\pm)-1 in d_6 -ethanol as 10 mM solutions at variable temperature.

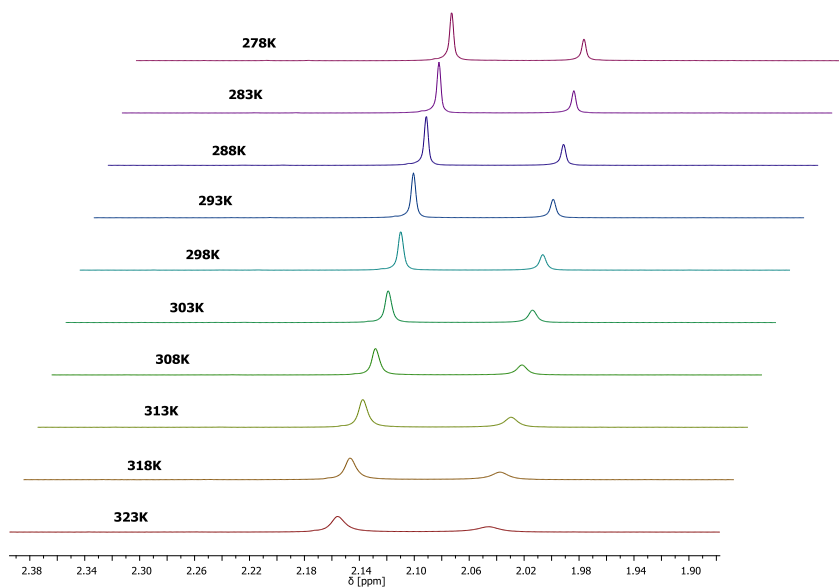


Figure S3.2. ^1H NMR spectra of (\pm)-2 in d_6 -ethanol as 10 mM solutions at variable temperature.

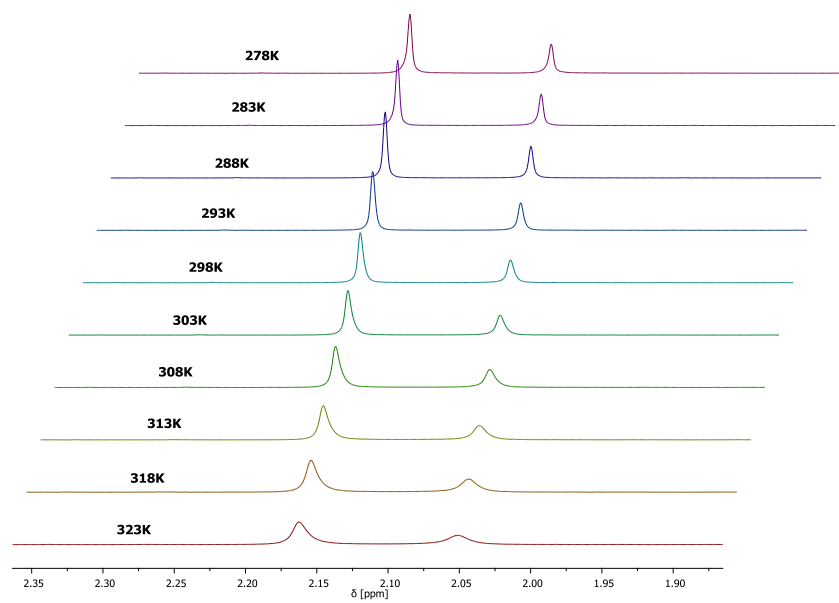


Figure S3.3. ^1H NMR spectra of (\pm)-3 in d_6 -ethanol as 10 mM solutions at variable temperature.

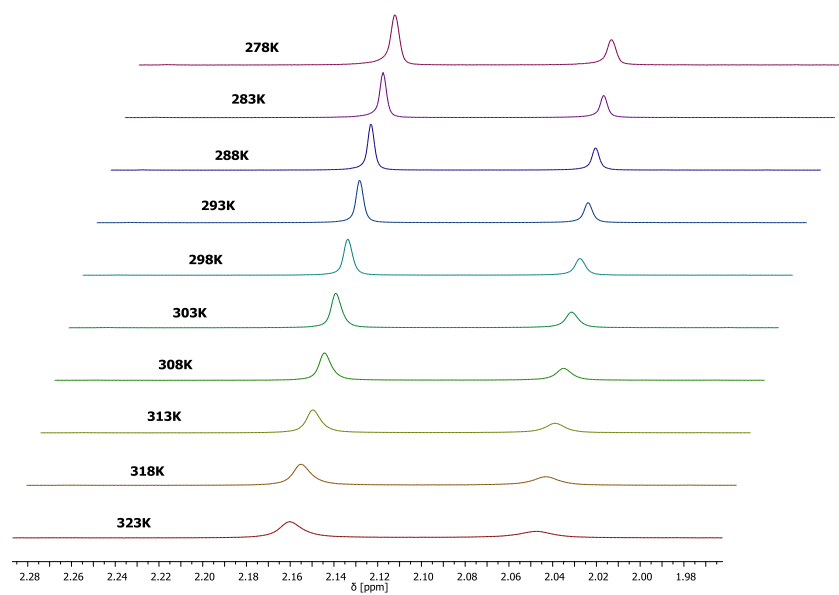


Figure S3.4. ^1H NMR spectra of (\pm)-4 in d_6 -ethanol as 10 mM solutions at variable temperature.

X-ray Crystallography

Crystals of (\pm)-**1** were grown by slow evaporation of methanol solution. Crystals were obtained as large transparent and colourless parallelogram body. CCDC-898520 crystallographic data is available from the Cambridge Crystallographic Data Centre.

Chemical formula (moiety)	$C_{42}H_{50}N_2O_2 \cdot CH_4O$	
Chemical formula (total)	$C_{43}H_{54}N_2O_3$	
Formula weight	646.88	
Temperature	120(2) K	
Radiation, wavelength	CuK α , 1.54184 Å	
Crystal system, space group	triclinic, $P\bar{1}$	
Unit cell parameters	$a = 9.4140(2)$ Å	$\alpha = 87.8308(17)^\circ$
	$b = 9.4615(2)$ Å	$\beta = 79.2432(18)^\circ$
	$c = 23.4843(5)$ Å	$\gamma = 63.911(2)^\circ$
Cell volume	$1843.32(7)$ Å ³	
Z	2	
Calculated density	1.165 g/cm ³	
Absorption coefficient μ	0.560 mm ⁻¹	
F(000)	700	
Crystal colour and size	colourless, 0.19 × 0.17 × 0.15 mm ³	
Reflections for cell refinement	30752 (θ range 3.8 to 76.4°)	
Data collection method	Agilent Technologies SuperNova	
	ω scans	
θ range for data collection	3.8 to 76.6°	

Index ranges	h -11 to 11, k -11 to 11, l -29 to 29
Completeness to $\theta = 76.6^\circ$	98.9 %
Reflections collected	45757
Independent reflections	7676 ($R_{\text{int}} = 0.0177$)
Reflections with $F^2 > 2\sigma$	7316
Absorption correction	Gaussian
Min. and max. transmission	0.9001 and 0.9202
Structure solution	charge-flipping
Refinement method	Full-matrix least-squares on F^2
Weighting parameters a, b	0.0824, 1.3610
Data / restraints / parameters	7676 / 27 / 585
Final R indices [$F^2 > 2\sigma$]	R1 = 0.0656, wR2 = 0.1689
R indices (all data)	R1 = 0.0675, wR2 = 0.1706
Goodness-of-fit on F^2	1.038
Extinction coefficient	0.0023(5)
Largest and mean shift/su	0.000 and 0.000
Largest diff. peak and hole	1.04 and -0.49 e \AA^{-3}

References

- (1) London, F. *Trans. Faraday Soc.* **1937**, *33*, 8b - 26.
- (2) Joh, N. H.; Oberai, A.; Yang, D.; Whitelegge, J. P.; Bowie, J. U. *J. Am. Chem. Soc.* **2009**, *131*, 10846-10847.
- (3) Autumn, K.; Sitti, M.; Liang, Y. A.; Peattie, A. M.; Hansen, W. R.; Sponberg, S.; Kenny, T. W.; Fearing, R.; Israelachvili, J. N.; Full, R. J. *Proc. Natl. Acad. Sci. U. S. A.* **2002**, *99*, 12252-12256.
- (4) Mengüç, Y.; Yang, S. Y.; Kim, S.; Rogers, J. A.; Sitti, M. *Adv. Funct. Mater.* **2012**, *22*, 1246-1254.
- (5) Yu, J.; Chary, S.; Das, S.; Tamelier, J.; Pesika, N. S.; Turner, K. L.; Israelachvili, J. N. *Adv. Funct. Mater.* **2011**, *21*, 3010-3018.
- (6) Novoa, J. J.; Whangbo, M.-H.; Williams, J. M. *J. Chem. Phys.* **1991**, *94*, 4835-4841.
- (7) Echeverria, J.; Aullon, G.; Danovich, D.; Shaik, S.; Alvarez, S. *Nat Chem* **2011**, *3*, 323-330.
- (8) Lüttschwager, N. O. B.; Wassermann, T. N.; Mata, R. A.; Suhm, M. A. *Angew. Chem., Int. Ed.* **2013**, *52*, 463-466.
- (9) Wodrich, M. D.; Wannere, C. S.; Mo, Y.; Jarowski, P. D.; Houk, K. N.; Schleyer, P. v. R. *Chem. Eur. J.* **2007**, *13*, 7731-7744.
- (10) Schreiner, P. R.; Chernish, L. V.; Gunchenko, P. A.; Tikhonchuk, E. Y.; Hausmann, H.; Serafin, M.; Schlecht, S.; Dahl, J. E. P.; Carlson, R. M. K.; Fokin, A. A. *Nature* **2011**, *477*, 308-311.
- (11) Fokin, A. A.; Chernish, L. V.; Gunchenko, P. A.; Tikhonchuk, E. Y.; Hausmann, H.; Serafin, M.; Dahl, J. E. P.; Carlson, R. M. K.; Schreiner, P. R. *J. Am. Chem. Soc.* **2012**, *134*, 13641-13650.
- (12) Hunter, C. A. *Angew. Chem., Int. Ed.* **2004**, *43*, 5310-5324.
- (13) *CRC Handbook of Chemistry and Physics. 84 edn*; CRC Press, 2003.
- (14) Mati, I. K.; Cockroft, S. L. *Chem. Soc. Rev.* **2010**, *39*, 4195-4205.
- (15) Paliwal, S.; Geib, S.; Wilcox, C. S. *J. Am. Chem. Soc.* **1994**, *116*, 4497-4498.
- (16) Cockroft, S. L.; Hunter, C. A. *Chem. Soc. Rev.* **2007**, *36*, 172-188.
- (17) Wohlfarth, C. in *Data extract from Landolt-Börnstein IV/17: Static Dielectric Constants of Pure Liquids and Binary Liquid Mixtures Vol. 17 Landolt-Börnstein - Group IV Physical Chemistry (ed M. D. Lechner)*; Springer-Verlag Berlin Heidelberg, 2008.
- (18) Oliferenko, A. A.; Oliferenko, P. V.; Huddleston, J. G.; Rogers, R. D.; Palyulin, V. A.; Zefirov, N. S.; Katritzky, A. R. *J. Chem. Inf. Comput. Sci.* **2004**, *44*, 1042-1055.
- (19) Bosque, R.; Sales, J. J. *J. Chem. Inf. Comput. Sci.* **2002**, *42*, 1154-1163.
- (20) Cabot, R.; Hunter, C. A.; Varley, L. M. *Org. Biomol. Chem.* **2010**, *8*, 1455-1462.
- (21) Fischer, F. R.; Wood, P. A.; Allen, F. H.; Diederich, F. *Proc. Natl. Acad. Sci. U. S. A.* **2008**, *105*, 17290-17294.
- (22) Tsuzuki, S.; Honda, K.; Uchamaru, T.; Mikami, M. *J. Phys. Chem. A* **2004**, *108*, 10311-10316.
- (23) Harry, A.; Scott, L. C.; Claudio, G.; Christopher, A. H.; Kevin, R. L.; Julie, P.; Sharon, E. S.;

- Christopher, J. U.; Rhonan, F. *Chembiochem* **2004**, *5*, 657-665.
- (24) Cabot, R.; Hunter, C. A. *Chem. Commun.* **2009**, *0*, 2005-2007.
- (25) Chamberlain, T. W.; Popov, A. M.; Knizhnik, A. A.; Samoilov, G. E.; Khlobystov, A. N. *ACS Nano* **2010**, *4*, 5203-5210.
- (26) Deshmukh, M. M.; Ohba, M.; Kitagawa, S.; Sakaki, S. *J. Am. Chem. Soc.* **2013**, *135*, 4840-4849.
- (27) Searle, M. S.; Westwell, M. S.; Williams, D. H. *J. Chem. Soc., Perkin Trans. 2* **1995**, *0*, 141-151.
- (28) Anslyn, E. V.; Dougherty, D. A. *Modern Physical Organic Chemistry*; University Science Books, 2005.
- (29) Chandler, D. *Nature* **2005**, *437*, 640-647.
- (30) Newcomb, L. F.; Gellman, S. H. *J. Am. Chem. Soc.* **1994**, *116*, 4993-4994.
- (31) Sherrill, C. D. *Computations of Noncovalent pi Interactions*; John Wiley & Sons, Inc., 2009.
- (32) Zhao, Y.; Truhlar, D. G. *Acc. Chem. Res.* **2008**, *41*, 157-167.
- (33) Chai, J.-D.; Head-Gordon, M. *Phys. Chem. Chem. Phys.* **2008**, *10*, 6615-6620.
- (34) Wodrich, M. D.; Corminboeuf, C.; Schleyer, P. v. R. *Org. Lett.* **2006**, *8*, 3631-3634.
- (35) Faroughi, M.; Zhu, K.-X.; Jensen, P.; Craig, D. C.; Try, A. C. *Eur. J. Org. Chem.* **2009**, *2009*, 4266-4272.
- (36) Hof, F.; Schär, M.; Scofield, D. M.; Fischer, F.; Diederich, F.; Sergeyev, S. *Helvetica Chimica Acta* **2005**, *88*, 2333-2344.

Chapter 4 Solvent effects on edge-to-face aromatic interactions

Abstract

Edge-to-face aromatic interactions are studied in a wide range of solvents using a Wilcox torsion balance. Patterns in the solvent effects were found to be too complicated to be rationalised by current approaches. Nevertheless, the edge-to-face aromatic interactions in solution are very small and sensitive to the solvent environment.

4.1 Introduction

Solvent effects are a complicated but useful phenomenon that can be exploited in chemical reactions¹ and molecular recognition processes.²⁻⁴ Numerous efforts have been made to rationalise solvent effects via experimental model studies. For example, both Still⁵ and Rebek⁶ have found that the stability of molecular inclusion complexes depend on solvent size and packing. Rebek *et al* proposed that the 55% packing coefficient found in his molecular capsules was the same as that found in organic liquids. Diederich *et al* reported that the complexation free energies of pyrene within cyclophanes increased linearly with solvent polarity, as measured using the E_T30 scale.⁷ Iverson also found this kind of relationship in aromatic stacking in folding molecules.⁸ Meanwhile, Hunter has developed a simple solvation model based on H-bond acceptor and donor ability for simple non-covalent systems.⁹ Considering the multitude of solvent studies, it becomes apparent that solvent effects on non-covalent

interactions vary from system to system and may not always be general. Here we start from the heavily studied edge-to-face aromatic interaction to see how solvent influences the interaction.

4.2 Project Design and Synthesis

Many variations of the classic Wilcox torsion balance have been used to study edge-to-face aromatic interactions, and in some cases contradictory models of the factors governing the behaviour of this system have been proposed.^{2,10-12} However, to date, solvent screens on the effects of solvents on these types of interactions have been limited to less than 10 different solvents, which are mostly polar solvents.¹²⁻¹⁴ Here we designed a simple experiment to study solvent effects on edge-to-face aromatic interactions.

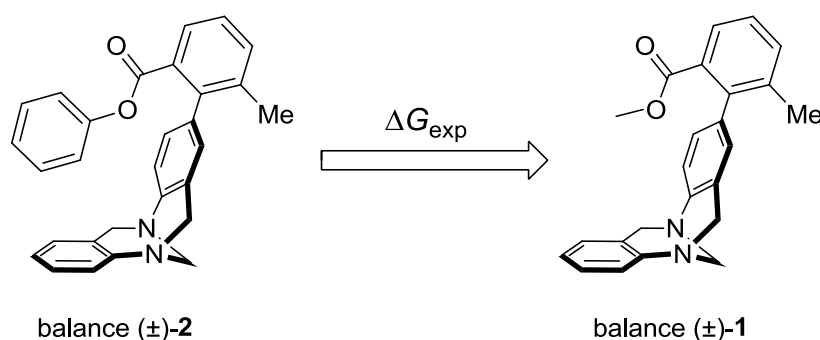


Figure 4.1. Balance (±)-2 and control balance (±)-1.

Balance (±)-2 features an edge-to-face aromatic interaction in the folded state (Fig 4.1 and Fig 4.2). As described in previous chapters, ¹H NMR provides a tool for measuring folding free energies in solution. Figure 4.2 shows that an unsolvated, vacuum-like region of space is generated in the folded state of balance (±)-1 as indicated in red. In contrast, the phenyl group occupies the entire space within the

cavity of the folded state in balance (\pm)-2. Control balance (\pm)-1 does not possess an effective interaction between the methyl and the face aromatic, since the CH \cdots aromatic distance is over 4.2Å (as shown by calculation using Spartan '08 in Fig 4.2). This distance is also too far for effective dispersion interactions to be formed between the methyl group and the lower aromatic ring, although the bite angle of the Tröger's base may be somewhat flexible.¹⁵ Similar torsion balances studied by other groups were demonstrated to have no CH \cdots π interaction.¹⁶⁻¹⁷

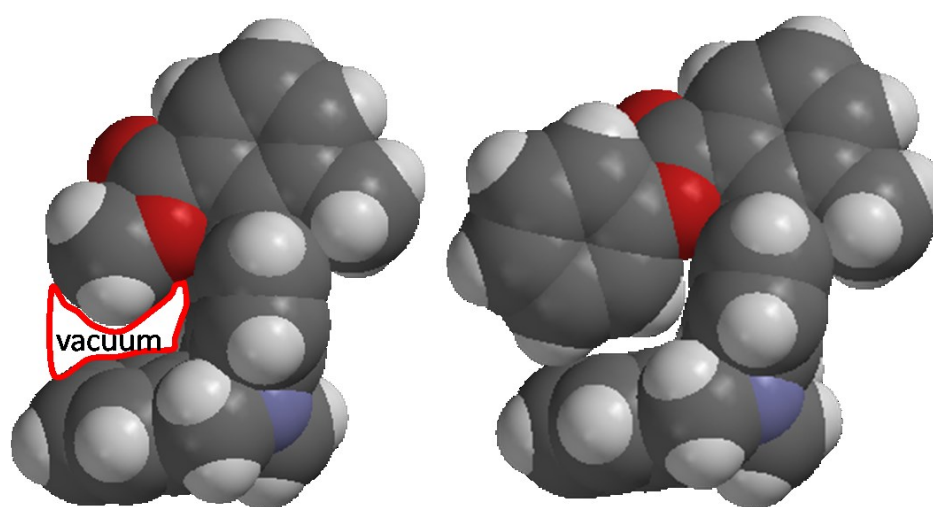


Figure 4.2. Space filling models of the folded conformations of Wilcox balances (\pm)-1 and (\pm)-2, geometries were optimised using DFT/B3LYP/6-31G*. The solvent-inaccessible “vacuum” area generated in balance (\pm)-1 is marked in red.

It is also important to note that the methyl group is large enough to cause desolvation of the aromatic ring on the base of the balance in folded conformation. This is an important feature of the current experimental design since solvation of this ring has been proposed as being a major contributor to governing the folding free energies of these types of molecules.² Given the design features discussed above, ΔG_{exp} should

represent the edge-to-face aromatic interaction, as given by the equation:

$$\Delta G_{\text{exp}} = \Delta G_{(\pm)\text{-}2} - \Delta G_{(\pm)\text{-}1} \quad \text{Equation 4.1}$$

Thus, building on our experience of the measuring folding free energies of Wilcox balances in many different solvents (Chapter 3), it should be possible to screen solvent effects readily following synthesis of the methyl ester control compound.

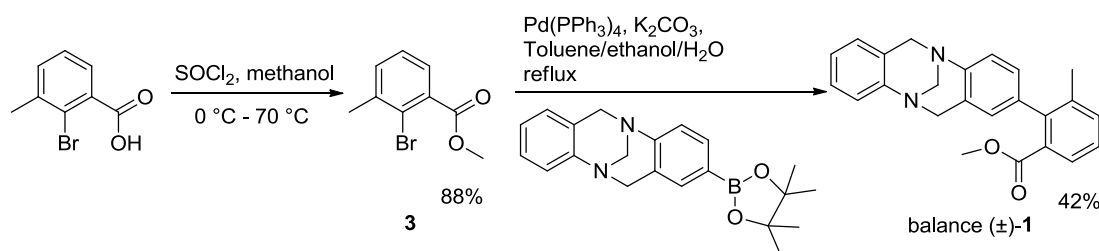


Figure 4.3. Syntheses of balance (±)-1.

Methylation of 2-bromo-3-methylbenzoic acid was carried out in methanol, where the methanol served as a solvent as well as a reactant. Suzuki coupling of compound 3 with the boronic ester successfully gave balance (±)-1 in 42% yield (Fig 4.3). Synthesis of balance (±)-2 was described earlier (refer to balance (±)-4 in Chapter 3).

4.3 Results and Discussion

Folding free energies of balances (±)-1 and (±)-2 were measured in a wide range of solvents (Table 4.1 and Fig 4.4), it can be seen that changes in ΔG_{exp} are very small with less than 1 kJ mol^{-1} difference among all the solvents tested. Notably, the experimental value in solution is much smaller than the 6 kJ mol^{-1} predicted for edge-to-face interactions in the gas phase.¹⁸ Upon classifying the data according to the types of solvents as previously employed successfully in Chapter 3, few obvious trends can be seen, except for in THF/water mixtures. Increased folding in the phenyl

balance relative to the methyl ester control can be rationalised on the basis of the increased hydrophobic effect.¹⁹ This contrasts with Wilcox's previous report that the folding ratio of balance (±)-**3** changed little as the solvent was varied (Fig 4.5 right).¹⁶

It is interesting to see that balance (±)-**1** and (±)-**2** behave differently in the THF/water mixtures. Due to the lack of significant CH \cdots π interactions in balance (±)-**1**, it might have been anticipated that $\Delta G_{(\pm)-1}$ values would not change much as the solvent was varied. However, the data in Table 1 shows that variation of the solvent has a significant impact on the folding of the control balance. $\Delta G_{(\pm)-1}$ is less favourable as the water content increases while $\Delta G_{(\pm)-2}$ changes in the opposite way. In fact, $\Delta G_{(\pm)-1}$ is determined by the relative solvation energies of the folded and unfolded conformations of the Wilcox balance, which clearly vary as the solvent is changed. Although there is no CH \cdots π interaction between methyl group and aromatic base of balance (±)-**1**, it is possible that small solvent molecules may possibly enter the internal cavity of the Tröger's base. Water is the smallest solvent examined in this screen and has two O-H functional groups. Thus, it might be possible that water forms one O-H \cdots O=C and one O-H \cdots π interaction within balance (±)-**1** (Fig 4.5a).

Table 4.1. Folding free energies of balance (±)-1 and balance (±)-2. ΔG_{exp} is interaction energy calculated by equation shown previously. Errors for $\Delta G_{(\pm)-1}$ and $\Delta G_{(\pm)-2}$ are within 0.12 kJ mol^{-1} .²⁰

Errors for ΔG_{exp} are calculated as $\delta\Delta G_{\text{exp}} = \sqrt{(\delta\Delta G_{(\pm)-1})^2 + (\delta\Delta G_{(\pm)-2})^2} = 0.17 \text{ kJ mol}^{-1}$.

	Surface area of solvent molecule ^a /Å ²	$\Delta G_{(\pm)-1}$ /kJ mol ⁻¹	$\Delta G_{(\pm)-2}$ /kJ mol ⁻¹	ΔG_{exp} /kJ mol ⁻¹
Cyclohexane	130	-2.29	-2.00	+0.30
<i>n</i> -Hexane	153	-1.03	-1.31	-0.28
Carbon disulfide	78	-0.43	-0.34	+0.09
Dichloromethane	84	-0.78	-0.87	-0.08
Chloroform	100	-0.83	-0.93	-0.10
Carbon tetrachloride	117	-1.32	-1.22	+0.09
Benzene	115	-0.99	-1.40	-0.40
Tetrahydrofuran	106	-1.35	-1.11	+0.24
Pyridine	110	-0.62	-1.09	-0.48
Acetone	96	-0.86	-0.78	+0.08
Acetonitrile	73	-0.39	-0.72	-0.33
Ethanol	82	-1.34	-1.33	+0.01
Methanol	61	-1.02	-1.28	-0.26
DMSO	104	-0.48	-1.05	-0.57
THF /9% water	-	-1.14	-1.10	+0.04
THF /15% water	-	-1.07	-1.19	-0.13
THF /20% water	-	-1.00	-1.33	-0.33
THF /25% water	-	-0.88	-1.33	-0.45
THF /30% water	-	-0.76	-1.46	-0.69
THF /35% water	-	-0.74	-1.49	-0.75
THF /40% water	-	-0.69	-1.60	-0.91
1-iodoperfluorohexane	244	-1.28	-1.23	+0.05
Hexafluorobenzene	149	-1.54	-2.10	-0.56

a. Surface area of solvent molecule are calculated by *Spartan*.

According to this hypothesis, the preference for folded state becomes less energetically favourable because water can solvate the folded and the unfolded states equally well. Thus the hydrophobic effect provides little driving force for folding in balance (±)-1. Compared to the previous reported balance (±)-3, the folding ratio changed little as the solvent was varied (Fig 4.5b).¹⁶ One possibility could be that

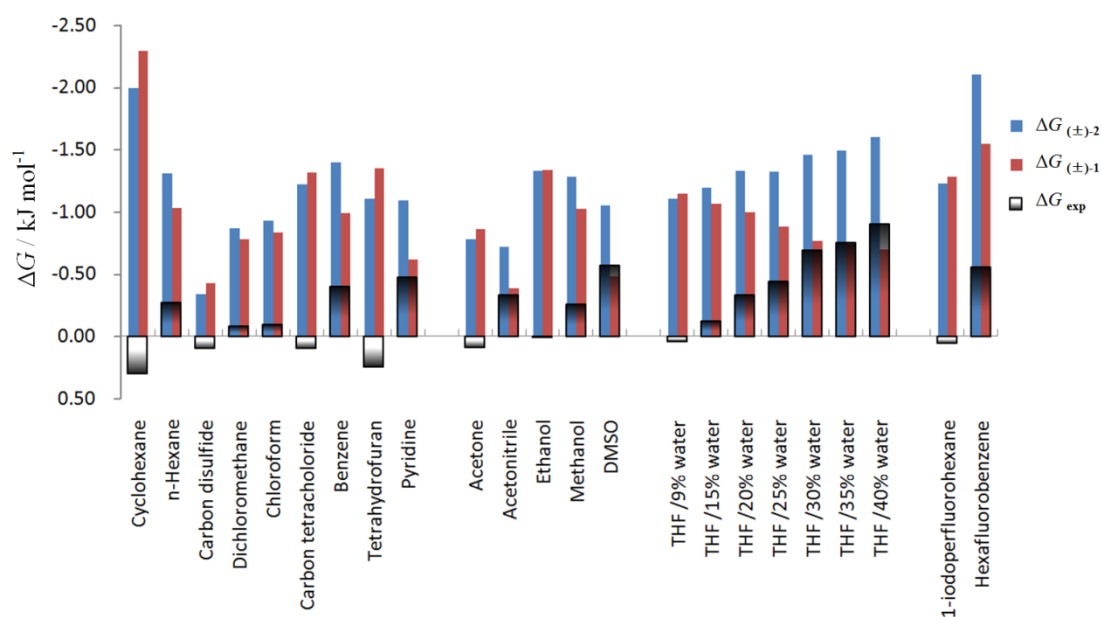


Figure 4.4. Folding free energies of balance (±)-1 and (±)-2, and ΔG_{exp} are shown in bar graph. Errors are discussed in Table 4.1.

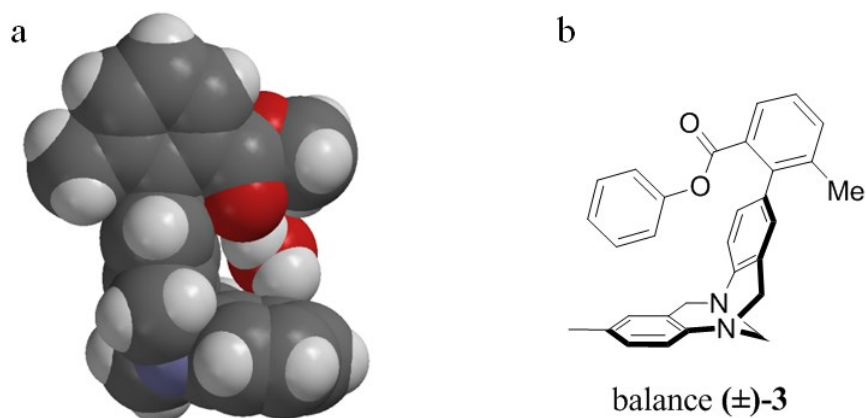


Figure 4.5. (a) Structure of water complexed to balance (±)-1, Spartan energy minimised using DFT/B3LYP/6-31G*, and (b) structure of balance (±)-3 used in Wilcox's study¹⁶

the methyl group on the face aromatic of the balance may play a role in occluding solvent from solvating the lower ring and the phenyl ring above it in the folded conformation. Thus, making the interaction is insensitive to the solvent. However, the scope of the solvents examined by Wilcox was very small.

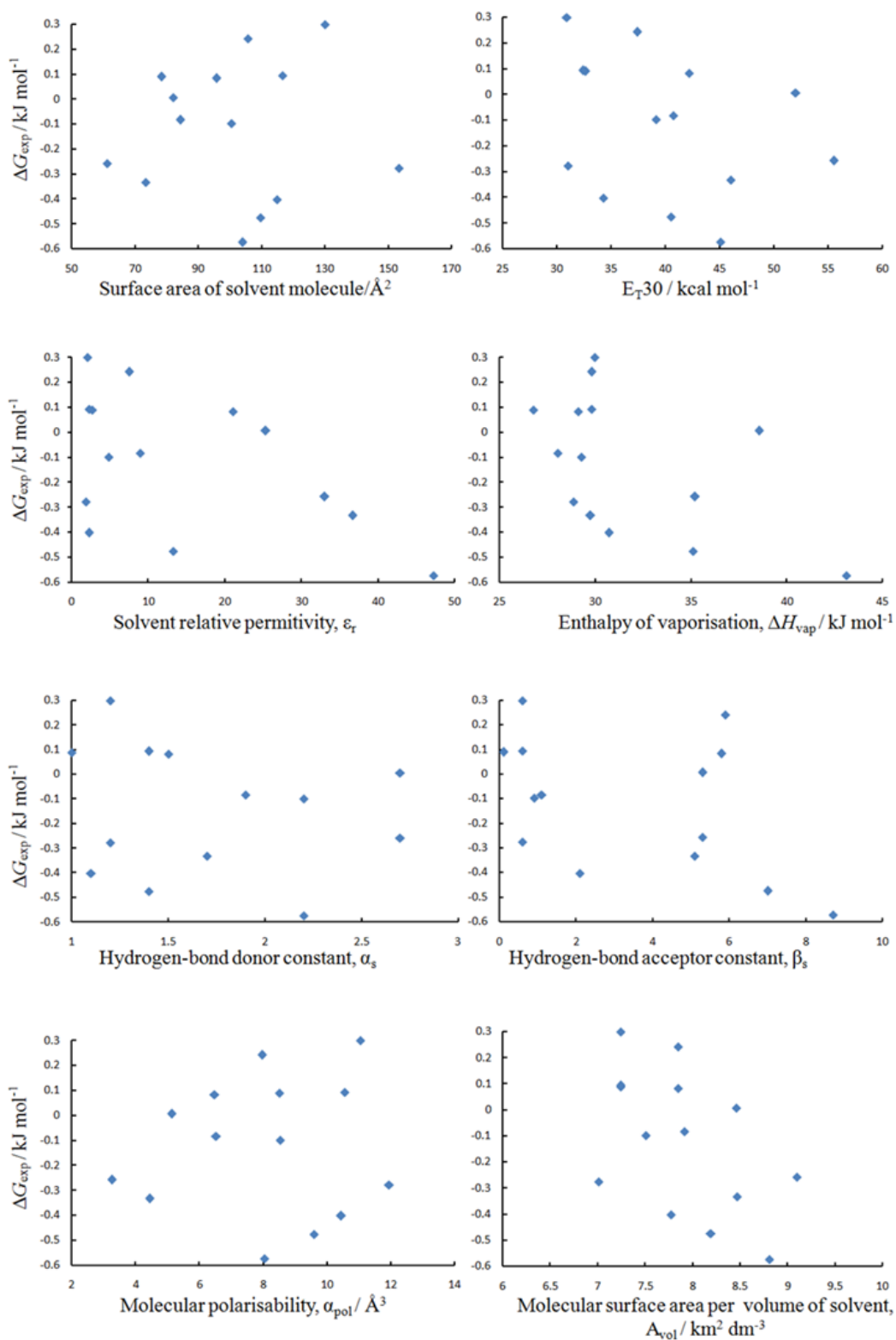


Figure 4.6. ΔG_{exp} (except mixed solvents and fluorinated solvents) plotted against a range of solvent property parameters.

Nonetheless, balance (\pm)-2 is more exposed to the solvent, and energetic effects of varying the solvent are clearly seen. The other solvent trends are harder to rationalise. To characterise solvent effects in normal organic solvents (mixed solvents and fluorinated solvents were excluded for simplicity), solvent parameters like solvent polarity, size and polarisability were employed (as listed in Chapter 3). None of these parameters gave good correlations (Fig 4.6). Hunter's solvation model was also employed in an attempt to fit the data, but no good results arose (Fig 4.7). The polarity dependence on edge-to-face aromatic interactions seen in metal tris-bipyridine complexes was not shown here.¹³ This suggests that even for the same kinds of interaction, the solvent effects behave differently and depends on the system being investigated. The interaction geometry, and solvent structure and sites may all matter.

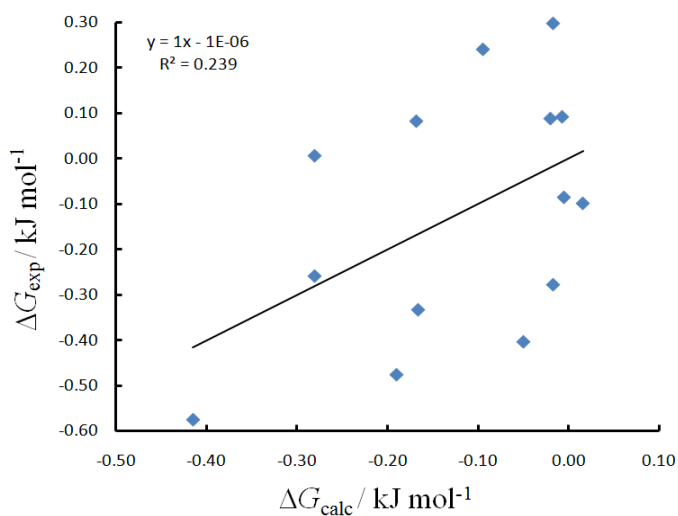


Figure 4.7. ΔG_{exp} plotted against ΔG_{calc} ($\Delta G_{\text{calc}} = a + b\alpha_s + c\beta_s + d\alpha_s\beta_s$ Where the empirically derived coefficients were determined to be $a = -0.089$, $b = 0.070$, $c = 0.018$, $d = -0.034$)

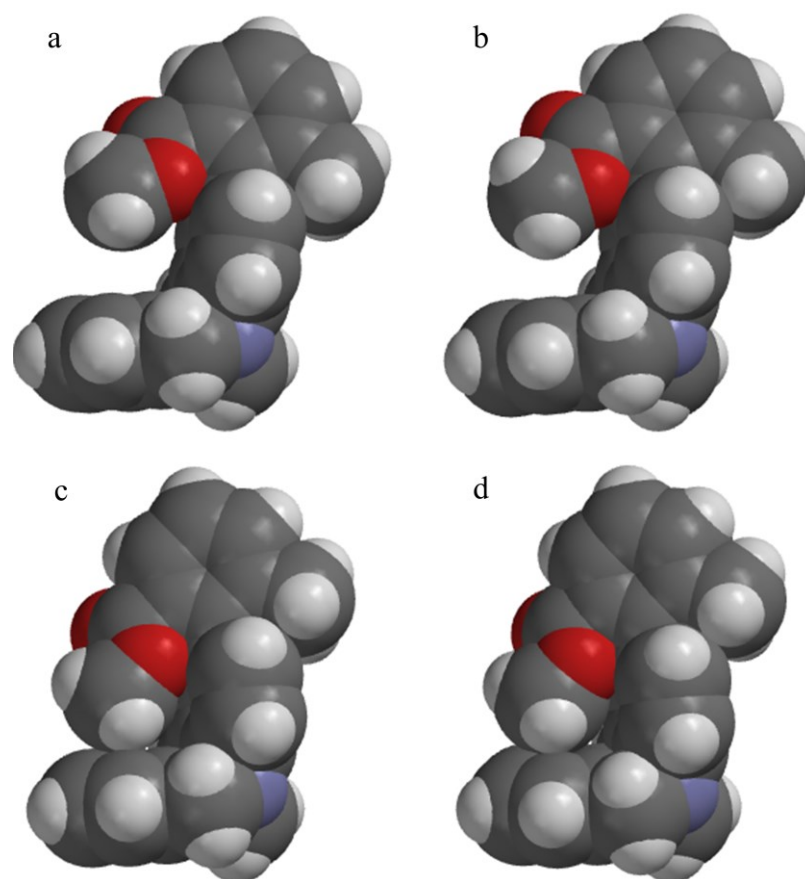


Figure 4.8. Optimised structure of balance (\pm)-**1** using Spartan at a) HF/6-31G*; b) DFT/B3LYP/6-31G*; c) DFT/M06/6-31G*; d) DFT/ ω B97X-D/6-31G* level.

Further computational analyses revealed that if dispersion interaction is important, the Tröger's base backbone might bend to form a dispersive CH \cdots π contact (Fig 4.8), giving a very favourable folding free energy (-8.6 and -10.0 kJ mol $^{-1}$ from DFT/M06/6-31G* and DFT/ ω B97X-D/6-31G* calculations respectively). However, calculations by HF/6-31G* ($+1.0$ kJ mol $^{-1}$) and DFT/B3LYP/6-31G* ($+0.6$ kJ mol $^{-1}$) method gave results closer to the experimental data. This is in consistent with our conclusion in Chapter 3 that dispersion interactions are mostly cancelled in solution.

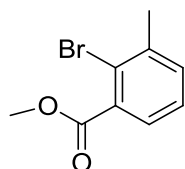
4.4 Conclusion and Future Work

The classic Wilcox torsion balance was applied in the solvent study of edge-to-face aromatic interactions. In the open system, edge-to-face aromatic interactions are small and sensitive to the solvents. Compared with previous findings, our study suggests that this type of weak non-covalent interaction is solvent dependent and the influence of solvent depends on the solvent accessibility of the system. This accounts for the different behaviours reported in closed systems such as capsules,^{6,21-22} partially open systems such as cyclophanes^{7,23} and open systems like that employed here. Further study on the origin of these solvent effects are required.

4.5 Experimental Section

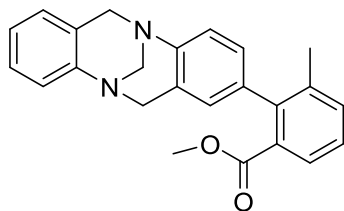
All compound numbers refer to compounds exclusively as presented in this chapter.

All of the compounds involved in the syntheses were purchased from *Sigma-Aldrich*, *VWR* or *FluoroChem* and used without further purification.



Methyl 2-bromo-3-methylbenzoate 3. SOCl₂ (160 μl) was added dropwise to 2-bromo-3-methylbenzoic acid (214 mg, 1 mmol) in 2 ml methanol at 0 °C. After complete addition, the solution was heated to reflux at 70 °C for 3 h. After cooling, the solvent was removed under reduced pressure. Then it was diluted with H₂O and extracted with DCM. The organic layer was washed with sat. NaHCO₃ and H₂O. Organic layer was dried over MgSO₄ and solvent was removed to give 200 mg pure product. 201 mg brownish oil. Yield 88%. ¹H NMR (500 MHz, CDCl₃) δ 7.47 (d, *J*=

7.6 Hz, 1H), 7.35 (d, $J = 7.5$ Hz, 1H), 7.25 (t, $J = 7.3$ Hz, 1H), 3.94 (s, 3H), 2.47 (s, 3H). ^{13}C NMR (101 MHz, CDCl_3) δ 167.72, 139.72, 134.02, 133.13, 127.89, 126.85, 123.08, 52.50, 23.78. MS (EI) m/z 228.0 (M^+)



2-(6H,12H-5,11-Methano-dibenzo[b,f][1,5]diazocin-2-yl)-3-methyl-benzoic acid

methyl ester balance (\pm)-1. Boronic ester (150 mg, 0.43 mmol), bromide (117 mg, 0.51 mmol), and $\text{Pd}(\text{PPh}_3)_4$ (50 mg 0.04 mmol) were mixed in 10 mL toluene and 2 mL ethanol. K_2CO_3 (179 mg, 1.30 mmol) in 1 mL water was added. The mixture was degassed and heated to 110 °C under N_2 overnight. Then the reaction was cooled to room temperature, diluted with DCM and washed with water. The organic layer was dried over MgSO_4 , filtered and solvent was removed under reduced pressure. The crude product was purified by column chromatography. 68 mg yellowish solid. Yield 42%. m.p. 136-138°C ^1H NMR (500 MHz, CDCl_3) δ 7.62/7.55 (2d, $J = 7.6$ Hz, 1H), 7.43 – 7.32 (m, 1H), 7.28 (m, 1H), 7.24 – 7.11 (m, 3H), 7.08 – 6.86 (m, 3H), 6.73/6.69 (2s, 1H), 4.78 – 4.27 (m, 2H), 4.52 – 4.31 (m, 2H), 4.30 – 4.12 (m, 2H), 3.60/2.80 (2s, 3H), 2.20/2.05 (2s, 3H). ^{13}C NMR (126 MHz, CDCl_3) δ 169.69/169.12, 148.30/147.89, 146.91/146.74, 140.98/140.66, 137.31/136.80, 135.95/135.75, 132.96/132.85, 132.75/132.12, 128.11/127.92, 127.89, 127.42/127.28, 127.20, 127.06/127.01, 126.94, 126.84, 126.75, 125.26/124.92, 124.57/124.23, 123.87/123.84, 67.36/66.79, 59.32/59.23, 58.60/58.55, 51.89/50.90, 20.92/20.71. MS (EI) m/z 370.2 (M^+)

References

- (1) Otto, R.; Brox, J.; Trippel, S.; Stei, M.; Best, T.; Wester, R. *Nat Chem* **2012**, *4*, 534-538.
- (2) Cockroft, S. L.; Hunter, C. A. *Chem. Commun.* **2006**, 3806-3808.
- (3) Cook, J. L.; Hunter, C. A.; Low, C. M.; Perez-Velasco, A.; Vinter, J. G. *Angew. Chem., Int. Ed.* **2007**, *46*, 3706-3709.
- (4) Sarwar, M. G.; Dragisic, B.; Salsberg, L. J.; Gouliaras, C.; Taylor, M. S. *J. Am. Chem. Soc.* **2010**, *132*, 1646-1653.
- (5) Chapman, K. T.; Still, W. C. *J. Am. Chem. Soc.* **1989**, *111*, 3075-3077.
- (6) Mecozzi, S.; Rebek, J. J. *Chem. Eur. J.* **1998**, *4*, 1016-1022.
- (7) Smithrud, D. B.; Diederich, F. *J. Am. Chem. Soc.* **1990**, *112*, 339-343.
- (8) Cubberley, M. S.; Iverson, B. L. *J. Am. Chem. Soc.* **2001**, *123*, 7560-7563.
- (9) Hunter, C. A. *Angew. Chem., Int. Ed.* **2004**, *43*, 5310-5324.
- (10) Kim, E.-i.; Paliwal, S.; Wilcox, C. S. *J. Am. Chem. Soc.* **1998**, *120*, 11192-11193.
- (11) Hof, F.; Scofield, D. M.; Schweizer, W. B.; Diederich, F. *Angew. Chem., Int. Ed.* **2004**, *43*, 5056-5059.
- (12) Fischer, F. R.; Schweizer, W. B.; Diederich, F. *Chem. Commun.* **2008**, 4031-4033.
- (13) Breault, G. A.; Hunter, C. A.; Mayers, P. C. *J. Am. Chem. Soc.* **1998**, *120*, 3402-3410.
- (14) Mati, I. K.; Cockroft, S. L. *Chem. Soc. Rev.* **2010**, *39*, 4195-4205.
- (15) Bhayana, B.; Ams, M. R. *J. Org. Chem.* **2011**, *76*, 3594-3596.
- (16) Paliwal, S.; Geib, S.; Wilcox, C. S. *J. Am. Chem. Soc.* **1994**, *116*, 4497-4498.
- (17) Bhayana, B.; Wilcox, C. S. *Angew. Chem., Int. Ed.* **2007**, *46*, 6833-6836.
- (18) Jennings, W. B.; Farrell, B. M.; Malone, J. F. *Acc. Chem. Res.* **2001**, *34*, 885-894.
- (19) Fischer, F. R.; Schweizer, W. B.; Diederich, F. *Angew. Chem., Int. Ed.* **2007**, *46*, 8270-8273.
- (20) Fischer, F. R.; Wood, P. A.; Allen, F. H.; Diederich, F. *Proc. Natl. Acad. Sci. U. S. A.* **2008**, *105*, 17290-17294.
- (21) Waller, M. P.; Kruse, H.; Muck-Lichtenfeld, C.; Grimme, S. *Chem. Soc. Rev.* **2012**, *41*, 3119-3128.
- (22) Hof, F.; Craig, S. L.; Nuckolls, C.; Rebek, J. J. *Angew. Chem., Int. Ed.* **2002**, *41*, 1488-1508.
- (23) Diederich, F. In *Modern Cyclophane Chemistry*; Wiley-VCH Verlag GmbH & Co. KGaA: 2005, p 519-546.

Chapter 5 Halogen bonding in solution

Abstract

Halogen $\cdots\pi$ interactions are rarely investigated in solution. In this chapter, two methods are attempted to measure the thermodynamic properties of this weak interaction in solution. Halogen-arene complexes are too weak to be measured even in non-competitive solvents. The synthesis of a new class of molecular torsion balance failed due to compound instability.

5.1 Introduction

In the most recent decades, halogen bonding has been recognised as an important class of non-covalent interaction. It has been treated as a novel interaction in organic chemistry, material science and medicinal chemistry.¹⁻³ Halogen-bond donor ability is generally attributed to the uneven electron distribution on halogen atoms, which generate an electron-positive σ hole.⁴ Commonly investigated halogen bond pairs are iodine-arene interactions,⁵⁻⁷ organic halide-anion interactions and organic halide-N/O/S interactions.^{3,8-9} However, organic halide-arene (C-X $\cdots\pi$) interactions have been less studied, although they have been suggested as providing attractive driving forces in crystal engineering.¹⁰⁻¹¹ Meanwhile, 33% of interactions involving halogen atoms seen in protein systems are X $\cdots\pi$ interactions,⁸ where the mean distance of the interaction ranges between 3.2 Å and 4.1 Å.^{8,12}

In contrast to the large amounts of structural data on X $\cdots\pi$ interactions, thermodynamic data is scarce. Organic chloride/bromide-benzene interactions have been analysed using different computational methods, and the results point to dominant contributions from dispersion forces.¹³ Hunter and co-workers¹⁴ applied thermodynamic double-mutant cycles to obtain experimental association free

energies for C-X-arene interactions, using zipper complexes in CDCl_3 . However, repulsive interactions were measured in all cases, which was attributed to the geometric constraints of the complexes, which were unable to fully accommodate steric bulk of the CX_3 groups. Very recently, the binding constants of 2- $\text{C}_3\text{F}_7\text{I}$ and 1- $\text{C}_3\text{H}_7\text{I}$ with d_8 -toluene were measured to be $K = 0.32 \text{ M}^{-1}$ and 0.43 M^{-1} .¹⁵ The very limited experimental thermodynamic data for $\text{X}\cdots\pi$ interactions obtained to date means that there is a great desire to study these types of interactions systematically to reveal their stabilities and physical origin in solution.

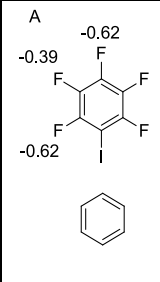
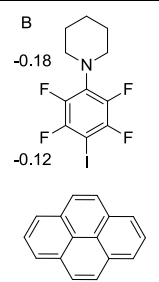
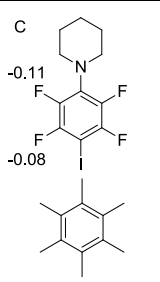
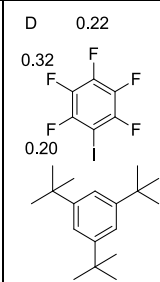
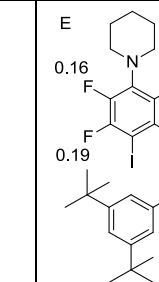
5.2 Iodide-aromatic complexes

According to ESPs of organic halogens, halogen-bond donor ability increases in the order of $\text{F} < \text{Cl} < \text{Br} < \text{I}$. Perfluorinated aromatic iodides are among the strongest, and most stable organic halogen-bond donors reported to date. They also enable ^{19}F -NMR experiments and allow more choices of organic solvents beside expensive deuterated solvents. Considering the important and often dominant effects of solvent competition, solvents need to be carefully chosen for the following study. CCl_4 and cyclohexane have no particularly electro-positive or negative sites, which makes them suitable for the investigation of halogen bonding interactions. A series of complexes were examined in both of these solvents by ^{19}F -NMR titration experiments.

Despite the weakly competitive solvents used, the binding constants were too low to be measured accurately by this method. This is consistent with the very recent result from Hansen's group, who measured binding constants less than 1 M^{-1} for $\text{I}\cdots\pi$ interactions without any solvent competition.¹⁵ Although the percentage bound could not be determined from the titration curves, significant chemical shift changes were observed upon binding. δ_{F} moved upfield as guests were added for complexes A, B and C. This suggests that stacking conformations may be adopted for these complexes, because upfield chemical shifts are often observed upon aromatic

stacking. For complexes D and E, downfield changes in δ_F were observed. This suggests that these two complexes adopt a T-shape conformation with the iodine atom pointing to the other ring. The different conformational preferences of complexes D and E compared to the other complexes might be attributed to the steric effects of the bulky *tert*-butyl which prevent stacking. Even with this chemical shift data, other conformations cannot be excluded. The flexibility in these systems results in loose geometric control, while the entropic penalty to bimolecular association of $\sim 6 \text{ kJ mol}^{-1}$,¹⁶ and the very weak nature of the interactions means that binding is too weak to be reliably measured using the complexes shown in Table 5.1. Therefore, an alternative approach needs to be established for the measurement of halogen $\cdots\pi$ interactions.

Table 5.1. Titration results of complexes investigated. numbers next to structure are the changes of chemical shift upon titration. C_{Host} is concentration of host molecule and C_{guest} is concentration of guest molecule.

					
solvent	CCl_4	CCl_4	cyclohexane	cyclohexane	cyclohexane
C_{Host}	0.56 M	0.001 M	0.2 M	1 M	0.5 M
C_{guest}	0-2.8 M	0-0.3M	0-0.25 M	0-1.6 M	0-2 M
δ_F movement	upfield shift	upfield shift	upfield shift	downfield shift	downfield shift

5.3 Molecular torsion balances

Molecular torsion balances provide a convenient tool for quantifying weak non-covalent interactions. A modified Wilcox balance was designed in which the benzoate group was replaced with phenol acetate-bearing halides with the aim of measuring halogen $\cdots\pi$ interactions (Fig 5.1e). Crystal structures of the main functional groups were obtained from the Cambridge Crystal Database (Fig 5.1a-c), and a target compound model was built based on these crystal data (Fig 5.1d). The space-filling model shows that the iodine atom is nicely positioned above the face of the aromatic ring with the σ hole pointing towards the ring.

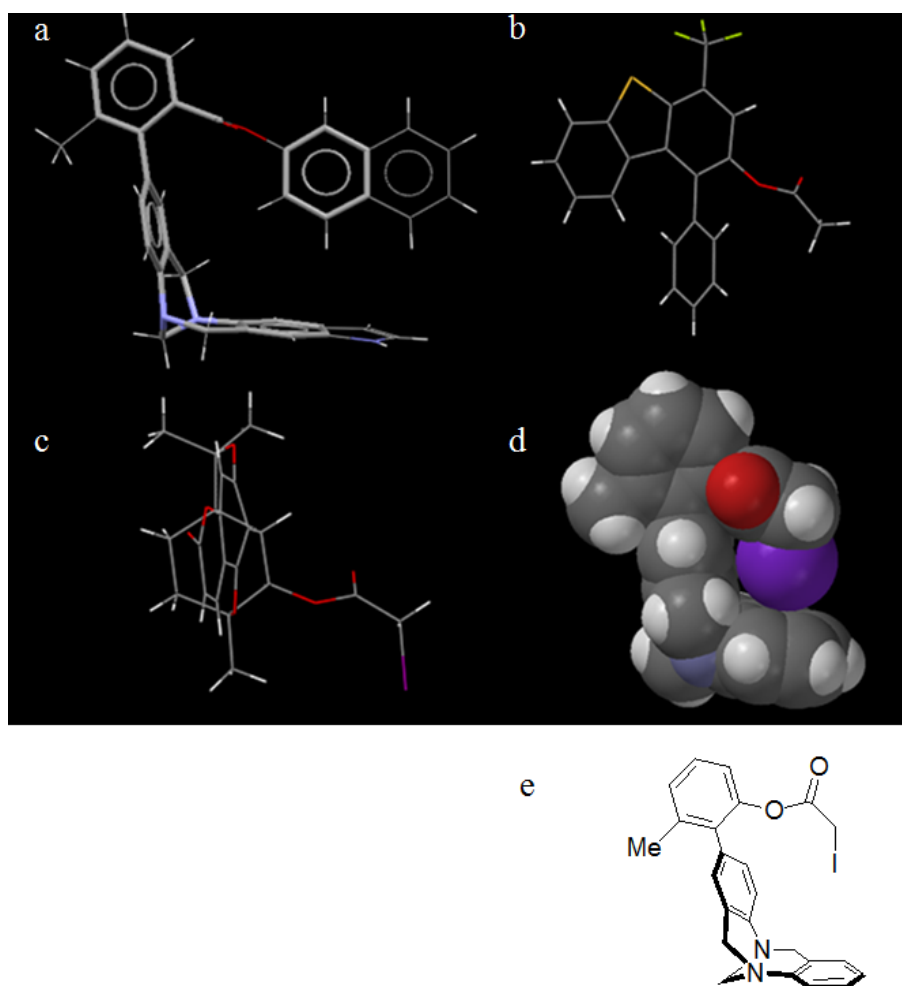


Figure 5.1. a) a crystal structure of a typical Wilcox balance (CDS entry GIPRAZ), b) a compound containing a phenol acetate fragment (CDS entry SORZAB), c) a compound containing an iodoacetic acid fragment (CDS entry BRUCLB), d) mimic space-filling model of target compound, and e) structure of target compound.

In addition to a suitable geometry to accommodate halogen $\cdots\pi$ interactions, a further essential requirement for operation as a molecular balance is that the rotation about the biphenyl bond is slow on the NMR timescale, such that different conformer signals can be observed at room temperature. Two classes of Wilcox balances have been reported in previous successful studies of non-covalent interactions that satisfy these barrier to rotation requirements: one has two ester groups in the *ortho* positions to hinder the rotation (Fig 5.2a),¹⁷⁻¹⁸ the other has one ester group and one methyl group in the *ortho* positions (Fig 5.2b).¹⁹ Rotational barrier calculations were carried out for the simplified model-biphenyl derivatives using B3LYP/6-31G*, and the barrier to rotation for our design (Fig 5.2c) was found to be -57 kJ mol^{-1} , which lies between those of the previously made Wilcox balances (-46 kJ mol^{-1} and -62 kJ mol^{-1}). Thus, it should be expected that our modified torsion balance is also likely to show conformers in the NMR signals at room temperature.

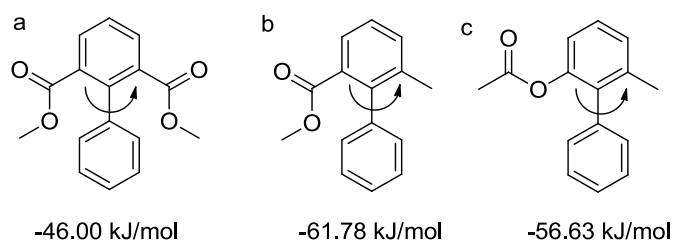


Figure 5.2. Rotation barriers calculated at DFT/B3LYP/6-31G* level.

Following this promising computational design, synthesis of the torsion balance shown in Figure 5.1e was initiated starting from readily available amines (Fig 5.3). The unsymmetrical Tröger's base was formed by condensation of two anilines and paraformaldehyde under acid catalyst. The desired product could be easily separated from the mixture of symmetrical Tröger's bases and side products. The second step was completed by boronation with a palladium-catalyst. The bromide compound was obtained via selective bromination of *m*-cresol using a novel brominating reagent. This compound was then coupled with previously made boronic ester by Suzuki

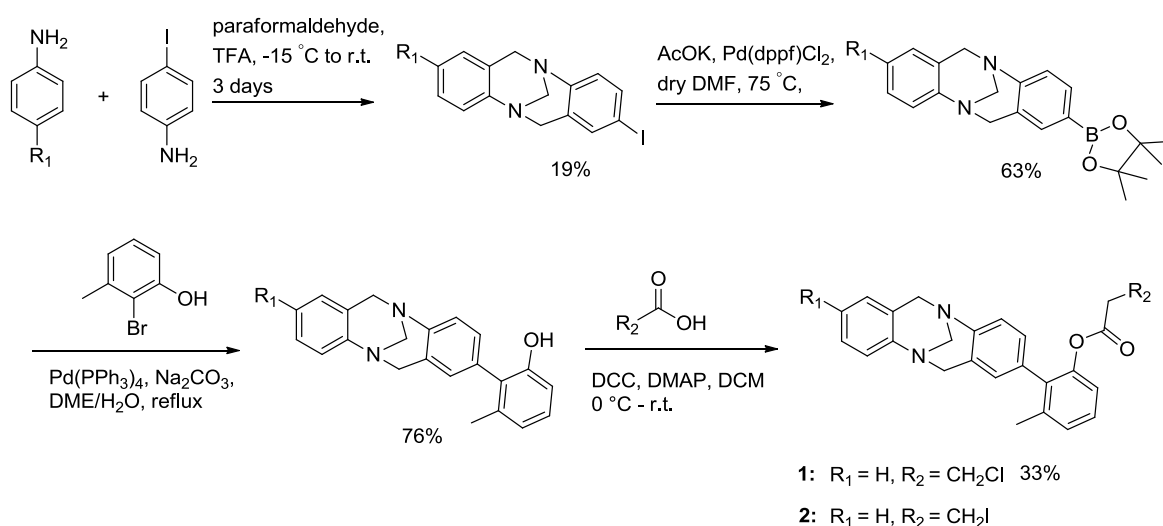


Figure 5.3. Synthesis of the proposed Wilcox balance for measuring halogen $\cdots\pi$ interactions.

coupling. The final esterification step was catalysed by DMAP with DCC serving as the coupling reagent.

Compound **1** was successfully made, however distinct folded and unfolded conformer signals could not be seen in the $^1\text{H-NMR}$ spectrum. One possible reason for this could have been that the rotational barrier calculation was not accurate. It might have been possible to examine this possibility further using variable-temperature NMR. However, the iodoacetic group is larger than the chloroacetic group, thus, there is a chance that the bulkier group may hinder the rotation by increasing the energetic barrier to rotation. Unfortunately, compound **2** was not stable at room temperature and was very hard to purify. The instability of the iodoacetyl compound can be attributed to its reactivity towards nucleophiles, it was likely undergoing aliphatic nucleophilic substitution, where the iodine serves as the leaving group.

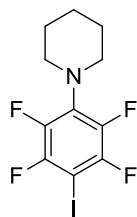
5.4 Conclusion and Future work

Preliminary NMR titration experiments showed some evidence of halogen $\cdots\pi$ interactions. However, the interactions are not measurable by this method. The subsequent design and synthesis of a new class of Wilcox balance to measure this interaction also failed due to the stability of the compound. Further work is required to design a new torsion balance which is stable and suitable for the quantification of halogen $\cdots\pi$ interactions.

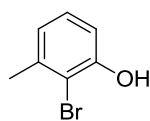
5.5 Experimental Section

All compound numbers refer to compounds exclusively as presented in this chapter.

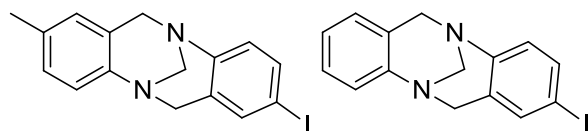
All of the compounds involved in the syntheses were purchased from *Sigma-Aldrich*, *VWR* or *FluoroChem* and used without further purification.



1-(2,3,5,6-Tetrafluoro-4-iodophenyl)-piperidine was synthesised according to literature.²⁰

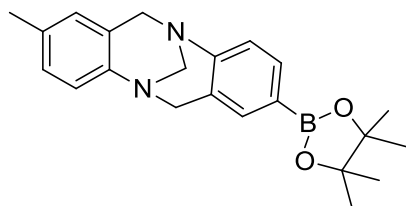


2-bromo-3-methylphenol was synthesised according to literature.²¹

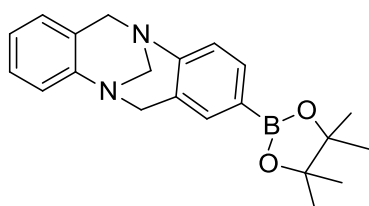


2-iodo-8-methyl-6,12-dihydro-5,11-methanodibenzo[b,f][1,5]diazocine and

2-iodo-6,12-dihydro-5,11-methanodibenzo[b,f][1,5]diazocine was made according to literature.²²



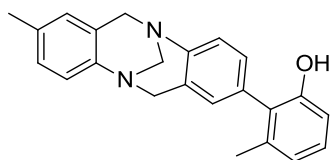
2-methyl-8-(4,4,5,5-tetramethyl-1,3,2-dioxaborolan-2-yl)-6,12-dihydro-5,11-methanodibenzo[b,f][1,5]diazocine was made according to literature.¹⁹



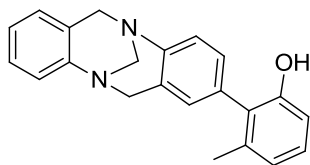
2-(4,4,5,5-tetramethyl-1,3,2-dioxaborolan-2-yl)-6,12-dihydro-5,11-methanodibenzo[b,f][1,5]diazocine was reported in Chapter 2

General synthetic procedure for Suzuki coupling

A mixture of 2-bromo-3-methylphenol (0.9 mmol, 170 mg), the corresponding boronic ester (0.6 mmol), Pd(PPh₃)₄ (0.05 mmol, 70 mg) and Na₂CO₃ (1.8 mmol, 191 mg) were added into 10 ml DME and 8 ml water solution. The resulting mixture was degassed and heated to reflux under N₂ for 24h. Then the solution was cooled down, acidified with 2M HCl aqueous solution, extracted with DCM and washed with sat. NaHCO₃. The solvent was evaporated, and the crude product was purified by column chromatography.



3-methyl-2-(8-methyl-6,12-dihydro-5,11-methanodibenzo[b,f][1,5]diazocin-2-yl)phenol. White solid. Yield 74%. ^1H NMR (500 MHz, CDCl_3) δ 7.19 (d, $J = 8.2$ Hz, 1H), 7.14 – 7.11 (m, 2H), 7.04 (dd, $J = 8.2, 1.4$ Hz, 1H), 7.00 (d, $J = 8.3$ Hz, 1H), 6.85 (d, $J = 1.8$ Hz, 1H), 6.81 (s, 1H), 6.73 (d, $J = 2.6$ Hz, 1H), 6.68 (dd, $J = 8.2, 2.5$ Hz, 1H), 6.03 – 5.59 (m, 1H), 4.77 (d, $J = 16.6$ Hz, 1H), 4.75 (d, $J = 16.7$ Hz, 1H), 4.41 (s, 2H), 4.25 – 4.19 (m, 2H), 2.28 (s, 3H), 2.20 (s, 3H). ^{13}C NMR (126 MHz, CDCl_3) δ 154.97, 145.67, 144.64, 137.83, 136.87, 134.11, 133.75, 130.97, 128.72, 128.42, 127.75, 127.35, 127.30, 126.96, 124.90, 124.49, 117.02, 112.74, 66.91, 58.50, 58.42, 20.93, 20.66. MS(EI) m/z 342.1 (M^+)

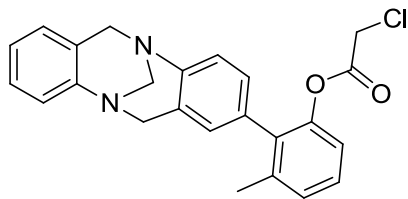


2-(6,12-dihydro-5,11-methanodibenzo[b,f][1,5]diazocin-2-yl)-3-methylphenol. White solid. Yield 76%. m.p. 223-224°C ^1H NMR (400 MHz, CDCl_3) δ 7.25 – 6.94 (m, 7H), 6.85 (d, $J = 1.5$ Hz, 1H), 6.71 (d, $J = 2.5$ Hz, 1H), 6.67 (dd, $J = 8.2, 2.6$ Hz, 1H), 5.94 (s, 1H), 4.78 (d, $J = 16.7$ Hz, 2H), 4.41 (s, 2H), 4.27 (d, $J = 16.6$ Hz, 1H), 4.24 (d, $J = 16.7$ Hz, 1H), 2.21 (s, 3H). ^{13}C NMR (101 MHz, CDCl_3) δ 154.89, 147.89, 146.16, 137.56, 136.94, 133.81, 131.01, 128.63, 127.93, 127.70, 127.44, 127.26, 127.07, 125.21, 124.56, 124.17, 117.02, 112.71, 66.76, 58.65, 58.54, 20.67. MS(EI) m/z 328.1 (M^+)

General synthetic procedure for esterification²³

Acid (1eq.) and 4-dimethylaminopyridine(3% mol) were dissolved in 5 ml dry DCM in ice bath. *N,N'*-Dicyclohexylcarbodiimide (1.1eq.) was added to this solution. The

mixture was stirred for 30 mins. Then this mixture was added dropwise to phenol (1eq.) solution in 5 ml dry DCM. The mixture was warmed to room temperature and stirred overnight. Water was added. The solution was extracted with DCM and washed with brine. Organic layer was dried over MgSO₄ and filtered. Solvent was removed and the crude was subjected to prep. TLC.



2-(6,12-dihydro-5,11-methanodibenzo[b,f][1,5]diazocin-2-yl)-3-methylphenyl 2-chloroacetate (Compound 1). 20 mg colourless waxy solid. Yield about 33%. ¹H NMR (500 MHz, CDCl₃) δ 7.24 – 7.10 (m, 5H), 7.07 – 6.95 (m, 4H), 6.86 (d, *J* = 1.2 Hz, 1H), 4.78 (d, *J* = 16.7 Hz, 2H), 4.39 (s, 2H), 4.32 (s, 2H), 4.29 – 4.18 (m, 2H), 2.26 (s, 3H). ¹³C NMR (126 MHz, CDCl₃) δ 166.07, 149.17, 148.04, 146.99, 139.70, 137.24, 136.63, 130.89, 128.35, 127.96, 127.57, 127.55, 127.41, 127.04, 125.23, 124.73, 124.09, 122.57, 118.27, 66.79, 58.65, 58.60, 40.92, 20.67. characterizations are incomplete due to the abandon of this design.

References

- (1) Metrangolo, P.; Meyer, F.; Pilati, T.; Resnati, G.; Terraneo, G. *Angew. Chem., Int. Ed.* **2008**, *47*, 6114-6127.
- (2) Erdelyi, M. *Chem. Soc. Rev.* **2012**, *41*, 3547-3557.
- (3) Beale, T. M.; Chudzinski, M. G.; Sarwar, M. G.; Taylor, M. S. *Chem. Soc. Rev.* **2013**.
- (4) Clark, T.; Hennemann, M.; Murray, J.; Politzer, P. *J. Mol. Model.* **2007**, *13*, 291-296.
- (5) McKinney, W. J.; Popov, A. I. *J. Am. Chem. Soc.* **1969**, *91*, 5215-5218.
- (6) Benesi, H. A.; Hildebrand, J. H. *J. Am. Chem. Soc.* **1949**, *71*, 2703-2707.
- (7) Bhowmik, B. B. *Spectrochimica Acta Part A: Molecular Spectroscopy* **1971**, *27*, 321-327.
- (8) Lu, Y.; Wang, Y.; Zhu, W. *Phys. Chem. Chem. Phys.* **2010**, *12*, 4543-4551.
- (9) Arman, H. D.; Giesecking, R. L.; Hanks, T. W.; Pennington, W. T. *Chem. Commun.* **2010**, *46*, 1854-1856.
- (10) Schollmeyer, D.; Shishkin, O. V.; Ruhl, T.; Vysotsky, M. O. *CrystEngComm* **2008**, *10*, 715-723.
- (11) Adams, C. J.; Bowen, L. E. *Dalton Trans.* **2005**, 2239-2240.
- (12) Saraogi, I.; Vijay, V. G.; Das, S.; Sekar, K.; Guru Row, T. N. *Cryst. Eng.* **2003**, *6*, 69-77.
- (13) Wallnoefer, H. G.; Fox, T.; Liedl, K. R.; Tautermann, C. S. *Phys. Chem. Chem. Phys.* **2010**, *12*, 14941-14949.
- (14) Harry, A.; Scott, L. C.; Claudio, G.; Christopher, A. H.; Kevin, R. L.; Julie, P.; Sharon, E. S.; Christopher, J. U.; Rhonan, F. *Chembiochem* **2004**, *5*, 657-665.
- (15) Hauchecorne, D.; van der Veken, B. J.; Herrebout, W. A.; Hansen, P. E. *Chem. Phys.* **2011**, *381*, 5-10.
- (16) Hunter, C. A. *Angew. Chem., Int. Ed.* **2004**, *43*, 5310-5324.
- (17) Paliwal, S.; Geib, S.; Wilcox, C. S. *J. Am. Chem. Soc.* **1994**, *116*, 4497-4498.
- (18) Hof, F.; Scofield, D. M.; Schweizer, W. B.; Diederich, F. *Angew. Chem., Int. Ed.* **2004**, *43*, 5056-5059.
- (19) Bhayana, B.; Wilcox, C. S. *Angew. Chem., Int. Ed.* **2007**, *46*, 6833-6836.
- (20) Sarwar, M. G.; Dragisic, B.; Salsberg, L. J.; Gouliaras, C.; Taylor, M. S. *J. Am. Chem. Soc.* **2010**, *132*, 1646-1653.
- (21) Borikar, S. P.; Daniel, T.; Paul, V. *Tetrahedron Lett.* **2009**, *50*, 1007-1009.
- (22) Faroughi, M.; Zhu, K.-X.; Jensen, P.; Craig, D. C.; Try, A. C. *Eur. J. Org. Chem.* **2009**, *2009*, 4266-4272.
- (23) Correa-Basurto, J.; Rodríguez-Páez, L.; Aguiar-Moreno, E. S.; López-Sánchez, P.; Espinoza-Fonseca, L. M.; Wong, C.; Trujillo-Ferrara, J. *Med. Chem. Res.* **2009**, *18*, 20-30.

Chapter 6 Hydrogen as a Hydrogen Bond Acceptor

Abstract

Hydrogen was investigated as H bond acceptor in a silane-perfluoro-*tert*-butanol complex. ^1H NMR showed an upfield shift of $\delta_{\text{Si-H}}$ upon binding with perfluoro-*tert*-butanol. The association constant was determined as $0.75 \pm 0.10 \text{ M}^{-1}$ in cyclohexane by ^{19}F NMR titration experiment. The $\text{H}\cdots\text{H}$ distance was found to be 1.786 \AA as computed by DFT/B3LYP/6-31G*.

6.1 Introduction

Hydrogen bonds (H-bonds) have been studied extensively. H-bonds are responsible for the precise organisation of the DNA double helix¹ and have become a building motif for material science.²⁻³ Classic H-bond acceptors are electronegative atoms, like N, O, S and inorganic F. Hydrogen atoms are rarely regarded as being able to serve as H-bond acceptors until very recently. Close $\text{H}\cdots\text{H}$ contacts observed in crystal structures are often referred to as dihydrogen bonds.⁴ Metal hydrides are now regarded as being very good H-bond acceptors, and many $\text{M-H}\cdots\text{H-O/N}$ interactions have been found where M is a transition metal such as Ir, Re, or Nb.⁴⁻⁶ Some thermodynamic data has been determined for these types of H-bond interactions and they were found to be comparable in strength to classical H-bonds.^{4-5,7-8} Other main group metal hydrides like LiH and BeH_2 have also been reported to serve as H-bond acceptors.⁶ Metalloids such as B and Si also form hydrides, which might be capable of forming dihydrogen bonds. Boron hydrides, such as that found in the ammonia-borane complex is a potential hydrogen storage material.⁹ Recently, Shore's group demonstrated that the $\text{B-H}\cdots\text{H-N}$ dihydrogen bond facilitates formation of the diammoniate (Fig 6.1a) involved in diborane formation, which is crucial to dihydrogen release.⁹ Meanwhile, McGrady and co-workers have shown that the

B-H \cdots H-B interaction may also accelerate the process.¹⁰

Geometrically, most B-H \cdots H-N interactions found in the crystal database are bent (Fig 6.1b). The common explanation is that the N-H bends towards the large electronegative B atom due to Coulombic interactions.⁵ However, it is possible that B-H \cdots H-N contacts observed in the solid-state are just a consequence of favourable N-H \cdots B interactions which bring the hydrogen atoms close in space. Silane (SiH₄) is often used as a reducing agent, which due to silicon being less electronegative than hydrogen, provides a rare example of a non-metallic compound that containing a weakly electron-rich hydrogen. The ability of Si-H to act as a H-bond acceptor was first reported in 2005 by Mikan and Ishikawa *et al.*, who identified dihydrogen bonds in phenol-diethylmethylsilane clusters via IR-UV double resonance spectroscopy.¹¹ A theoretical study has also claimed that Si-H \cdots H-C interactions assist Si-C bond formation.¹² However, no further study has been carried out to further investigate the thermodynamic properties of Si-H \cdots H interactions. Fully understanding dihydrogen bonds may be helpful in revealing organic mechanisms, and for exploring new reactions and efficient hydrogen storage materials.

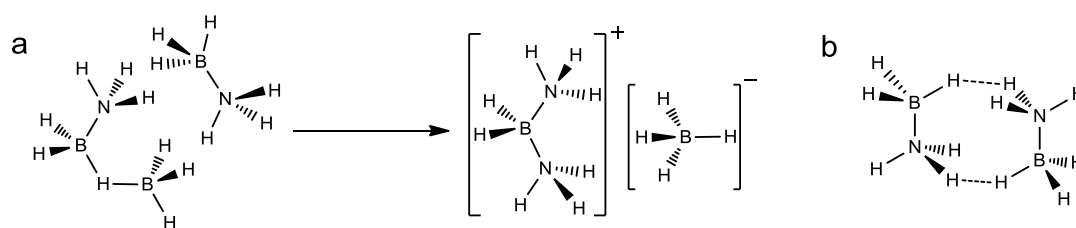


Figure 6.1. a) The formation of diammoniate of diborane⁹ and b) bent B-H \cdots H-N¹³.

6.2 Design and Aims

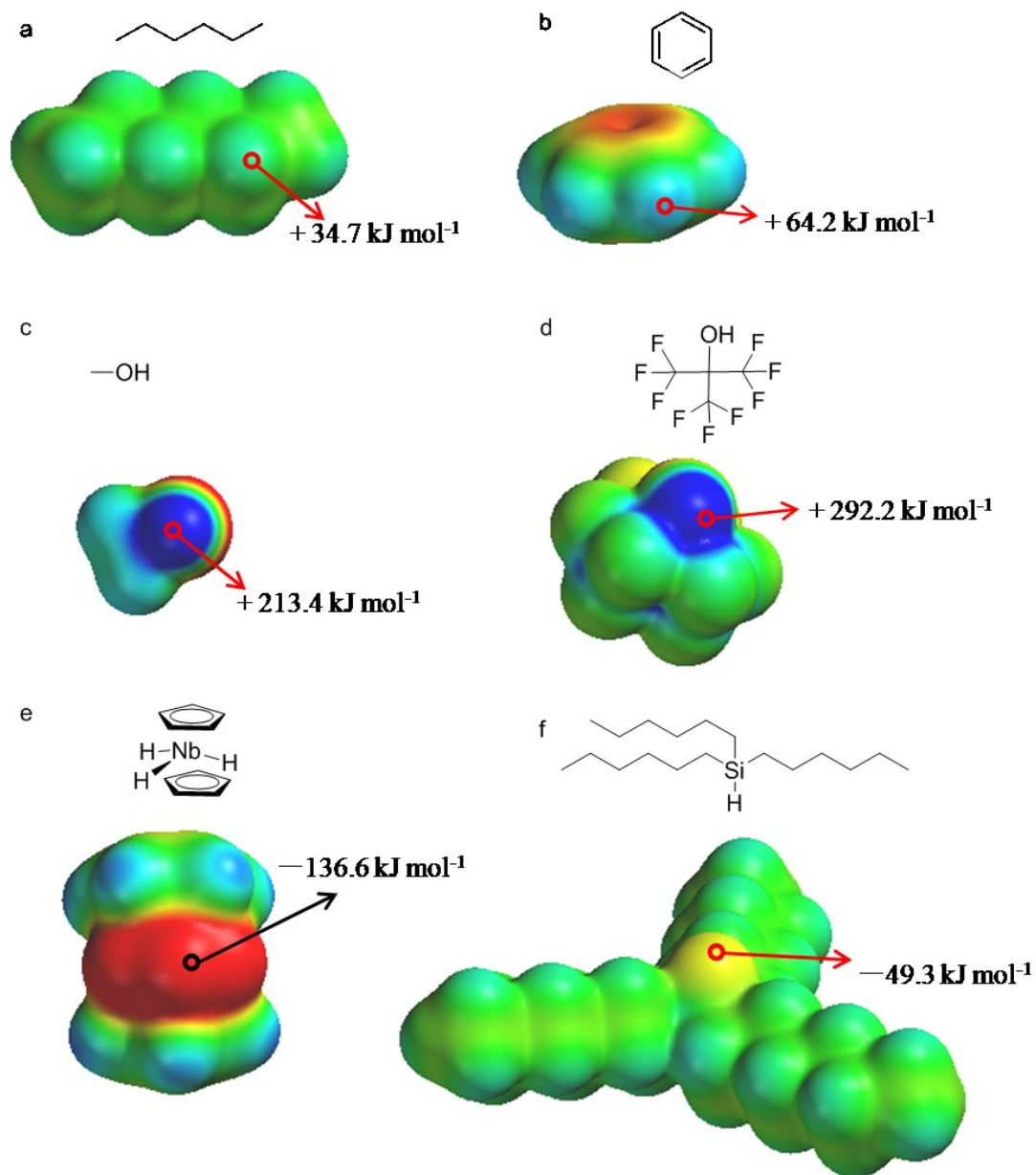


Figure 6.2. Electrostatic surface potentials (ESPs) of a) hexane, b) benzene, c) methanol, d) perfluoro-*tert*-butanol, e) NbCp_2H_3 metal hydride and f) tri-*n*-hexylsilane. ESPs are scaled from -100 kJ mol^{-1} (red) to $+100 \text{ kJ mol}^{-1}$ (blue). ESPs were calculated using B3LYP/6-31G*.

Normally protons in organic compounds are electron-positive, as illustrated by the electrostatic potentials (ESPs) shown for alkanes, benzene and alcohols in Figure 6.2. The ESP of the OH in alcohol is over $+200 \text{ kJ mol}^{-1}$ (Fig 6.2c), which is consistent with its good H-bond donor properties. Perfluoro-*tert*-butanol (PFTB) is very strong H-bond donor with an ESP of $+292 \text{ kJ mol}^{-1}$ and is often employed in the study of H-bonds (Fig 6.2d).¹⁴⁻¹⁵ In contrast, metal hydrides have very electron-negative protons -132 kJ mol^{-1} (Fig 6.2e), and accordingly, the dihydrogen bond energy in the NbCp₂H₃ and trifluoroethanol complex was determined to be $18.8 \pm 1.3 \text{ kJ mol}^{-1}$ through IR examination of the OH stretch region.⁷ In comparison, the Si-H in trihexylsilane has a much less negative ESP of -44 kJ mol^{-1} (Fig 6.2f).

The aim of this project is to investigate the Si-H group in trihexylsilane as a weak H-bond acceptor (Fig 6.3a). Two H-bonds are to be tested, one with a strong H-bond donor perfluoro-*tert*-butanol (PFTB) and the other a weaker donor, 1*H*-perfluorohexane (Fig 6.3b-c). Since Si-H is also a potential halogen-bond acceptor, iodopentafluorobenzene will be employed as halogen-bond donor in this study (Fig 6.3d). As the H-bond donors are fluorinated compounds, ¹⁹F-NMR titrations can be used to obtain thermodynamic data about the interactions of interest.

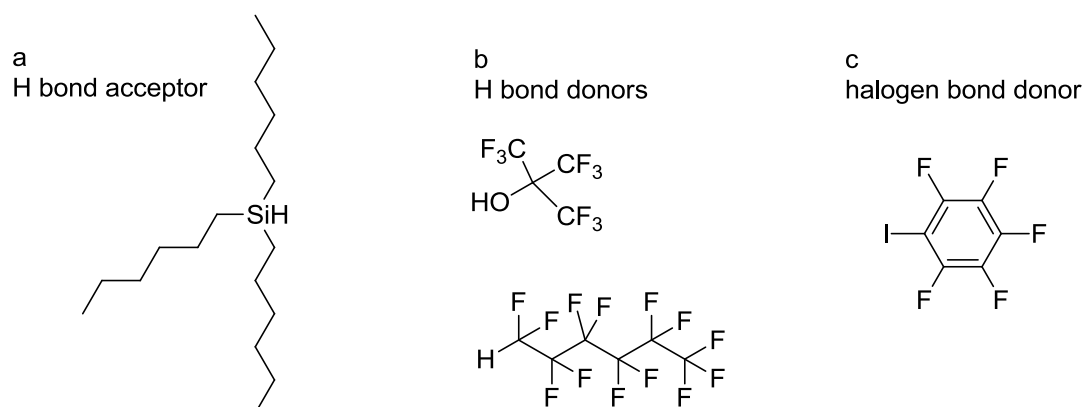


Figure 6.3. Structures of a) trihexylsilane, b) perfluoro-*tert*-butanol (PFTB), c) 1*H*-perfluorohexane and d) iodopentafluorobenzene

6.3 Results and Discussion

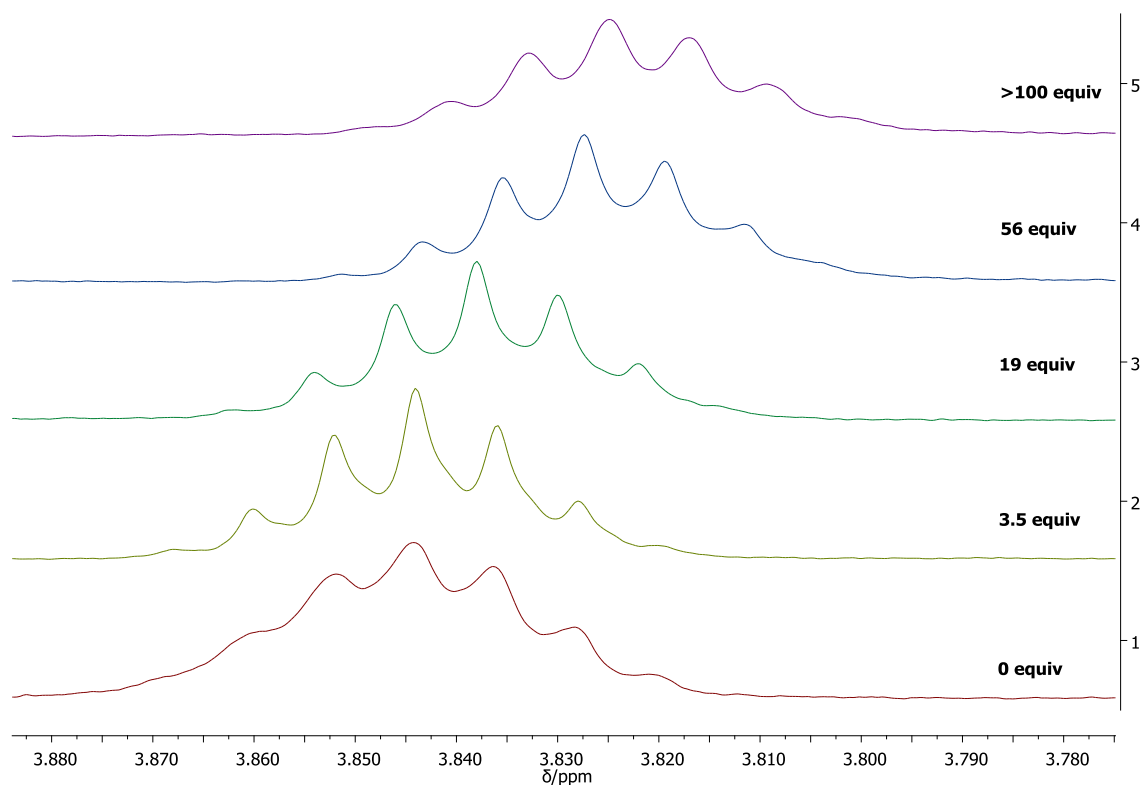


Figure 6.4. ^1H -NMR spectra of tri-*n*-hexylsilane (20mM) with different equivalents of PFTB in d_{12} -cyclohexane..

When hydrogen acts as a H-bond donor, a downfield shift is seen upon complexation with a H-bond acceptor. However, an upfield shift was observed in $\delta_{\text{Si-H}}$ of the silane upon addition of perfluoro-*tert*-butanol in d_{12} -cyclohexane (Fig 6.4). Although the movement is small (0.02 ppm), it provides evidence that Si-H is acting as a H-bond acceptor rather than a H-bond donor. An upfield shift was also reported in the complex between $[\text{NEt}_4][\text{HRe}_2(\text{CO})_9]$ and trifluoroethanol.⁸

Due to the small change in the observed ^1H NMR chemical shifts, ^{19}F NMR was introduced for determining thermodynamic data. During the titration, δ_{F} was seen to move downfield as the concentration of silane was increased, implicating the

formation of the desired complex between the very weak H-bond acceptor of silane and the strong H-bond donor PFTB. Using this titration data it was also possible to determine the binding constant as $0.75 \pm 0.10 \text{ M}^{-1}$ in cyclohexane at 298 K (Fig 6.5). The small binding constant indicates that Si-H is indeed a very weak H-bond acceptor, which is likely weakened further by solvent interactions. The binding constant of the silane with the weaker H-bond donor 1*H*-perfluorohexane and the halogen-bond donor were too weak to be measured using this method.

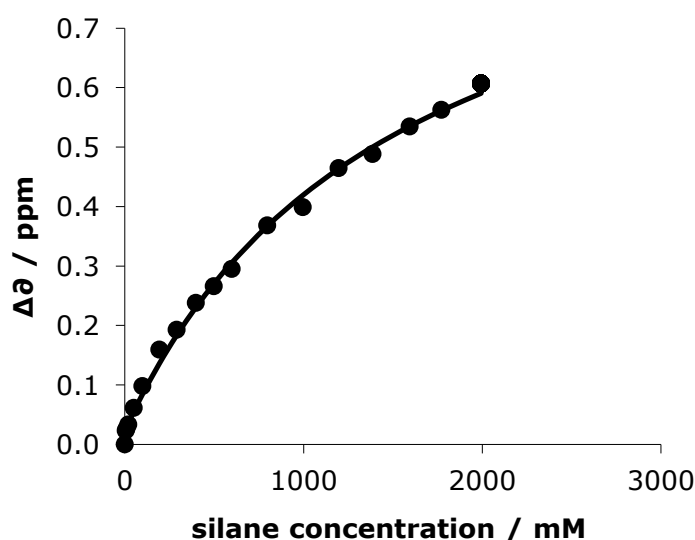


Figure 6.5. An example of tri-*n*-hexylsilane and perfluoro-*tert*-butanol complex binding isotherm.

Further support for the dihydrogen bond between tri-*n*-hexylsilane and PFTB was provided by density functional theory (DFT) calculations. After geometry minimisation, the Si-H proton was found to be in close contact with the strong H-bond donor OH as shown in Figure 6.6. The H \cdots H distance was 1.786 Å, which falls within the range of classic H-bond lengths (1.6 Å- 2.0 Å).¹⁶ The OH \cdots H angle was 161.8° and the H \cdots H-Si angle was 149.7°. The bent geometry can be attributed to steric hindrance between the bulky perfluoro-*tert*-butyl and hexyl groups. The H \cdots H interaction energy was computed as 23 kJ mol⁻¹, but since this value did not include correction of the basis set superposition error (BSSE), the error may be large. A calculation using a larger basis set like aug-cc-pVQZ should be performed if time

permits. The O-H bond was also elongated compared to its free form (0.978Å vs 0.973Å). Meanwhile, the Si-H bond was elongated by 0.008Å (from 1.499Å for the free silane).

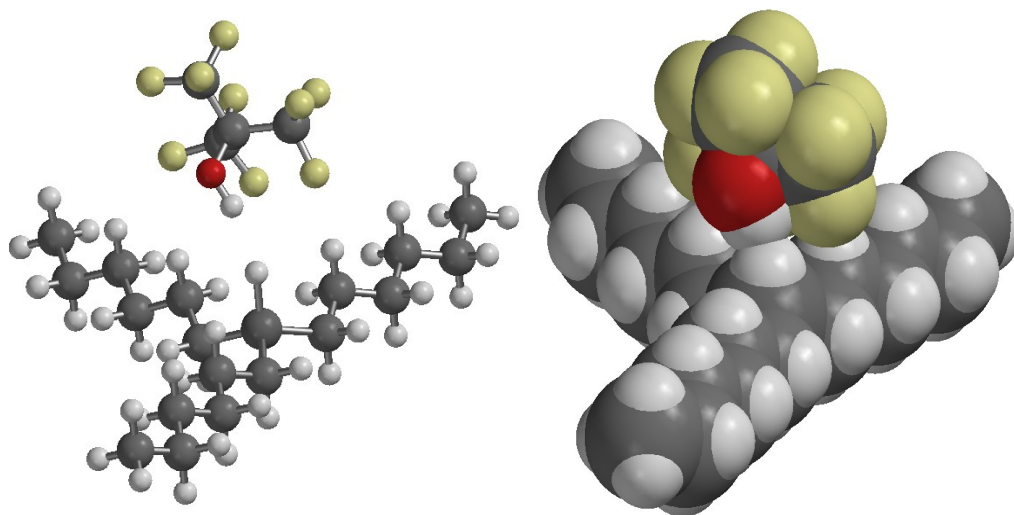


Figure 6.6. Optimized complex structure calculated at DFT/B3LYP/6-31G* level.

6.4 Conclusion and Future work

To conclude, the binding constant of the dihydrogen bond involving Si-H as a H-bond acceptor was determined for the first time, confirming that Si-H acts as a weak H-bond acceptor. The interacting complex was also examined by DFT and with ^1H and ^{19}F NMR studies. Further work might examine the interaction using molecular torsion balances, or using a supramolecular balance that exploits cooperativity to amplify weak interaction as small as 60 J/mol.¹⁷

6.5 Experimental Section

All compounds were purchased from *Sigma-Aldrich*, *VWR* or *Fluoro Chem*. Solvents were dried over 4Å molecular sieves. 20mM trifluoroacetic acid in D_2O was used as an internal standard during ^{19}F NMR experiments. Fluorinated compounds served as the host in titration experiments. Silane guest solutions were prepared using host stock solution, so that the host concentration remained constant during the titration

experiments. Fitting was performed using an Excel spreadsheet provided by Prof. Christopher A. Hunter. DFT calculations were carried out using the program *Spartan '08*.

References

- (1) Watson, J. D.; Crick, F. H. C. *Nature* **1953**, *171*, 737-738.
- (2) Ciesielski, A.; Palma, C.-A.; Bonini, M.; Samori, P. *Adv. Mater.* **2010**, *22*, 3506-3520.
- (3) Otero, R.; Gallego, J. M.; de Parga, A. L. V.; Martín, N.; Miranda, R. *Adv. Mater.* **2011**, *23*, 5148-5176.
- (4) Custelcean, R.; Jackson, J. E. *Chem. Rev.* **2001**, *101*, 1963-1980.
- (5) Siegbahn, P. E. M.; Eisenstein, O.; Rheingold, A. L.; Koetzle, T. F. *Acc. Chem. Res.* **1996**, *29*, 348-354.
- (6) Alkorta, I.; Elguero, J. *Chem. Soc. Rev.* **1998**, *27*, 163-170.
- (7) Bakhmutova, E. V.; Bakhmutov, V. I.; Belkova, N. V.; Besora, M.; Epstein, L. M.; Lledós, A.; Nikonov, G. I.; Shubina, E. S.; Tomàs, J.; Vorontsov, E. V. *Chem. Eur. J.* **2004**, *10*, 661-671.
- (8) Donghi, D.; Beringhelli, T.; D'Alfonso, G.; Mondini, M. *Chem. Eur. J.* **2006**, *12*, 1016-1025.
- (9) Chen, X.; Bao, X.; Zhao, J.-C.; Shore, S. G. *J. Am. Chem. Soc.* **2011**, *133*, 14172-14175.
- (10) Wolstenholme, D. J.; Traboulsee, K. T.; Hua, Y.; Calhoun, L. A.; McGrady, G. S. *Chem. Commun.* **2012**, *48*, 2597-2599.
- (11) Ishikawa, H.; Saito, A.; Sugiyama, M.; Mikami, N. *J. Chem. Phys.* **2005**, *123*, 224309.
- (12) Juárez-Pérez, E. J.; Viñas, C.; Teixidor, F.; Núñez, R. *J. Organomet. Chem.* **2009**, *694*, 1764-1770.
- (13) Richardson, T.; de Gala, S.; Crabtree, R. H.; Siegbahn, P. E. M. *J. Am. Chem. Soc.* **1995**, *117*, 12875-12876.
- (14) Cabot, R.; Hunter, C. A.; Varley, L. M. *Org. Biomol. Chem.* **2010**, *8*, 1455-1462.
- (15) Cook, J. L.; Hunter, C. A.; Low, C. M.; Perez-Velasco, A.; Vinter, J. G. *Angew. Chem., Int. Ed.* **2007**, *46*, 3706-3709.
- (16) Steiner, T. *J. Phys. Chem. A* **1998**, *102*, 7041-7052.
- (17) Roman, M.; Cannizzo, C.; Pinault, T.; Isare, B.; Andrioletti, B.; van der Schoot, P.; Bouteiller, L. *J. Am. Chem. Soc.* **2010**, *132*, 16818-16824.